Model Predictive Approaches for Automated Emergency Maneuvers

A Comparative Analysis of Hybridization for Vehicle Control

Master Thesis

Roald Bruinsma

Delft University of Technology

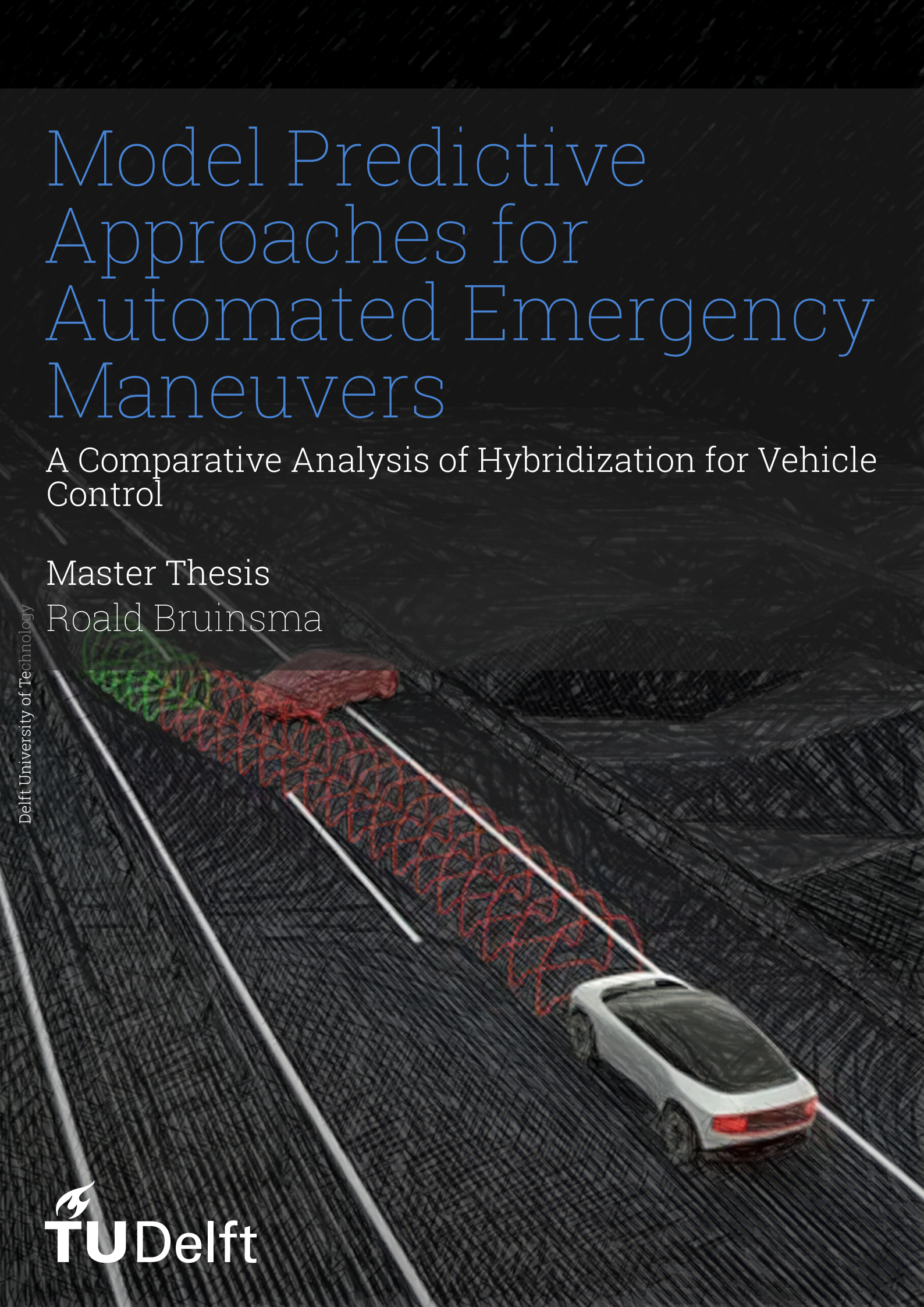

TU Delft

Model Predictive Approaches for Automated Emergency Maneuvers

A Comparative Analysis of Hybridization for Vehicle Control

by

Roald Bruinsma

to obtain the individual double degree of Master of Science in Systems & Control and in Mechanical Engineering at the Delft University of Technology,
to be defended publicly on Friday July 5, 2024 at 09:00 AM.

Student number:	4455509	
Graduation Committee:	Dr. ir. A.J.J. van den Boom,	Delft University of Technology, Chair
	Dr. ir. B. Shyrokau,	Delft University of Technology, Chair
	Ir. A. Bertipaglia, PhD Candidate,	Delft University of Technology, Supervisor
	Ir. L. Gharavi, PhD Candidate,	Delft University of Technology, Daily Supervisor

TU Delft Delft University of Technology

Cognitive Robotics

DCSC

Acknowledgements

I would like to express my heartfelt gratitude to all those who have provided invaluable support and assistance throughout my graduation project.

First, I sincerely thank my supervisors, Ton van den Boom, Barys Shyrokau, and Alberto Bertipaglia. Their supervision, time, invaluable insights, and critical perspectives have been instrumental in guiding me through this project. Their expertise and feedback helped me structure my approach to tackling problems, interpreting the results, and maintaining a critical outlook throughout the process.

A special thanks goes to my daily supervisor, Leila Gharavi. Her support and willingness to assist with any questions, doubts, or issues I encountered at any time significantly enhanced the quality of this work as well as my mental state. Her guidance in both theoretical and practical aspects, along with her encouragement, provided me with the confidence to persevere through the most challenging moments and kept me motivated when I needed it the most.

I also wish to thank my family—my brother, sister, and especially my parents—for their support (and financial assistance), which has been immensely helpful throughout this journey.

Of course, I also want to extend my gratitude to my roommates and friends, who had to endure my fluctuating moods and live through one of the most challenging periods of my life. Despite my repeated declarations that I was finished with the project, their constant motivation and encouragement helped me push through.

Last but certainly not least, I want to thank my girlfriend, Mathilde. Without her support, I would never have finished this project. Listening to me complain might not always have been enjoyable, but her patience and understanding provided me with the strength to carry on. Moreover, she was able to keep my mind off studying on the moments I needed to. Her unwavering support and belief in me has been a crucial factor in the completion of this work.

Roald Bruinsma
Delft, June 2024

Abstract

Model Predictive Control (MPC) is widely recognized for its efficacy in executing emergency evasive maneuvers, yet it often necessitates high-fidelity vehicle models to manage nonlinearities and uncertainties, which significantly increases computational demand. Hybrid systems modeling frameworks offer a promising solution by approximating said nonlinearities, thus reducing computational complexity while striving to maintain satisfactory control performance. However, there is a notable lack of benchmarks evaluating the impact of hybrid approximations on performance metrics.

This thesis presents a detailed comparative analysis of various levels of hybrid model complexity, assessing their impact on tracking performance and computational demand within both the classic MPC and Model Predictive Contouring Control (MPCC) frameworks. The study employs four hybrid approximations of the vehicle model, each with a distinct level of complexity, as prediction models in both MPC and MPCC optimization problems. The closed-loop behavior of these systems is simulated during emergency maneuvers of varying aggressiveness, and their robustness against different levels of road friction and vehicle velocities is assessed.

The results indicate that the MPC formalism offers a more robust approach to tracking performance and provides a feasible solution in a broader range of scenarios than the MPCC framework. Furthermore, the analysis reveals that higher model complexity, while potentially improving tracking accuracy, also significantly increases computational demands. Conversely, simpler models offer more consistent performance with reduced computational requirements.

This work offers comprehensive insights into the trade-offs between model complexity, control performance, and computational efficiency. By clarifying the effects of hybrid approximation levels on the control system's behavior, this thesis provides valuable guidelines for implementing hybrid MPC in automated driving systems, particularly for emergency maneuvers. The findings contribute to the development of more efficient and robust control strategies for advanced driver assistance systems and autonomous vehicles.

Keywords: Automated vehicles, emergency evasive maneuvers, model predictive control, hybridization, benchmark

Contents

List of Figures

Nomenclature

Abbreviations

Abbreviation	Definition
AV	Automated Vehicle
CoM	Center of Mass
DLC	Double Lane Change
IQR	Inter-Quartile Range
KPI	Key Performance Indicator
MIP	Mixed-Integer Program
MIQCP	Mixed-Integer Quadratically Constrained Program
MPC	Model Predictive Control
MPCC	Model Predictive Contouring Control
NLP	Nonlinear Program
NMPC	Nonlinear Model Predictive Control
PWA	Piecewise Affine
PWL	Piecewise Linear
RMSE	Root-Mean-Square-Error

Symbols

Symbol	Definition	Unit
A_f	Frontal area of vehicle	[m^2]
a_i	Slope of PWA approximation at local mode i	[N/rad]
a_x	Longitudinal acceleration	[$\mathrm{m/s}^2$]
a_y	Lateral acceleration	[$\mathrm{m/s}^2$]
C_c	Curvature scaling factor	[-]
C_d0	Rolling resistance coefficient	[-]
C_d1	Aerodynamic drag coefficient	[-]
c_i	Offset of PWA approximation at local mode i	[N]
C_y	Tire cornering stiffness	[-]
F_x	Longitudinal tire force	[N]
$F_\mathrm{x,Drag}$	Longitudinal drag force	[N]
F_y	Lateral tire force	[N]
F_z	Vertical tire load	[N]
g	Gravitational constant	[$\mathrm{kg/m}^3$]
h_CoM	Height CoM	[m]
I_zz	Vehicle moment of inertia around vertical axis	[kgm^2]
J	Cost function	[-]
k	Timestep	[-]
l_f	Front axle to CoM distance	[m]
l_r	Rear axle to CoM distance	[m]
m	Vehicle mass	[kg]
N_p	Prediction horizon	[-]
q	Cost term	[-]
r	Yaw rate	[rad/s]

Symbol	Definition	Unit
r_i	Breakpoint of PWA approximation after local mode i	[rad]
t_{MPC}	Sampling time MPC	[s]
t_{plant}	Sampling time plant	[s]
v_{x}	Longitudinal velocity	[m/s]
v_{y}	Lateral velocity	[m/s]
X	Global x position	[m]
Y	Global y position	[m]
α	Tire slip angle	[rad]
α_{sat}	Saturating slip angle	[rad]
δ_{f}	Front tire steering angle	[rad]
ϵ^{c}	Contouring error	[m]
ϵ^{l}	Lag error	[m]
θ	Traveled vehicle distance (path parameter)	[m]
κ	Curvature function	[1/m]
μ	Tire-road friction coefficient	[-]
ρ	Air density	[kg/m^3]
ϕ	Angle of tangent to the path	[rad]
χ	Drive/brake force distribution	[-]
ψ	Yaw angle	[rad]

1 Introduction

1.1. Motivation

Each year, an estimated 1.35 million people lose their lives and 20 to 50 million others sustain non-fatal injuries, often resulting in disabilities, due to traffic incidents [1]. Traffic accidents not only cause immense personal suffering but also impose a substantial economic burden, with costs related to medical expenses, lost productivity, and property damage running into billions of euros annually. According to the National Motor Vehicle Crash Causation Survey conducted in the U.S. from 2005 to 2007, most traffic accidents are caused by human error, with drivers found accountable for 94% of all accidents. This highlights the need for interventions that can mitigate human error and improve driving safety. As vehicle speeds increase and road conditions worsen, the severity of these statistics becomes more apparent. High-speed driving reduces reaction time and increases the likelihood of severe outcomes in the event of a crash. Poor road conditions, such as potholes, debris, and severe weather conditions, further worsen the risk of accidents [2]. These factors collectively underscore the urgency of finding effective solutions to enhance road safety.

Automated Vehicles (AVs) offer a promising solution to mitigate human errors on the road [3]. Equipped with advanced sensors, algorithms, and control systems, AVs can navigate complex environments without human intervention. They continuously monitor their surroundings, detect potential hazards, and make split-second decisions to avoid collisions. The integration of real-time environmental data enables AVs to adapt swiftly and effectively to changing conditions, ensuring optimal performance even in challenging scenarios where human drivers fail. This capability is particularly important during emergency evasive maneuvers, where AVs can leverage their full range of control to avoid obstacles and prevent collisions. AVs with Level 4 and Level 5 autonomy, as defined by the Society of Automotive Engineers J3016 standard [4], can execute complex last-minute maneuvers with high precision. These levels of autonomy signify that the vehicles can operate without human input in most or all circumstances, further reducing the risk of accidents caused by human error. Studies have shown that AVs have the potential to significantly reduce human error and enhance road safety [5, 6].

The extensive use of AVs could result in benefits in a variety of other domains. With fewer accidents, there would be a reduction in the burden on emergency services and healthcare systems. Traffic flow could become smoother and more predictable, reducing congestion and emissions. However, despite the potential benefits, the widespread adoption of AVs hinges significantly on societal acceptance and trust in this emerging technology. Addressing safety, reliability, and privacy concerns will be crucial in garnering public support for AVs [7]. To fully realize these benefits and account for societal acceptance, addressing the complex challenges of AV control is essential. Emergency evasive maneuvers are one of the most complex AV challenges in highway driving. In emergency evasive maneuvers, the AV needs to perform sudden and rapid movements to avoid an unexpected obstacle on the road, pushing the vehicle to its handling limits. When a collision-free trajectory has been planned by the planning algorithm, these maneuvers require highly complex and real-time feasible trajectory-tracking algorithms to follow the reference trajectory [8]. While this remains a widely studied topic, effective reference tracking in

emergency evasive maneuvers remains a challenge to this day.

1.2. Model Predictive Approaches

In recent decades, Model Predictive Control (MPC) has become a cornerstone in automated driving research due to its structured constraint handling and dynamic control capabilities [9]. Its ability to optimize actions in a finite horizon while updating the solution in real-time helps adaptability to evolving conditions [10]. This adaptability is crucial in the context of Automated Vehicle (AV) control, where unpredictable environments require robust and adaptive control strategies.

Achieving high-speed automated driving faces significant challenges, particularly in handling model complexity and control methods during emergency evasive maneuvers. These maneuvers require quick and precise responses from the vehicle's control system to maintain safety on the road. However, as model complexity increases to enhance tracking performance, so does the computational demand, potentially resulting in delayed responses and increased risks of accidents.

To address the need for precise tracking, the Model Predictive Contouring Control (MPCC) framework, initially developed for high-precision machining applications [11, 12], can be adapted for automated driving. MPCC relies on the assumption of minor lateral deviations from the reference path, which is often the case in high-precision applications where the quality specifications require maximum lateral errors in the order of microns. However, this assumption may not hold in automated driving since satisfying safety and stability constraints is prioritized over limiting the deviation from the reference path.

Unlike reference-tracking MPC [9], MPCC incorporates an analytical description of the reference path in terms of a customized path parameter [11]. By minimizing the distance to the reference path while maximizing progress along it in a receding horizon fashion, MPCC offers enhanced control capabilities, particularly in high-speed maneuvers where precision and agility are paramount. MPCC has been incorporated in robot motion planning at low speeds [13], trajectory planning in the presence of vulnerable road users [14], complex urban driving scenarios [15], lap-time optimization for racing RC cars [16], and high-speed drone flights [17, 18].

Recent advancements have seen MPCC applied to vehicle control in high-speed emergency maneuvers [19], where it has exhibited superior performance compared to baseline MPC controllers. Moreover, its application in car racing contexts suggests that MPCC exhibits control actions closer to human-like driving than classic MPC formalism [16]. Consequently, this study aims to comprehensively evaluate and compare both MPC and MPCC frameworks, shedding light on their respective strengths and limitations in high-speed automated driving scenarios.

1.3. Model Simplifications

The performance of Nonlinear MPC (NMPC) in extreme maneuvers is often compromised by nonlinear vehicle dynamics, leading to two main issues: computational complexities for solving the NonLinear Program (NLP), which increase the time and resources needed for processing, and stability and tracking issues due to convergence to a local optimum, which can cause the vehicle to deviate from its intended path [20].

Addressing the NLP and stability concerns involves various strategies within NMPC design. One prevalent approach involves adjusting model fidelity to strike a balance between accuracy and computational demand [21, 22, 23]. By tailoring the model complexity to the specific maneuver requirements, researchers aim to optimize computational efficiency while ensuring accurate trajectory tracking. However, varying model fidelity can lead to increased computational demands and complexity in model calibration, especially when integrating high-dimensional vehicle dynamics.

Another avenue explores cascaded complexities within the NMPC framework [24]. This approach involves decomposing the control problem into hierarchically organized subproblems, each addressing specific aspects of the maneuver. By breaking down the complexity into manageable components,

computational efficiency can be improved without sacrificing control performance. While promising, this method requires meticulous tuning of hierarchical control layers and may not generalize well across diverse driving scenarios.

Customized modeling of coupled dynamics and control represents a promising direction in addressing NMPC challenges [8]. By integrating vehicle dynamics and control algorithms in a synergistic manner, researchers seek to exploit the inherent relationships between these components to enhance overall system performance. This integrated approach offers the potential for more robust and efficient control solutions in high-speed maneuvering scenarios but demands extensive parameterization and validation efforts, which can be time-consuming and resource-intensive.

Online successive linearizations around the current operating point present another avenue for simplifying model complexity within NMPC frameworks [25, 26]. By linearizing the nonlinear model at each time step, this approach effectively reduces computational burden while maintaining accuracy in trajectory prediction. However, its effectiveness is contingent upon the accuracy of the linearization and the maneuver.

Research on explicit NMPC represents another strategy for addressing nonlinearities efficiently [27, 28, 9]. By precomputing control laws for a range of operating conditions, explicit NMPC circumvents the need for online optimization, thereby reducing computational overhead. However, the memory requirements for storing precomputed control laws can be substantial, particularly for large-scale problems.

Complex NMPC frameworks often employ variable models [29], time-step discretizations [30], or prediction horizons [31] to balance accuracy and computational efficiency. By adapting these parameters dynamically based on the current maneuver characteristics, researchers aim to optimize control performance while minimizing computational costs. However, achieving this balance requires careful consideration of the trade-offs between model accuracy and computational efficiency.

Furthermore, data-driven approaches offer a promising avenue for addressing NMPC challenges [32]. By leveraging large datasets to learn complex vehicle dynamics and control behaviors, data-driven NMPC algorithms can achieve a balance between accuracy and computational demand. However, the reliance on extensive datasets may limit the applicability of these approaches in emergency scenarios where real-time responses are crucial.

1.4. Hybridization

Hybridization techniques offer a powerful alternative for simplifying the intricate dynamics of nonlinear models. By breaking down these models into local modes, each of which is described by a linear relationship and activated within specific regions, hybridization offers a more manageable framework for analysis and control [33]. This approach is particularly advantageous in switched control-based methods, where effectively addressing nonlinearities is crucial. Hierarchical rule-based control architectures further enhance hybridization by adapting to different risk levels, seamlessly transitioning between models based on state and nonlinearity considerations [34, 35]. Moreover, these architectures can dynamically adjust to higher-fidelity models based on computational errors, thereby integrating continuous and discrete dynamics to efficiently manage complex system behaviors [36, 37]. The corresponding hybrid MPC formulations result in Mixed-Integer Programming (MIP) problems, which, by leveraging deterministic solving methods, are capable of finding global optima given sufficient computational resources.

The concept of hybridizing vehicle models for real-time implementation traces back to early research in nonlinear MPC [38]. Since then, diverse hybridizations of the nonlinear vehicle model have been explored. Due to the equivalences between hybridization techniques, each with its characteristics, different hybrid approaches can be used to approximate model nonlinearities [39]. Notably, the lateral tire force model, which introduces significant nonlinearities in automated driving near control limits, has been represented using hybrid parameter varying [40], piecewise affine [41], and mixed-logical dynamical approximations [42, 43]. Recent studies have extended hybridization to scenarios involving

emergency evasive maneuvers and highly nonlinear vehicle dynamics [44, 45, 46]. For instance, in [46], the entire nonlinear vehicle model is approximated using the max-min-plus-scaling systems formalism.

These hybridization techniques have significantly improved computational efficiency and control accuracy under complex driving conditions. Leveraging these benefits, this study adopts hybrid system formulations to approximate all nonlinear elements of the vehicle model. This comprehensive approach aims to capitalize on the advantages of hybridization, ensuring that the control strategies developed are robust and capable of handling the intricate dynamics encountered in automated driving, especially during emergency scenarios.

1.5. Contribution

To the best of the authors' knowledge, no studies have evaluated the impact of hybrid approximations on control performance in emergency evasive maneuvers. This paper provides a comparison benchmark to analyze and improve the computational and tracking performance of model predictive optimization problems in emergency evasive maneuvers scenarios through a simulation study. Various complexity levels of hybrid formulations are employed to approximate tire nonlinearities and the coupling between longitudinal and lateral dynamics. The approximations of the nonlinear vehicle model are used to formulate and solve the MPC problems as Mixed-Integer Quadratically-Constrained Programs (MIQCPs). The trade-off between the accuracy and the computation speed of the resulting hybrid MPC controllers is investigated in a comparative analysis. The controllers are simulated to track a Double Lane Change (DLC) maneuver in varying scenarios to test their robustness in terms of tracking, model uncertainty, and feasibility and to assess their computational demand. This work is divided into two parts: the first part is dedicated to hybridizations of the nonlinear model, and the second part evaluates the complexity of the hybridizations for both MPC and MPCC frameworks. The corresponding contributions of this paper are three-fold:

- hybridization of the lateral tire model for different levels of complexity to assess its impact on vehicle performance and computational efficiency
- integration of the hybrid model approximations within the MPCC framework
- presentation of a comparison benchmark for a comparative analysis on different levels of hybrid complexity and two model predictive approaches, and corresponding guidelines to signify their impact in emergency maneuvers

1.6. Thesis Structure

The remainder of the thesis is structured as follows. In chapter 2, the primary contributions of this graduation project are detailed in the format of a research paper. This chapter encapsulates the core findings and methodologies developed throughout the course of the project, providing a structured and in-depth presentation of the research outcomes. chapter 4 presents an extended conclusion to this work and chapter 3. In Appendix A, hybrid approximations of several nonlinear elements are presented. A validation of the hybrid models by means of open-loop simulations is given in Appendix B. Finally, the tuning of the hybrid model predictive frameworks is carried out by means of a sensitivity analysis, which is discussed in Appendix C.

2

Research Paper

This chapter provides the academic research paper outlining the research conducted as part of this graduation project.

Model Predictive Approaches for Automated Emergency Maneuvers: A Comparative Analysis of Hybridization for Vehicle Control

Roald Bruinsma

***Abstract*—Model Predictive Control (MPC) is an effective reference tracking strategy for automated vehicle control, particularly useful during emergency evasive maneuvers such as double lane changes. This control method often requires a high-fidelity vehicle model to accurately capture nonlinearities and uncertainties, significantly increasing computational demand. Hybrid systems modeling frameworks have been developed to approximate these nonlinearities, thereby reducing computational complexities while maintaining satisfactory tracking performance. However, existing benchmarks that evaluate the impact of these hybrid approximations on tracking performance and computational demands are lacking. Establishing such comparative benchmarks is crucial for understanding how different levels of model complexity affect the overall efficiency and effectiveness of model predictive approaches in automated driving scenarios. This paper addresses this gap by presenting a comparative analysis of various levels of hybrid model complexity. It assesses their tracking performance and computational demand using both MPC formulation and Model Predictive Contouring Control (MPCC) formalism in different emergency maneuver scenarios. Four hybrid approximations of the nonlinear single-track vehicle model with varying complexity levels are considered and employed as prediction models in both MPC and MPCC optimization problems. The closed-loop behavior of these control frameworks is simulated in double-lane change maneuver scenarios, evaluating tracking performance scenarios with varying levels of curvature. Additionally, variations in friction and velocity are evaluated in different scenarios to assess controller robustness to model uncertainty. Results indicate that reducing the complexity of hybrid approximations can decrease computational demand, albeit at the expense of tracking performance. Moreover, MPC formalism offers a more robust approach to tracking performance and provides a feasible solution in a broader range of scenarios than the MPCC framework. By shedding light on the impact of different complexity levels for the hybrid approximation of the nonlinear model and the control optimization problem formulation, this work offers comprehensive guidelines for hybrid MPC applications for automated driving in emergency scenarios.**

***Index Terms*— Automated vehicles, emergency evasive maneuvers, model predictive control, hybridization, benchmark**

I. Introduction

In recent decades, Model Predictive Control (MPC) has become a cornerstone in automated driving research due to its structured constraint handling and dynamic control capabilities [1]. Its ability to optimize actions in a finite horizon while updating the solution in real-time helps adaptability to evolving conditions [2]. This adaptability is crucial in the context of Automated Vehicle (AV) control, where unpredictable environments require robust and adaptive control strategies.

Achieving high-speed automated driving faces significant challenges, particularly emergency evasive maneuvers such as Double-Lane Changes (DLCs). These maneuvers require quick and precise responses from the vehicle's control system to maintain safety on the road. However, the performance of nonlinear MPC in extreme maneuvers is often compromised by nonlinear vehicle dynamics, leading to two main issues: computational complexities for solving the NonLinear Program (NLP), which increase the time and resources needed for processing, and stability and tracking issues due to convergence to a local optimum, which can cause the vehicle to deviate from its intended path [3]. As model complexity increases to enhance tracking performance, so does the computational demand, potentially resulting in delayed responses and increased risks of accidents, highlighting the need for precise path tracking.

To address the need for precise tracking, the Model Predictive Contouring Control (MPCC) framework, initially developed for high-precision machining applications [4], [5], can be adapted for automated driving. MPCC relies on the assumption of minor lateral deviations from the reference path, which is often the case in high-precision applications where the quality specifications require maximum lateral errors in the order of microns. However, this assumption may not hold in automated driving since satisfying safety and stability constraints is prioritized over limiting the deviation from the reference path. Unlike reference-tracking MPC [1], MPCC incorporates an analytical description of the reference path in terms of a customized path parameter [4]. It minimizes the distance to the reference while maximizing progress along it in a receding horizon fashion. This is achieved by considering the projection of the vehicle's position onto the reference line, offering enhanced control capabilities.

MPCC has been incorporated in robot motion planning at low speeds [6], trajectory planning in the presence of vulnerable road users [7], complex urban driving scenarios [8], lap-time optimization for racing RC cars [9], and high-speed drone flights [10], [11]. Recent advancements have seen MPCC applied to vehicle control in high-speed emergency maneuvers [12], where it has exhibited superior performance compared to baseline MPC controllers. Moreover, its application in car racing contexts suggests that MPCC exhibits control actions closer to human-like driving than classic MPC formalism [9]. Consequently, this study aims to comprehensively evaluate and compare both MPC and MPCC frameworks, shedding light on their respective strengths and limitations in high-speed automated driving scenarios.

Approaches to address the aforementioned issues related to the nonlinear vehicle dynamics include varying model fidelity [13]–[15], cascaded complexities [16], and customized modeling of coupled dynamics and control [17]. However, these methods involve managing increased computational demands, complexity in model calibration, hierarchical control

layer tuning, and extensive parameterization and validation efforts, which are particularly challenging in diverse driving scenarios. Online successive linearizations around the current operating point simplify model complexity but depend heavily on model nonlinearities and maneuvers and are sensitive to uncertainties [18], [19]. Research on explicit MPC addresses nonlinearities efficiently but requires substantial memory for large-scale problems [1], [13], [20], [21]. Other complex frameworks use variable models, variable time-step discretizations, or variable prediction horizons to balance accuracy and computational efficiency [22]–[24]. However, these methods face implementation challenges in maintaining computational tractability and adapting to rapid changes in environmental dynamics. A data-driven approach could offer a balance between accuracy and computational demand but needs large data sets that are not available in emergency scenarios [25].

A different approach to the nonlinear vehicle model problem is to employ hybridization techniques that simplify nonlinear models by dividing them into local modes, each described by a linear relation and activated within specific regions [26]. Switched control-based approaches leverage this method to effectively address the challenges of modeling nonlinearities. Hierarchical rule-based control architectures adapt to different risk levels [27], [28], switching models based on the given states and nonlinearities [29], or transitioning to higher-fidelity models depending on computational errors [30]. These methods introduce the concept of hybrid systems, integrating continuous and discrete dynamics to manage complex system behaviors efficiently. The corresponding hybrid MPC formulations result in Mixed-Integer Programming (MIP) problems, which are guaranteed to find global optima given sufficient computational resources thanks to deterministic solving methods.

The suggestion to hybridize the vehicle model for real-time implementation stems from early nonlinear MPC research [31]. Since then, different hybridizations of the nonlinear vehicle model have been employed. The lateral tire force model, a major source of nonlinearities in automated driving near the limits of control, has received particular attention. This model has been represented by hybrid parameter varying [32], piecewise affine [33], [34], or mixed-logical dynamical approximations [35]. Recent work incorporated hybridization into emergency evasive maneuvers and highly nonlinear vehicle dynamics [36]–[38]. These hybridization techniques have proven to improve the computational efficiency and control accuracy of vehicle models under complex driving conditions. Therefore, this study will employ hybrid system formulations to approximate all nonlinear elements of the vehicle model to account for the computational complexities and tracking problems.

To the best of the authors' knowledge, no studies have evaluated the impact of hybrid approximations on control performance in emergency evasive maneuvers. This paper provides a comparison benchmark to analyze and improve the computational and tracking performance of model predictive optimization problems in emergency evasive maneuvers scenarios through a simulation study. Various complexity levels of hybrid formulations are employed to approximate tire nonlinearities and the coupling between longitudinal and lateral dynamics. The approximations of the nonlinear vehicle model are used to formulate and solve the MPC problems as Mixed-Integer Quadratically-Constrained Programs (MIQCPs). The trade-off between the accuracy and the computation speed of the resulting hybrid MPC controllers is investigated in a comparative analysis. The controllers are simulated to track a Double Lane Change (DLC) maneuver in varying scenarios to test their robustness in terms of tracking, model uncertainty, and feasibility and to assess their computational demand. This work is divided into two parts: the first part is dedicated to hybridizations of the nonlinear model, and the second part evaluates the complexity of the hybridizations for both MPC and MPCC frameworks. The corresponding contributions of this paper are three-fold:

- hybridization of the lateral tire model for different levels of complexity to assess its impact on vehicle performance and computational efficiency
- integration of the hybrid model approximations within the MPCC framework
- presentation of a comparison benchmark for a comparative analysis on different levels of hybrid complexity and two model predictive approaches, and corresponding guidelines to signify their impact in emergency maneuvers

The paper is structured as follows. First, Sec. II provides background information on the hybrid approximation of nonlinear elements and the control methods employed in this study and explains the DLC maneuver considered in this study. Sec. III explains the nonlinear vehicle and tire model that will be employed as the plant model in this study. Sec. IV details the hybridization and the corresponding hybrid MPC controllers. In Sec. V, an overview of the scenarios that will be considered for the comparative analysis is given. Moreover, this section presents performance criteria for the objective assessment of the controllers, which serves as the comparative benchmark. Sec. VI presents the most noteworthy results for all scenarios. The results are discussed in Sec. VII, and future research directions are recommended. Finally, Sec. VIII provides a conclusion on this work.

II. Background

This section provides an overview of the key concepts and frameworks employed in this study. First, the Piecewise-Affine (PWA) approximation method for scalar nonlinear functions is discussed. Next, the MPC framework is introduced as a reference tracking strategy widely used for AV control. Following this, the MPCC formalism is presented by extending the MPC framework. The hybrid control optimization problem is then described, where the objective function from either the MPC or MPCC framework is minimized subject to system dynamics and constraints. Finally, the DLC maneuver that will be evaluated in this work is explained.

A. Model Element Approximation

In this study, nonlinear elements of the model will be hybridized separately. A scalar nonlinear function $f(z)$ can

be approximated by a hybrid formulation $\hat{f}(z)$ by solving the nonlinear optimization problem to find the slopes a_i, offsets c_i, and breakpoints r_i of the local modes of the PWA approximations [39], as is given in (1).

$$\min_{a_i,c_i,r_i} \int_{r_0}^{r_n} \Big(f(z) - \hat{f}(z)\Big)^2 dz, \tag{1a}$$

$$\text{s.t.} \quad \hat{f}(z) = \begin{cases} a_1^T z + c_1 & \text{if} \quad z \in \mathcal{R}_1 \\ \vdots & \\ a_n^T z + c_n & \text{if} \quad z \in \mathcal{R}_n \end{cases}, \tag{1b}$$

$$,]\underline{z} = r_0 \leq r_1 \leq \cdots \leq r_{n-1} \leq r_n = \overline{z}, \tag{1c}$$

$$a_i r_i + c_i = a_{i+1} r_i + c_{i+1}, \quad \forall i = 1, \ldots, n-1, \tag{1d}$$

where it holds that $\mathcal{R}_i \in [r_{i-1}, r_i]$ and n is the number of local modes of the approximation. The higher the number of local modes, the more accurate the approximation concerning the nonlinear element. Constraint (1d) guarantees the continuity of the PWA approximation at the breakpoints. The nonlinear optimization problem in (1) can be solved to local optimality using MATLAB's `fmincon` function with the interior-point algorithm.

B. MPC Cost Function

The MPC optimization problem is solved in each time step by minimizing a cost function over a prediction horizon of N_p steps such that the resulting MPC controller penalizes deviations from the desired lateral position, heading, and the reference vehicle velocity, as well as the control effort. To ensure smoother and more gradual changes in control actions, the rates of the control inputs are penalized. The cost function for the MPC controllers using the l_1-norm is as follows:

$$\begin{aligned} J_k = \sum_{i=1}^{N_\mathrm{p}} \Big(& \|\Delta \mathrm{Y}_{k+i}\|_1^{q_{\Delta Y}} + \|\Delta\psi_{k+i}\|_1^{q_{\Delta\psi}} + \|\Delta v_{\mathrm{x},k+i}\|_1^{q_{\Delta v_\mathrm{x}}} \\ & + \left\|\dot{\delta}_{\mathrm{f},k+i}\right\|_1^{q_{\dot{\delta}_\mathrm{f}}} + \left\|\dot{F}_{\mathrm{x},k+i}\right\|_1^{q_{\dot{F}_\mathrm{x}}} \Big), \end{aligned} \tag{2}$$

where N_p is the prediction horizon, $\Delta \mathrm{Y}_k = \mathrm{Y}_{\mathrm{ref},k} - \mathrm{Y}_k$, $\Delta\psi_k = \psi_{\mathrm{ref},k} - \psi_k$, $\Delta v_{\mathrm{x},k} = v_{\mathrm{x,ref}} - v_{\mathrm{x},k}$, and the weights of the cost function are

$$q_{\Delta \mathrm{Y}}, q_{\Delta\psi}, q_{\Delta v_\mathrm{x}}, q_{\dot{\delta}_\mathrm{f}}, q_{\dot{F}_\mathrm{x}} > 0. \tag{3}$$

The tuning of cost function weights $q_{\Delta \mathrm{Y}}, q_{\Delta\psi}, q_{\dot{\delta}_\mathrm{f}}, q_{\dot{F}_\mathrm{x}}$ involves determining their values based on the respective significance of positional accuracy, path speed, and control deviations.

C. MPCC Cost Function

The MPCC controllers extend the model predictive path-tracking control approach with the contouring control problem [4]. Instead of parameterizing by time, the contouring control problem utilizes parameterization of the desired path $(x_\mathrm{d}(\theta), y_\mathrm{d}(\theta))$ by the arc length $\frac{ds}{d\theta} = 1$, where s is the traveled vehicle distance along the path. The splines of the reference path are obtained by offline fitting. As a result, any point $(x(\theta), y(\theta))$ can be obtained by evaluating the reference path for its argument θ.

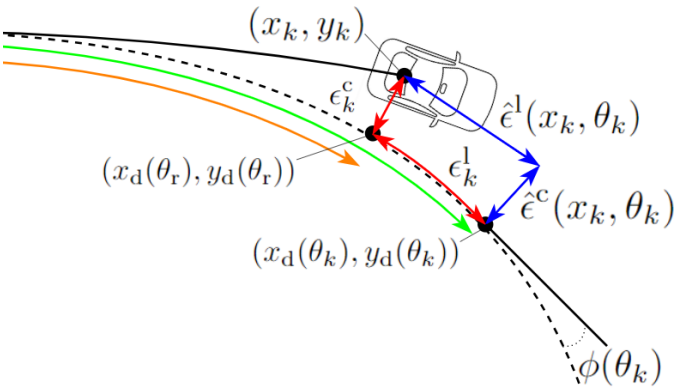

Fig. 1: Approximation of the contouring error ϵ^c and the lag error ϵ^l with respect to the reference trajectory.

The formulation of the MPCC problem requires error terms that describe the deviation of the vehicle's current position (x_k, y_k) from the desired reference point $(x_\mathrm{d}(\theta_k), y_\mathrm{d}(\theta_k))$ as can be observed in Fig. 1. The orthogonal distance of the vehicle from the reference path can be described by the contouring error ϵ_k^c and is given as follows [40]:

$$\epsilon_k^\mathrm{c} = \sin\phi(\theta_\mathrm{r})(x_k - x_\mathrm{d}(\theta_\mathrm{r})) - \cos\phi(\theta_\mathrm{r})(y_k - y_\mathrm{d}(\theta_\mathrm{r})), \tag{4a}$$

$$\phi(\theta_\mathrm{r}) = \arctan\left(\frac{\nabla y_\mathrm{d}(\theta_\mathrm{r})}{\nabla x_\mathrm{d}(\theta_\mathrm{r})}\right), \tag{4b}$$

where the distance between the point $(x_\mathrm{d}(\theta_\mathrm{r}), y_\mathrm{d}(\theta_\mathrm{r}))$ and (x_k, y_k) is minimal for the value of the path parameter $\theta_\mathrm{r}(x_k, y_k)$ and $\phi(\theta_\mathrm{r})$ is the angle of the tangent to the path at the reference point with respect to the X-axis. To approximate the path parameter, θ_k will be used instead of $\theta_\mathrm{r}(x_k, y_k)$, as a direct calculation of $\theta_\mathrm{r}(x_k, y_k)$ is not possible. This, in turn, leads to an introduction of the lag error that describes the norm between the reference traveled distance θ_r and the vehicle traveled distance θ_k. These errors are approximated as follows:

$$\begin{aligned} \hat{\epsilon}^\mathrm{c}(x_k, \theta_k) = & \sin\big(\phi(\theta_k)\big)\big(x_k - x_\mathrm{d}(\theta_k)\big) \\ & - \cos\big(\phi(\theta_k)\big)\big(y_k - y_\mathrm{d}(\theta_k)\big), \end{aligned} \tag{5a}$$

$$\begin{aligned} \hat{\epsilon}^\mathrm{l}(x_k, \theta_k) = & -\cos\big(\phi(\theta_k)\big)\big(x_k - x_\mathrm{d}(\theta_k)\big) \\ & - \sin\big(\phi(\theta_k)\big)\big(y_k - y_\mathrm{d}(\theta_k)\big), \end{aligned} \tag{5b}$$

where $\big(x_\mathrm{d}(\theta_k), y_\mathrm{d}(\theta_k)\big)$ is the desired reference point with desired heading angle $\phi(\theta_k)$. To allow θ_k to be an approximation of θ_r, it is desired to decrease the lag error approximation as much as possible by increasing its relative weight in the cost function. It can be observed in Fig. 1 that the approximation of the lag error decreases if $\theta_k \approx \theta_\mathrm{r}(x_k, y_k)$. This gives rise to the cost function for the MPCC controllers:

$$J_k = \sum_{i=1}^{N_\mathrm{p}} \Big(\|\hat{\epsilon}^\mathrm{c}(x_{k+i}, \theta_{k+i})\|_1^{q_{\hat{\epsilon}^\mathrm{c}}} + \left\|\hat{\epsilon}^\mathrm{l}(x_{k+i}, \theta_{k+i})\right\|_1^{q_{\hat{\epsilon}^\mathrm{l}}} + \|\Delta v_{\mathrm{x},k+i}\|_1^{q_{\Delta v_\mathrm{x}}} + \left\|\dot{\delta}_{\mathrm{f},k+i}\right\|_1^{q_{\dot{\delta}_\mathrm{f}}} + \left\|\dot{F}_{\mathrm{x},k+i}\right\|_1^{q_{\dot{F}_\mathrm{x}}} \Big), \tag{6}$$

where the weights of the cost function are

$$q_{\hat{\epsilon}^\mathrm{c}}, q_{\hat{\epsilon}^\mathrm{l}}, q_{\Delta v_\mathrm{x}}, q_{\dot{\delta}_\mathrm{f}}, q_{\dot{F}_\mathrm{x}} > 0. \tag{7}$$

The tuning of cost function weights $q_{\hat{\epsilon}^\mathrm{c}}, q_{\Delta v_\mathrm{x}}, q_{\dot{\delta}_\mathrm{f}}, q_{\dot{F}_\mathrm{x}}$ involves determining their values based on the respective significance of contouring accuracy, path speed, and control deviations. To maintain the validity of the lag error approximation, the cost function weight $q_{\hat{\epsilon}^\mathrm{l}}$ must be scaled accordingly, ensuring $\hat{\epsilon}^\mathrm{l}(x_k, \theta_k) \approx 0$.

D. Hybrid Control Optimization Problem

Depending on the objective function of the controller frameworks, the optimization problem for MPC using (2) or MPCC using (6) is formulated as follows:

$$\begin{aligned} \min \ & J_k && \text{(8a)} \\ \text{s.t. } & x_{k+i} = f(x_{k+i-1}, u_{k+i-1}, X_{\mathrm{ref},k+i-1}), && \text{(8b)} \\ & g_\mathrm{lb} \le g(x_{k+i}, u_{k+i-1}) \le g_\mathrm{ub}, && \text{(8c)} \\ & x_0 = x_\mathrm{initial}, \quad i = 1, \ldots, N_p, && \text{(8d)} \end{aligned}$$

where the function f represents the discretized version of the hybrid prediction model described in (18) and $g_\mathrm{lb,ub}$ represent the bounds on the constraints g. The MPC and MPCC controllers are implemented by solving the prediction model optimization at each time step. By minimizing the cost function J_k, an optimal control input $\mathbf{u}_k^*$ is obtained. This input is applied to the discretized version of the nonlinear plant model. The optimization is repeated for the next prediction model time step in a receding horizon fashion.

E. DLC Maneuver

This paper will employ a DLC maneuver to evaluate the designed controllers. Performing a DLC maneuver requires a high level of vehicle dynamics control to ensure safety and avoid collisions. In this maneuver, a vehicle executes two consecutive lane changes within a brief time frame, moving from its current lane to an adjacent one and returning to its original lane. The purpose of this maneuver is to navigate around a stationary obstacle or vehicle blocking the lane. Given a two-lane road, swift reversion to the initial lane becomes crucial to prevent collisions with oncoming traffic. The reference path for this maneuver is obtained from a predefined trajectory detailed in [12]. The segments and curvatures in Table I describe the path, where C_c is the curvature scaling factor.

The corresponding reference trajectory $(\mathrm{X}_\mathrm{ref}(s), \mathrm{Y}_\mathrm{ref}(s))$ of the DLC is then generated by integrating the curvature to obtain the desired heading angle $\psi_\mathrm{ref}(s)$ and then integrating the heading to obtain the coordinates:

TABLE I: Length and curvature for all path segments of the DLC maneuver.

Segment	Length [m]	Curvature [1/m]
L_in	75	0
L_1	$10C_\mathrm{c}$	$-0.049/C_\mathrm{c}^2$
L_2	$8.75C_\mathrm{c}$	$+0.049/C_\mathrm{c}^2$
L_3	$10C_\mathrm{c}$	$+0.049/C_\mathrm{c}^2$
L_4	$8.75C_\mathrm{c}$	$-0.049/C_\mathrm{c}^2$
L_5	$10C_\mathrm{c}$	0
L_exit	150	0

$$\begin{aligned} \psi_\mathrm{ref}(s) &= \int_0^s \kappa(x)dx, \\ \mathrm{X}_\mathrm{ref}(s) &= \int_0^s \cos(\psi_\mathrm{ref}(x))dx, \\ \mathrm{Y}_\mathrm{ref}(s) &= \int_0^s -\sin(\psi_\mathrm{ref}(x))dx, \end{aligned} \tag{9}$$

where $\kappa(x)$ represents the piecewise-defined curvature function based on the curvatures, and s is a parameter that represents the current position along the read trajectory being computed. The reference velocity throughout the maneuver is given as a fixed value.

III. Vehicle Model

This section details the nonlinear single-track vehicle model utilizing the Fiala brush tire force model. It explains all the elements of the nonlinear plant model, elaborates on the corresponding states and inputs, and highlights the nonlinear lateral tire model.

A. Nonlinear Bicycle Model

The vehicle model considered in this study is the nonlinear single-track bicycle model, illustrated in Fig. 2. For this model, it is assumed that the tires on each axle are lumped together. Moreover, only the in-plane dynamics are considered, ignoring the lateral weight transfer and additional roll and pitch dynamics. The following equations describe the nonlinear vehicle model:

$$\dot{\mathrm{X}} = v_\mathrm{x}\cos(\psi) - v_\mathrm{y}\sin(\psi), \tag{10a}$$
$$\dot{\mathrm{Y}} = v_\mathrm{x}\sin(\psi) + v_\mathrm{y}\cos(\psi), \tag{10b}$$
$$\dot{\psi} = r, \tag{10c}$$
$$\dot{v}_\mathrm{x} = \frac{-F_{\mathrm{y,f}}\sin(\delta_\mathrm{f}) + F_{\mathrm{x,f}}\cos(\delta_\mathrm{f}) + F_{\mathrm{x,r}} - F_{\mathrm{xDrag}}}{m} + rv_\mathrm{y}, \tag{10d}$$
$$\dot{v}_\mathrm{y} = \frac{F_{\mathrm{y,f}}\cos(\delta_\mathrm{f}) + F_{\mathrm{x,f}}\sin(\delta_\mathrm{f}) + F_{\mathrm{y,r}}}{m} - rv_\mathrm{x}, \tag{10e}$$
$$\dot{r} = \frac{F_{\mathrm{y,f}}\cos(\delta_\mathrm{f})l_\mathrm{f} + F_{\mathrm{x,f}}\sin(\delta_\mathrm{f})l_\mathrm{f} - F_{\mathrm{y,r}}l_\mathrm{r}}{I_\mathrm{zz}}, \tag{10f}$$
$$\dot{\theta} = \sqrt{v_\mathrm{x}^2 + v_\mathrm{y}^2}, \tag{10g}$$
$$\dot{\delta}_\mathrm{f} = \dot{\delta}_\mathrm{f}, \tag{10h}$$
$$\dot{F}_\mathrm{x} = \dot{F}_\mathrm{x}, \tag{10i}$$

TABLE II: The fixed vehicle and tire model parameters.

Parameter	Explanation	Value	Unit
l_f	Front axle to CoM distance	1.4360	[m]
l_r	Rear axle to CoM distance	1.4490	[m]
h_CoM	Height Center of Mass	0.566	[m]
I_zz	Vehicle moment of inertia around vertical axis	2985.216	[kgm^2]
m	Vehicle mass	1708	[kg]
A_f	Frontal area of vehicle	2.4	[m^2]
ρ	Air density	1.204	[kg/m^3]
C_d0	Rolling resistance coefficient	45	[N]
C_d1	Aerodynamic drag coefficient	0.25	[Ns/m]
$C_\mathrm{y,f}$	Front tire cornering stiffness	157450	[N/rad]
$C_\mathrm{y,r}$	Rear tire cornering stiffness	164260	[N/rad]
μ_f	Front tire friction coefficient	0.8	[-]
μ_r	Rear tire friction coefficient	0.9	[-]
$\mathcal{X}_\mathrm{d}$	Drive distribution	0	[-]
$\mathcal{X}_\mathrm{b}$	Brake distribution	0.5	[-]
t_MPC	Step size MPC	0.2	[s]
t_plant	Step size plant	0.001	[s]
N_p	Prediction horizon	5	[-]

where F_xDrag is the longitudinal aerodynamic drag force that has a quadratic dependence on the vehicle speed:

$$F_\mathrm{xDrag} = 0.5\rho A_\mathrm{f} C_\mathrm{d1} v_\mathrm{x} + C_\mathrm{d0}. \tag{11}$$

In (10), an additional state corresponding to the vehicle traveled distance θ is introduced and used for the MPCC cost function to compute the vehicle position relative to the reference. The vehicle parameter values are based on an experimentally validated model and are given in Table II. Moreover, all vehicle variables can be found in Table III.

The vehicle model inputs are the road-wheel angle rate ($\dot{\delta}_\mathrm{f}$) and the total longitudinal force rate applied at the CoG ($\dot{F}_\mathrm{x}$). The distribution of drive/brake force, denoted as $\mathcal{X}$, establishes the relationship between the total longitudinal force and the longitudinal force applied at individual axles:

$$F_\mathrm{x,f} = \mathcal{X}_\mathrm{f} F_\mathrm{x}, \tag{12a}$$
$$F_\mathrm{x,r} = \mathcal{X}_\mathrm{r} F_\mathrm{x}, \tag{12b}$$

where $\mathcal{X} = \mathcal{X}_\mathrm{f} + \mathcal{X}_\mathrm{r} = 1$. However, since the front/rear force distribution is unequal for drive and brake forces, this expression must be extended separately for braking and driving. The expression is reformulated as:

$$F_\mathrm{x,f} = \begin{cases} \mathcal{X}_\mathrm{b} F_\mathrm{x} & \text{if} \quad F_\mathrm{x} \leq 0 \\ \mathcal{X}_\mathrm{d} F_\mathrm{x}, & \text{otherwise,} \end{cases} \tag{13a}$$

$$F_\mathrm{x,r} = \begin{cases} (1-\mathcal{X}_\mathrm{b})\, F_\mathrm{x} & \text{if} \quad F_\mathrm{x} \leq 0 \\ (1-\mathcal{X}_\mathrm{d})\, F_\mathrm{x}, & \text{otherwise,} \end{cases} \tag{13b}$$

where $\mathcal{X}_\mathrm{d}$ and $\mathcal{X}_\mathrm{b}$ are the drive and brake distributions. The resulting nonlinear vehicle model is described by the states $\mathbf{x} = [\mathrm{X}, \mathrm{Y}, \psi, v_\mathrm{x}, v_\mathrm{y}, r, \theta, \delta_\mathrm{f}, F_\mathrm{x}]$ and inputs $\mathbf{u} = [\dot{\delta}_\mathrm{f}, \dot{F}_\mathrm{x}]$.

B. Fiala Brush Tire Model

In this paper, the nonlinear Fiala brush tire model is considered due to its demonstrated accuracy in describing tire behavior up to the limits of tire saturation, coupled with its computational efficiency, facilitating real-time implementation. We examine an adapted iteration of this model, as proposed by Pacejka [41], where the maximum lateral tire force is given as

TABLE III: The vehicle and tire model variables with bounds.

Variable	Explanation	Bounds	Unit
X	Global x position	[-10, 1000]	[m]
Y	Global y position	[-80, 80]	[m]
ψ	Yaw angle	[-3.4907, 3.4907]	[rad]
v_x	Longitudinal velocity	[10, 25]	[m/s]
v_y	Lateral velocity	[-8, 8]	[m/s]
r	Yaw rate	[-1.0472, 1.0472]	[rad/s]
θ	Vehicle traveled distance	[0, 1000]	[m]
δ_f	Road-wheel angle	[-1.5708, 1.5708]	[rad]
F_x	Total longitudinal force	[-7200, 7200]	[N]
$F_\mathrm{x,f}$	Front tire longitudinal force	[-3600, 0]	[N]
$F_\mathrm{x,r}$	Rear tire longitudinal force	[-3600, 7200]	[N]
$F_\mathrm{y,f}$	Front tire lateral force	-	[N]
$F_\mathrm{y,r}$	Rear tire lateral force	-	[N]
F_xDrag	Longitudinal drag force	-	[N]
α_f	Front tire slip angle	-	[rad]
α_r	Rear tire slip angle	-	[rad]

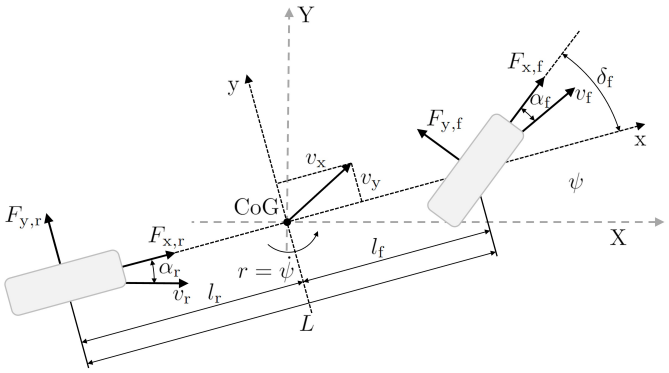

Fig. 2: Illustration of the single-track vehicle model.

$$F_\mathrm{y,i}^\mathrm{max} = \sqrt{(\mu_\mathrm{i} F_\mathrm{z,i})^2 - (F_\mathrm{x,i})}, \tag{14}$$

where $F_\mathrm{z,i}$ is the front or rear tire nominal load. Under these assumptions, the relationship between the front or rear lateral tire force and the front or rear tire slip angle is given as follows:

$$F_\mathrm{y,i} = \begin{cases} -C_\mathrm{y,i} \tan(\alpha_\mathrm{i}) \\ \quad + \frac{C_\mathrm{y,i}^2}{3F_\mathrm{y,i}^\mathrm{max}} |\tan(\alpha_\mathrm{i})| \tan(\alpha_\mathrm{i}) \\ \quad - \frac{C_\mathrm{y,i}^3}{27(F_\mathrm{y,i}^\mathrm{max})^2} \tan^3(\alpha_\mathrm{i}), & \text{if } |\alpha_\mathrm{i}| \leq \alpha_\mathrm{sat,i}, \\ -F_\mathrm{y,i}^\mathrm{max} \mathrm{sign}(\alpha_\mathrm{i}), & \text{otherwise.} \end{cases} \tag{15}$$

The tire model is defined by the axle's cornering stiffness C_y, which values are optimized by performing quasi-steady-state circular driving in a high-fidelity simulation based on a Delft-Tyre model 6.1 [12], and its value can be found in Table II. The front and rear tire slip angles are represented by:

$$\alpha_\mathrm{f} = \tan^{-1}\left(\frac{l_\mathrm{f} r + v_\mathrm{y}}{v_\mathrm{x}}\right) - \delta_\mathrm{f}, \tag{16a}$$
$$\alpha_\mathrm{r} = \tan^{-1}\left(\frac{-l_\mathrm{r} r + v_\mathrm{y}}{v_\mathrm{x}}\right). \tag{16b}$$

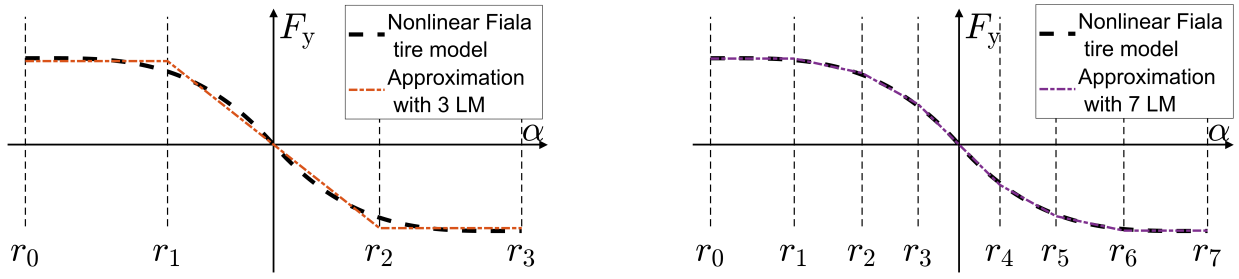

(a) Lateral tire force approximation with three local modes.

(b) Lateral tire force approximation with seven local modes.

Fig. 3: Lateral tire force approximations of the nonlinear Fiala tire model with three and seven local modes and breakpoints r_i.

TABLE IV: Settings for all DLC scenarios.

Scenario	**Curvature [-]**	**Friction [-]**	**Velocity [m/s]**
1	$C_c \in \{1.0, 1.2, ..., 2.0\}$	$\mu_f = 0.8, \quad \mu_r = 0.9$	$v_x = 17.5$
2	$C_c = 1$	$\mu \in \{0.7, 0.75, ..., 1.0\}$	$v_x = 17.5$
3	$C_c = 1$	$\mu_f = 0.8, \quad \mu_r = 0.9$	$v_x \in \{12.5, 15.0, 17.5, 20.0\}$
4	$C_c = 1$	$\mu \in \{0.5, 0.6, 0.7\}$	$v_x \in \{14.0, 14.5, ..., 20.0\}$

Saturation, or full sliding of the front or rear tire slip angle, occurs at the saturating slip angle $\alpha_{\text{sat,i}}$ [16]:

$$\alpha_{\text{sat,i}} = \arctan\left(\frac{3F_{\text{y,i}}^{\max}}{C_{\text{y,i}}}\right). \tag{17}$$

All relevant variables for the nonlinear vehicle model and tire model are shown in Table III.

IV. Hybrid Controller Design

This section describes the design and implementation of the proposed hybrid model predictive controllers employed in this study. First, simplifications are introduced, and nonlinear elements are hybridized to obtain the hybrid prediction models. Then, the physical bounds and constraints of the model are elaborated. Thereafter, the hybrid controllers are explained, and the tuning process of the controllers is discussed.

A. Hybrid Prediction Models

The proposed hybrid vehicle models considered in this study are approximations of the nonlinear model described in Sec. III-B. To simplify and approximate the nonlinear model, the following assumptions and simplifications are employed:

- Small angle approximation of steering angle.
- Small angle approximation of tire slip angles:
  $\tan^{-1}\left(\frac{l_f r + v_y}{v_x}\right) \approx \frac{l_f r + v_y}{v_x}$,
  $\tan^{-1}\left(\frac{-l_r r + v_y}{v_x}\right) \approx \frac{-l_r r + v_y}{v_x}$.
- Front and rear lateral tire model approximations for fixed total longitudinal force, friction coefficients, and longitudinal velocity:
  $F_x = 0N$, $\mu_f = 0.8$, $\mu_r = 0.9$, $v_x = 17.5$m/s.
- F_{xDrag} is fixed due to fixed velocity.
- Hybrid approximations of the sine, cosine, and norm terms.

The nonlinear front and rear lateral tire forces are approximated using the PWA approximation method outlined in (1).

As shown in Fig. 3, the lateral tire forces F_y are symmetric in the origin. Hence, it is necessary to approximate the lateral tire forces using a PWA approximation characterized by an uneven number of local modes. Examples of this approximation complexity are illustrated with three local modes in Fig. 3a and seven local modes in Fig. 3b, where it can be observed that increasing the number of local modes will lead to a more accurate representation of the nonlinear lateral tire model. Detailed derivations and models for all lateral tire forces and other nonlinear vehicle elements are provided in Appendix A. Using the hybrid approximation for the lateral tire forces and including the aforementioned simplifications and assumptions gives rise to the continuous hybrid vehicle model given in (18), where hybrid approximated elements are denoted with HYBR.

$$\dot{X} = v_x \cos^{\text{HYBR}}(\psi) - v_y \sin^{\text{HYBR}}(\psi), \tag{18a}$$
$$\dot{Y} = v_x \sin^{\text{HYBR}}(\psi) + v_y \cos^{\text{HYBR}}(\psi), \tag{18b}$$
$$\dot{\psi} = r, \tag{18c}$$
$$\dot{v}_x = \frac{F_{\text{y,f}}^{\text{HYBR}}\delta_f + F_{\text{x,f}} + F_{\text{x,r}} - F_{\text{xDrag}}}{m} + r v_y, \tag{18d}$$
$$\dot{v}_y = \frac{F_{\text{y,f}}^{\text{HYBR}} + F_{\text{x,f}}\delta_f + F_{\text{y,r}}^{\text{HYBR}}}{m} - r v_x, \tag{18e}$$
$$\dot{r} = \frac{F_{\text{y,f}}^{\text{HYBR}} l_f + F_{\text{x,f}}\delta_f l_f - F_{\text{y,r}}^{\text{HYBR}} l_r}{I_{zz}}, \tag{18f}$$
$$\dot{\theta} = [\|v_x, v_y\|_2]^{\text{HYBR}}, \tag{18g}$$
$$\dot{\delta}_f = \dot{\delta}_f, \tag{18h}$$
$$\dot{F}_x = \dot{F}_x. \tag{18i}$$

In Appendix B, open-loop simulations are employed to evaluate the effects of the different levels of complexity and to confirm the accuracy and performance of the proposed hybrid approximations.

B. Constraints

The limitations of the actuators, state boundaries, and physics-based constraints determine the feasible control region. In Table III, all constraints related to the states and the inputs are listed. It can be observed that the vehicle's longitudinal velocity is restricted between 10 and 25m/s to ensure proper forward motion. The road-wheel angle and the total longitudinal force are also limited to ensure the actuator behaves within its feasible range. The difference in constraint bounds between the front and the rear tire longitudinal force can be attributed to the rear-wheel driving characteristics of the vehicle.

The Fiala brush tire model model incorporates the Kamm circle constraint as a fundamental characteristic by including (14) for the maximum lateral tire force. Therefore, predetermined limits restrict the lateral forces exerted by the front and rear tires. They are determined by (14), based on the longitudinal force $F_{\mathrm{x,i}}$, vertical force $F_{\mathrm{z,i}}$, and road friction coefficient μ_{i} where $i \in \{\mathrm{f}, \mathrm{r}\}$. The Kamm circle constraint limits the attainable tire forces under combined lateral and longitudinal load conditions, preventing loss of contact and control. For the vertical forces, the following equations hold:

$$F_{\mathrm{z,r}} = \frac{1}{l_{\mathrm{f}} + l_{\mathrm{r}}} \big(m l_{\mathrm{r}} g - h_{\mathrm{CoM}} \left(F_{\mathrm{x,f}} + F_{\mathrm{x,r}} - F_{\mathrm{x,Drag}} \right) \big), \tag{19a}$$

$$F_{\mathrm{z,r}} = \frac{1}{l_{\mathrm{f}} + l_{\mathrm{r}}} \big(m l_{\mathrm{f}} g + h_{\mathrm{CoM}} \left(F_{\mathrm{x,f}} + F_{\mathrm{x,r}} - F_{\mathrm{x,Drag}} \right) \big), \tag{19b}$$

where h_{CoM} is the height of the Center of Mass (CoM), given in Table II. These constraints are expected to be maintained throughout the prediction horizon of the MPC and MPCC controllers.

C. Control parameters

The prediction model is discretized using the forward Euler method. A sampling time t_{MPC} = 0.2 s for the prediction model of the controllers was determined through computation time analysis. Additionally, the plant model uses a discretization time step of t_{plant} = 0.001s. Different time spans of the prediction in the range 0.8s to 1.60s are evaluated in Sec. VI-A, corresponding to $N_{\mathrm{p}} \in \{4, 5, 6, 7, 8\}$. Higher prediction horizons were found to be excessively computationally demanding.

D. MPC controllers

This comparative analysis considers two controller frameworks: hybrid MPC and hybrid MPCC. Both controller frameworks incorporate the hybrid prediction model given in (18) with varying complexity levels determined by the number of local modes of the lateral tire force approximations. The MPC controllers are based on (2) and are labeled as MPC1, MPC3, MPC5, and MPC7, corresponding to the number of local modes used for hybridizing the nonlinear lateral tire models. Likewise, the MPCC controllers are based on (6) and are labeled MPCC1, MPCC3, MPCC5, and MPCC7. The comparative analysis includes and compares a total of eight MIQCP controllers. The nonlinear single-track vehicle model described by (10) serves as the plant model across all controllers in the simulation study.

E. Weight Tuning

To guarantee accurate tracking, weights of the cost function in (2) or (6) need to be tuned. Achieving an optimal balance between minor tracking errors and control action usage is challenging since these weights hinge on the vehicle model, (physical) constraints, and the optimization solver itself. The tuning iterations involved systematic simulations where individual weights were introduced and adjusted one at a time. Time-domain trajectories and resulting Key Performance Indicators (KPIs) (as outlined in Sec. V-B) were evaluated throughout this process. The following general relations for tuning have been found:

- A trade-off is identified in the positional tracking of MPC controllers. Excessive weighting of the lateral position error $q_{\Delta \mathrm{Y}}$ increases computational demand, whereas insufficient weighting decreases positional accuracy. Additionally, the weight of the heading angle error should be larger than that of the lateral position error $q_{\Delta\psi}$ to guarantee tracking of the reference.
- Positional tracking of the MPCC controllers is improved by increasing the weight for contouring error $q_{\hat{e}^{\mathrm{c}}}$ relative to the lag error weight $q_{\hat{e}^{\mathrm{l}}}$. However, a substantial increase in the lag error weight increases computational demands. Conversely, reducing the lag error is required to guarantee the approximation of the path parameter, but excessively decreasing the weight can induce instabilities.
- A trade-off exists in velocity tracking: Insufficient weight on the velocity tracking error $q_{\Delta v_{\mathrm{x}}}$ yields inadequate velocity tracking, while excessive weight requires increased control input. However, this is feasible only if the weight on the total longitudinal force rate $q_{\dot{F}_{\mathrm{x}}}$ is not too high.
- Increasing the weight on the control inputs $q_{\dot{\delta}_{\mathrm{f}}}$ and $q_{\dot{F}_{\mathrm{x}}}$ will remove chattering and resulting oscillations, but too high a weight will result in a lack of control and tracking.

Based on these findings, manual tuning has been conducted for both the MPC and the MPCC controller frameworks. A sensitivity analysis for both frameworks was conducted to improve the manual tuning. This sensitivity analysis builds on the manual tuning and can be found in Appendix C. To guarantee fair comparisons, the manual tuning and the sensitivity analyses are conducted on the most complex models (i.e., the highest complexity approximations, MPC7 and MPCC7) for both frameworks. The tuning parameters derived from each framework were applied uniformly across all controller models within that framework.

V. Maneuvers and Assessment Criteria

This section details the different DLC maneuver scenarios that will be considered and the metrics employed to evaluate the tracking performance and robustness of the control frameworks in these scenarios. These maneuvers and assessment criteria will serve as the comparison benchmark.

A. Driving Scenarios

The DLC maneuver was evaluated for different levels of curvature, friction coefficients, and velocities to assess and compare the computational performance and tracking accuracy of the different control frameworks and hybrid models. The settings for these scenarios are given in Table IV. Prior to the scenarios, a prediction horizon assessment is conducted to determine the most suitable length for the prediction horizon N_p for all controllers. This assessment ensures that all controllers can simulate with reasonable computational demand and achieve acceptable tracking performance. The DLC maneuver is evaluated for $N_\mathrm{p} \in \{4, 5, ..., 8\}$. After finding a suitable value for the prediction horizon, the following scenarios are considered:

1) Varying Curvature: In this scenario, varying levels of curvature of the DLC maneuver are employed to assess the tracking performance of the controllers. The curvature level is adjusted by scaling the DLC maneuver with the curvature scaling factor C_c given in Table I. Increasing the scaling factor implies increasing the length of the path segments of the DLC reference trajectory and decreasing the corresponding curvature, thus making the lane changes less sharp.

2) Varying Friction Coefficient μ: In this scenario, the controllers are evaluated for varying friction coefficients while keeping the velocity constant. This setup aims to assess their robustness in handling model uncertainties arising from different friction properties. Since the prediction models are hybridized around fixed friction coefficients ($\mu_\mathrm{f} = 0.8, \mu_\mathrm{r} = 0.9$), it emphasizes the evaluation of controller performance under conditions where there might be mismatches between the plant and prediction models due to varying friction characteristics of the road.

3) Varying Velocity v_x: This scenario evaluates the controllers' performance under varying velocities while maintaining fixed friction coefficients. Since the prediction models are hybridized around a fixed velocity ($v_\mathrm{x} = 17.5$m/s), this scenario specifically examines model deviations due to changes in vehicle velocity, complementing the second scenario by assessing robustness in the face of model uncertainties related to varying vehicle velocity.

4) Feasibility of Optimal Solution: In this scenario, the feasibility of the controllers' solutions under low friction conditions is evaluated across a large range of velocities. This scenario assesses the robustness in terms of sensitivity to infeasibilities. Infeasibilities can be categorized into three different classes. The first class denotes scenarios where no feasible solution can be found at all, while the second class indicates situations where no feasible solution can be found within a specified timeframe. The final class means an undesired solution is found, which is infeasible in practice. In this study, the first two classes are classified as *Infeasible* since the simulations terminated prematurely. The third class is categorized as *Infeasible in practice* and will be highlighted separately as it produces results throughout the entire simulation, albeit with undesired outcomes.

B. Performance Criteria

To assess the performance of the controllers across various scenarios outlined in Sec. V-A, KPIs will be employed. The root mean square of the tracking errors (RMSE) over the horizon length of the controller is analyzed to assess the tracking abilities. The RMSE is given as

$$x_\mathrm{RMSE} = \sqrt{\frac{1}{N}\sum_{i=1}^{N}\big(x(i) - x_\mathrm{ref}(i)\big)^2}, \tag{20}$$

where x represents the following states $\mathrm{X}, \mathrm{Y}, \psi, v_\mathrm{x}$ and x_des the corresponding reference signals. Moreover, when considering the inputs, the RMSE can be evaluated for $x_\mathrm{ref} = 0$, where the inputs u are given as $\dot{\delta}_\mathrm{f}, \dot{F}_\mathrm{x}$. Other KPIs are the total computation time T_tot and the median computation time per time step T_med. Finally, for the scenarios involving varying curvature in Sec. V-A1, the maximum absolute lateral acceleration $|a_\mathrm{y,max}|$ is evaluated for each simulation to indicate the level of curvature. Instead of using the curvature scaling factor C_c, the maximum lateral acceleration is used, as it directly relates to the handling limits reached during the maneuver.

Lower values of the RMSEs indicate high control performance of the controller in tracking the reference trajectory, while lower values for T_tot and T_med indicate lower computational demand.

C. Solver Selection

The MIQCP problems are solved by the GUROBI optimizers [42], using MATLAB as the interface and overall computation environment. The simulations were conducted on a PC with a 6-core Intel Xeon W-2133 CPU 3.60GHz and 64GB RAM, using the MATLAB R2020a environment on Windows 10 Pro 64-bit.

VI. Results

This section states the results of the tracking and computational performance of all MPC and MPCC controllers. First, the computational performance is evaluated by using a varying prediction horizon. Then, the scenarios outlined in Sec. V-A are examined for a fixed prediction horizon. Based on a comparative analysis of the RMSEs of the states $\mathrm{X}, \mathrm{Y}, \psi, v_\mathrm{x}$, the controllers with the lowest and the highest errors from both frameworks are selected for Scenario 1, 2, and 3. Finally, the computation time for the first three scenarios is analyzed.

A. Prediction Horizon Assessment

The computational performance of the hybrid MPC controllers during the DLC is illustrated in Fig. 4, highlighting their mean and maximum relative tracking errors as well as computation time per control sampling interval. It can be observed that MPC1 and MPCC1 are not able to provide results for $N_\mathrm{p} = 4$, which is directly related to the oversimplification of the tire model that does not capture the full range of the

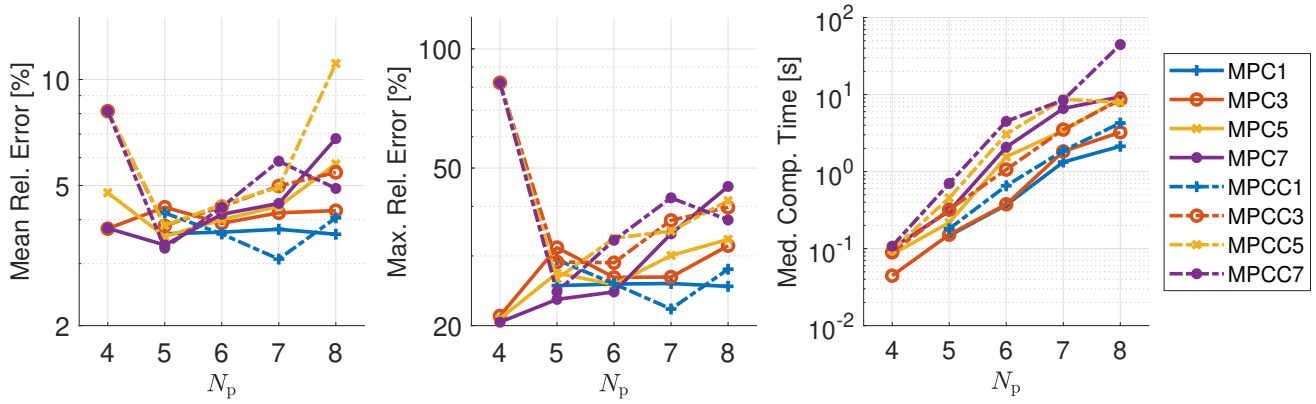

Fig. 4: Tracking and computational performance of the hybrid controllers in the double-lane change for different prediction horizons.

nonlinear tire model. Due to the low prediction horizon, the frameworks with the linear tire model are not able to provide feasible control.

For the controllers with 3 to 7 local modes, the MPC controllers outperform the MPCC controllers in terms of tracking. Especially at $N_\mathrm{p} = 4$, the MPCC controllers exhibit poor tracking performance while the MPC controllers demonstrate low maximum relative errors.

Higher-complexity models show increased relative errors as the horizon increases. The mean relative errors for MPC1 and MPC3 remain almost constant, while higher-complexity models suffer from an increase in error as the prediction horizon increases. This phenomenon can be attributed to the expanding search space dimensions. The higher the complexity of the model, the higher the increase in the dimension of the optimization problem and the potential accumulation of numerical errors.

All controllers exhibit a steady increase in computation time with increasing model complexity. MPC demonstrates superior computational speed compared to MPCC, reflecting the latter's more complex representation of the MPC problem. Regarding $N_\mathrm{p} = 5$, all controllers achieve low relative errors while maintaining a low computational demand compared to higher prediction horizons.

B. Scenario 1: Varying Curvature

In Scenario 1, the controllers were evaluated with a fixed prediction horizon of $N_\mathrm{p} = 5$, and the controllers are simulated for different curvature factors in the range of $C_\mathrm{c} \in \{1.0, 1.2, ..., 2.0\}$ to vary the curvature of the reference trajectory. The controllers with the lowest errors are MPC7 and MPCC7, and those with the highest errors are MPC3 and MPCC3.

Fig. 5 visualizes the performance of the aforementioned controllers in terms of tracking errors and median computation time. For all controllers, an increase in trajectory curvature generally also results in an increase in relative errors. The results show that the MPC controllers exhibit lower relative errors than the MPCC controllers when considering the same number of local modes.

In Fig. 6, the trajectories of the controllers with respect to the highest and the lowest level of curvature reference trajectories are visualized. For low trajectory curvature, the mean and maximum errors are more similar for all controllers, which is confirmed by the similarities in trajectories in Fig. 6b. However, for the reference trajectory with $C_\mathrm{c} = 1$, the mean and maximum errors of the controllers increase, resulting in more deviating trajectories in Fig. 6a, where MPCC controllers show higher performance in the positional trajectory tracking.

In terms of hybridization complexity, it can be observed that high complexity results in low relative errors in Fig. 5. MPC7 outperforms all other controllers in terms of relative errors. The other controllers have a higher rate of errors as the curvature increases, and the mean and maximum relative errors of MPC7 also remain lower than those of the other controllers in the same range of maximum lateral accelerations. However, results show that MPCC7 exhibits a lower mean relative error in the curvature trajectory where the highest maximum lateral accelerations are observed.

An increase in approximation complexity also results in an increase in maximum lateral acceleration for the same maneuver, indicating that the limits of vehicle control are higher. This can be attributed to the fact that with an increased approximation complexity, the prediction model is more accurate to the plant model, and thus, the controller is better able to exploit the vehicle model and provide more effective control to the plant. At the same time, the lower complexity hybridizations cannot capture the nonlinear behavior as well, thus resulting in a more conservative estimation of the vehicle capabilities due to under-approximations at the limits of handling.

As can be observed from Fig. 3, the higher complexity approximation closer approximates the nonlinear tire model for higher tire slip angles, thus being better able to capture the nonlinear behavior. However, an increase in framework complexity results in the opposite. This is related to the distinct control objective of MPC, which directly targets lateral position, heading, and velocity. This approach can result in unconventional maneuvers that a real vehicle would not typically perform to track the reference. At the same time, MPCC has a dual objective of minimizing the deviation from the desired

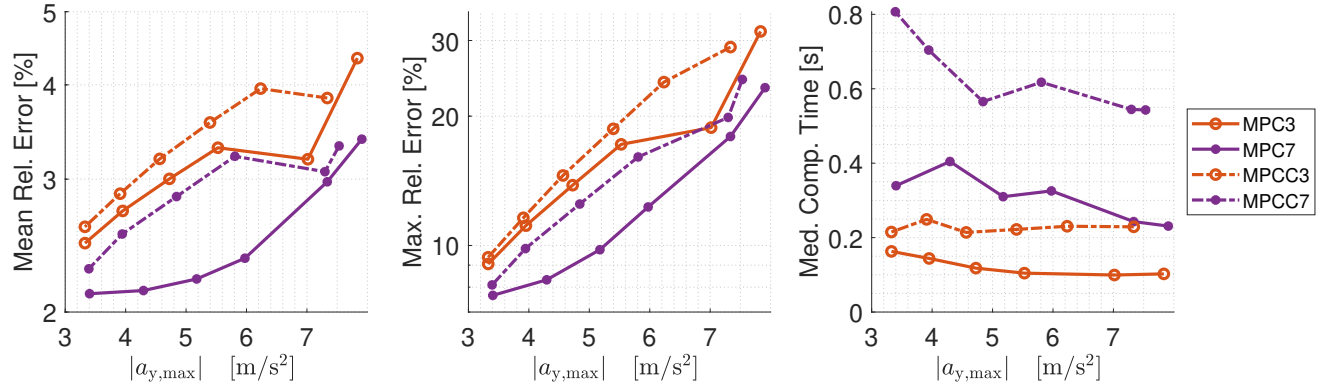

Fig. 5: Scenario 1: Tracking and computational performance of the best and the worst hybrid controllers.

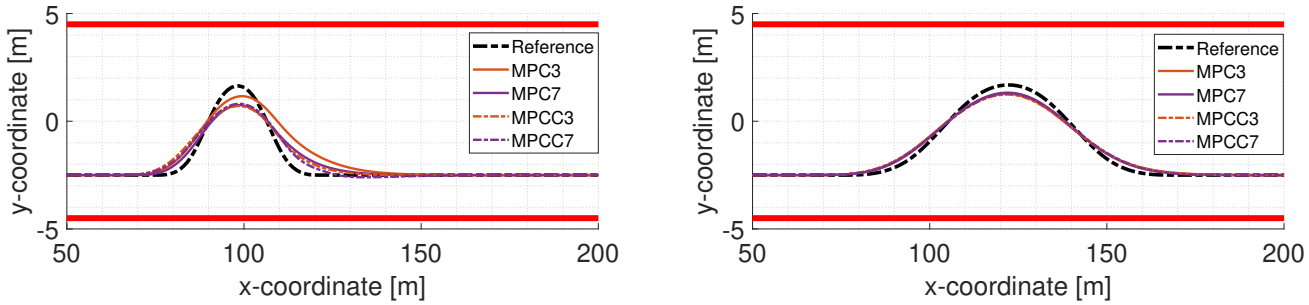

(a) $C_c = 1$. (b) $C_c = 2$.

Fig. 6: Scenario 1: DLC maneuvers of best and worst controllers for two curvatures.

path (contouring error) and optimizing the progress along the path (lag error), which can lead to a more balanced and conservative approach to handling the reference trajectory. Due to these differences, MPC7 exhibits the most aggressive behavior with the highest maximum lateral acceleration, whereas MPCC3 is able to execute this maneuver with the lowest maximum lateral acceleration. However, MPCC3 performs a significantly less extreme maneuver, as observed in Fig. 6a, which could explain the lower maximum lateral acceleration.

C. Scenario 2: Varying Friction Coefficient μ

The prediction horizon is fixed for $N_p = 5$, and the controllers are simulated for different road friction coefficients in the range of $\mu \in \{0.7, 0.75, ..., 1.0\}$ to ensure friction uncertainty in the prediction model due to the fixed road friction in the front and rear tire approximations. The controllers with the lowest errors for both frameworks in this scenario are MPC7 and MPCC7, and those with the highest are MPC3 and MPCC1.

Based on the results in Fig. 7, there is no clear best controller framework in terms of tracking performance since both MPC7 and MPCC7 show similar trends in the mean relative errors. MPC7 performs slightly better than MPCC7, considering maximum relative errors, but this is not the case at low road frictions. Moreover, MPCC1 has the worst tracking performance for high road friction coefficients, and for lower friction coefficients, MPC3 is worse.

For lower road friction coefficients, the mean and maximum errors deviate more for all controllers, which is confirmed by the differences in trajectories in Fig. 8a. The range of mean and maximum errors in Fig. 7 decreases for high road friction, resulting in more similar trajectories in Fig. 8b. In both figures, it can be observed that MPCC7 outperforms the other controllers in terms of tracking the reference.

Fig. 7 shows that increased approximation complexity generally results in higher tracking performance. An exception to this relation is the peaks for MPC7 and MPCC7 at $\mu = 0.9$. As road friction increases, the mean and maximum relative tracking errors decrease for MPC3, MPC7, and MPCC7. For MPC3, mean relative errors decrease steadily, and maximum relative errors decrease steeply. For MPC7 and MPCC7, the decrease in errors stops after $\mu = 0.9$, after which the errors again increase. This can directly be related to the hybrid approximations of the lateral tire forces, which are approximated for the front tire at $\mu_f = 0.8$ and at the rear tire at $\mu_r = 0.9$. The higher the approximation complexity, the more the effect of these fixed approximations is visible in the errors since the approximations are most valid on $\mu = 0.8$ or 0.9. Although the effect is less apparent for MPC3, it can still be observed that the decrease in relative errors stagnates after $\mu = 0.9$.

For MPCC1 with the linear tire force model, the uncertainty of the friction coefficient does not affect the relationship between the plant and the prediction model in the same way

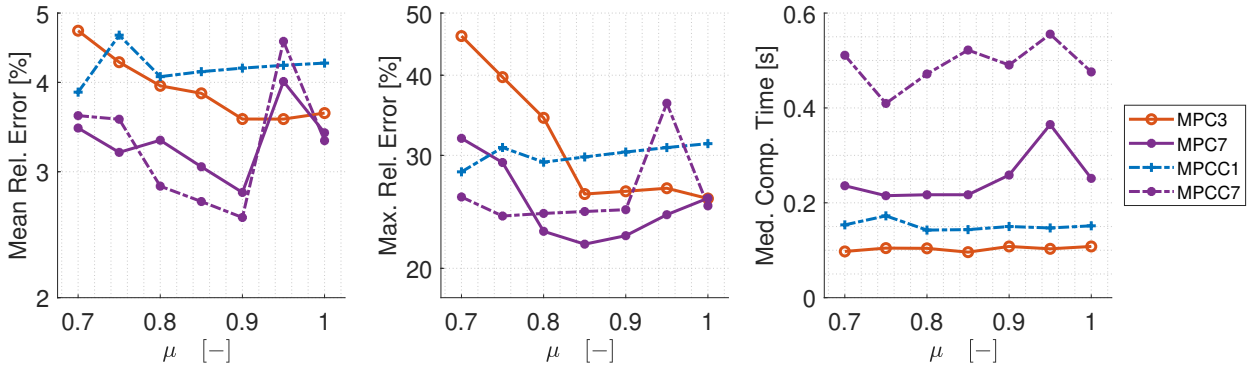

Fig. 7: Scenario 2: Tracking and computational performance of the best and the worst hybrid controllers.

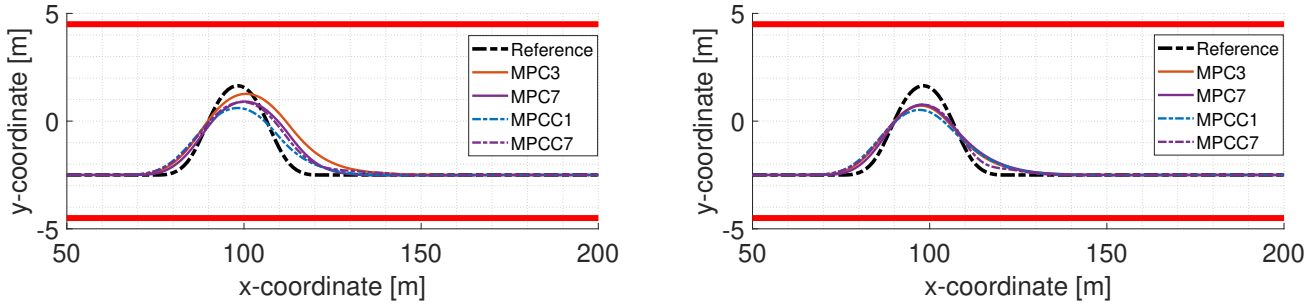

(a) $\mu = 0.7$. (b) $\mu = 1.0$.

Fig. 8: Scenario 2: DLC maneuvers of best and worst controllers for two road friction coefficients.

it does for higher complexity approximations because the friction coefficient does not influence the linear regime of the nonlinear tire model. Instead, it can be observed in Fig. 7 that the relative tracking errors decrease as the friction coefficient decreases. This could be explained by realizing that due to the linear tire force model, the controller will try to decrease the tire slip angles in order to avoid excessive tire forces. Since a decrease in road friction means a decrease in maximum lateral tire forces for the nonlinear plant model, the linear tire model has more over-approximation, which causes the controller to be even more conservative in lower friction circumstances.

D. Scenario 3: Varying Velocity v_x

The prediction horizon is fixed for $N_p = 5$, and the controllers are simulated for different desired velocities in the range of $v_{x,des} \in \{12.5, 15.0, 17.5, 20.0\}$m/s to ensure uncertainty in the prediction model due to the fixed velocity in the front and rear tire approximations as well as the drag force. In this scenario, the controllers with the errors for both frameworks are MPC7 and MPCC7, and those with the highest are MPC3 and MPCC1.

Increased desired velocity results in higher tracking errors for all controllers, as shown in Fig. 9. Particularly, the maximum relative errors increase significantly, which could be attributed to the fact that the drag force in the plant model is quadratically dependent on the velocity, as is given in (11). Due to the fixed approximations of the drag force as well as the lateral tire forces at $v_x = 17.5$m/s, the error between the prediction and the plant model increases significantly for higher velocities.

Similarly, the deviation between the plant and the prediction model also becomes higher for very low velocities, as Fig. 9 shows increasing mean and maximum errors at 12.5m/s. The reason that all controllers show more accurate tracking performance at lower velocities can also be attributed to the controllers having more time to solve the optimization problem. Moreover, the vehicle does not operate near the limits of handling as much as during high velocities, where the aggressiveness of the maneuver is significantly higher.

When comparing the controllers with the highest RMSEs of the states, MPC3 performs better at lower velocities, whereas MPCC1 has better mean relative tracking at higher velocities. The mean and maximum errors are lower for all controllers for lower desired velocities, which is confirmed by the similarities in trajectories in Fig. 10a. The variation in mean and maximum errors increases for higher desired velocities, resulting in more deviating trajectories in Fig. 10b. In both figures, it can be observed that MPCC7 has the best positional tracking with respect to the reference trajectory.

In Fig. 9, the mean relative tracking errors decrease as approximation complexity increases when comparing the same frameworks. The exception is for a desired velocity of $v_x = 20$m/s, where MPCC1 and MPCC7 show similar tracking performance. In terms of both mean and maximum relative errors, MPC7 and MPCC7 show similar performance.

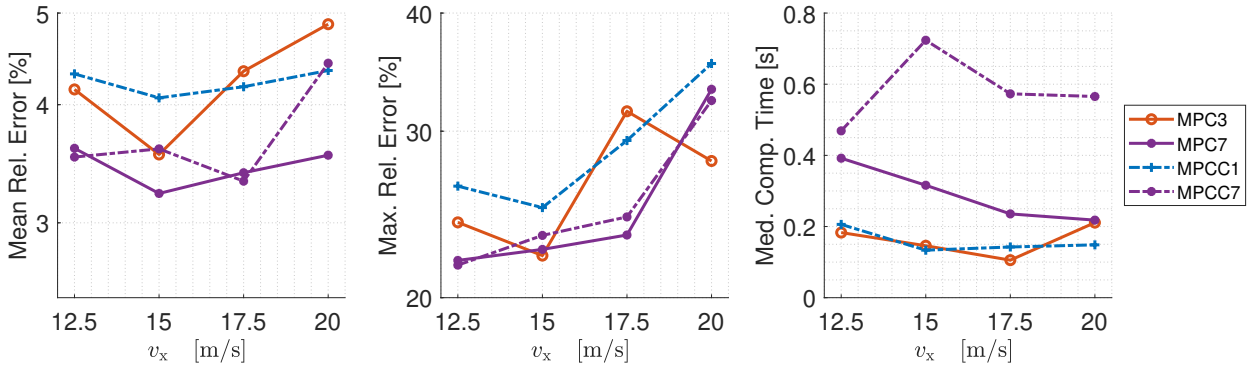

Fig. 9: Scenario 3: Tracking and computational performance of the best and the worst hybrid controllers.

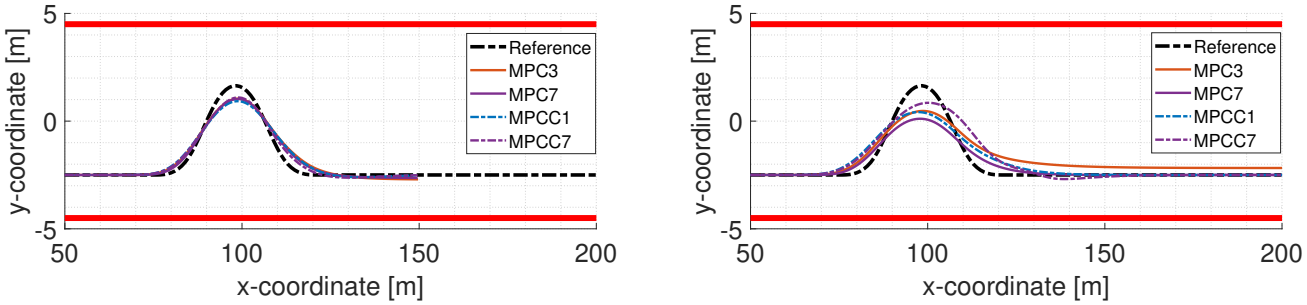

(a) $v_x = 12.5$m/s. (b) $v_x = 20.0$m/s.

Fig. 10: Scenario 3: DLC maneuvers of best and worst controllers for two desired velocities.

E. Scenario 4: Feasibility of Optimal Solution

For this scenario, all controllers are evaluated by assessing the limits of feasible control for varying desired velocities at low road friction. The prediction horizon is fixed for $N_p = 5$, and the controllers are simulated for different desired velocities in the range of $v_{x,des} \in \{12.5, 15.0, 17.5, 20.0\}$m/s and friction coefficients in the range of $\mu \in \{0.5, 0.6, 0.7\}$.

In Fig. 11, the feasible control limits for all controllers are illustrated, and the feasibility results of all controllers are summarized in Table V. At $\mu = 0.5$, MPC1 exhibits the highest number of infeasibilities among MPC controllers. Furthermore, MPC3 is best able to resist infeasibilities as its limit of control is at 17 m/s, which tops all other MPC controllers at that friction coefficient. MPC3 has the highest percentage of feasible results, as can be found in Table V. The results show that the higher the approximation complexity, the lower the feasible results and the higher the risk for practical infeasibilities. Among MPCC controllers, all feasible results are practically viable, with MPCC3 showing the highest control limit of 16.5m/s and the most feasible outcomes. For the other MPCC controllers, the limit of feasible control is lower. The MPC controllers have 71.15% feasible results, of which 51.35% is practically viable. MPCC only has 29.41% feasible results, indicating that for lower friction coefficients, MPCC is less robust to infeasibilities.

For $\mu = 0.6$, the feasibility of all controllers increases while the practical infeasibility decreases. MPC has 86.54% feasible results, of which 80% are practically viable, whereas MPCC only has 42.31% feasible results.

There are no practically infeasible results for the highest road friction coefficient of $\mu = 0.7$. Moreover, the feasibility again increases for all controllers. MPC1 has a limit of feasible control at 18 m/s, whereas the other MPC controllers are feasible for the entire velocity range. MPCC5 suffers from the most infeasible results of all MPCC controllers. MPC has 92.31% feasible results, and MPCC has 88.46%, indicating that the feasibility for MPC controllers is higher.

TABLE V: Scenario 4: Feasibility and practical feasibility of all controllers for different road friction coefficients.

	Feasibility (in practice) [%]					
	$\mu = 0.5$		$\mu = 0.6$		$\mu = 0.7$	
MPC1	23.08	(100)	53.85	(100)	69.23	(100)
MPC3	92.31	(58.33)	100	(76.92)	100	(100)
MPC5	85.62	(45.45)	92.31	(83.33)	100	(100)
MPC7	85.62	(36.36)	100	(69.23)	100	(100)
MPCC1	38.46	(100)	69.23	(100)	92.31	(100)
MPCC3	46.15	(100)	61.54	(100)	92.31	(100)
MPCC5	23.08	(100)	53.85	(100)	69.23	(100)
MPCC7	7.69	(100)	46.15	(100)	100	(100)

F. Computational Performance

For Scenario 1 visualized in Fig. 5, it can be observed that increasing the approximation complexity level and the framework complexity increases the computational demand. MPC3 shows the best computational performance, while MPCC7 shows the worst. At the same time, MPC7 and MPCC3 show computation times that are similar. Therefore, the MPC controllers have lower median computation times than the MPCC

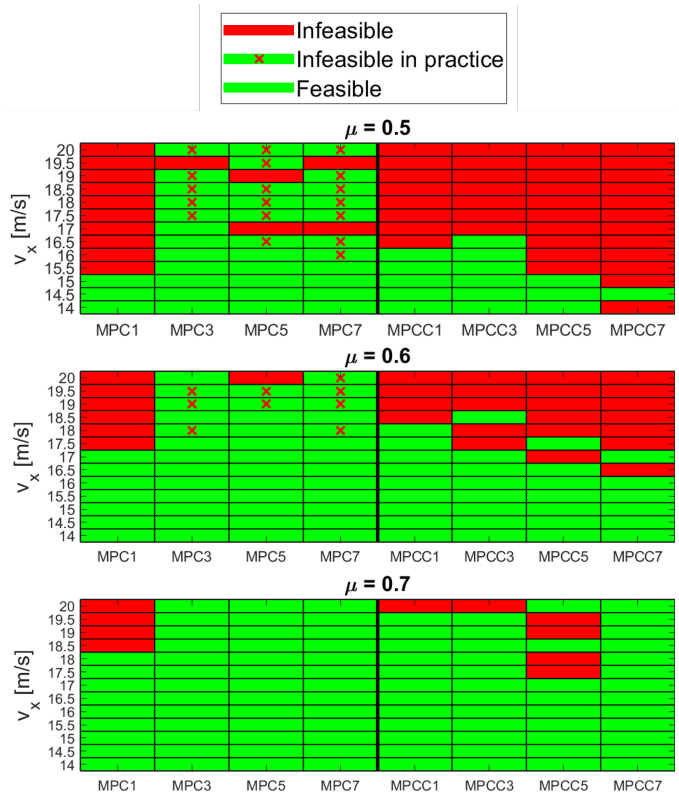

Fig. 11: Scenario 4: Limits of feasibility control for varying velocities and friction coefficients. The first two classes of infeasibility are solution infeasibility and time-limited infeasibility, which are indicated by a red box. The third class of infeasibility is practical infeasibility, which is indicated by a green box with a red cross as it does provide a feasible solution, but this solution is not feasible in practice. A green box indicates the feasible solutions.

controllers. Similar results can be observed for Scenario 2 and 3 in Fig. 7 and 9, where varying friction coefficients and velocities show no clear relation to the computation times. Combining and comparing the first three scenarios in Fig. 12 highlights the computational efficiency of the hybrid MPC controllers over the hybrid MPCC controllers. In every scenario, MPCC controllers consistently exhibit higher median computation times than MPC controllers and display greater variability in their computation times. This variability, indicated by a larger interquartile range (IQR) and a wider range of computation times, is particularly evident in scenarios with varying curvature where the median computation time of MPCC controllers is twice the computation time of MPC controllers (0.1535s versus 0.3037s). Similar results are found for scenarios with varying friction coefficients and desired velocities, where the IQR is narrower but still larger than that of MPC controllers. The increased complexity of MPCC controllers with respect to the MPC controllers contributes to this variability. The presence of higher whiskers for the MPCC controllers indicates that there are cases where the computation time can be substantially higher than the typical range. The median computation times, IQRs, and whiskers of the box

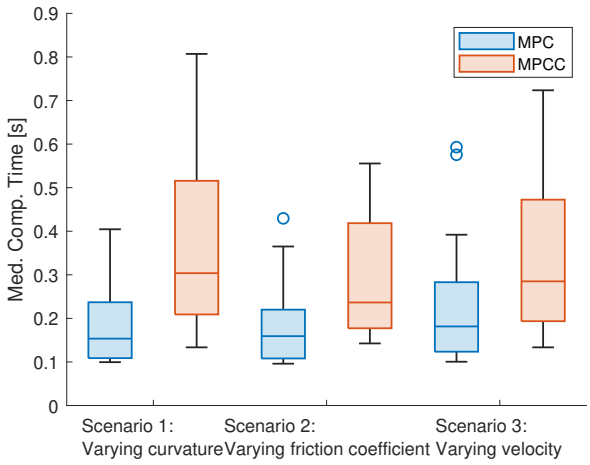

Fig. 12: Median computation time for different scenarios.

plots for the MPC controllers remain relatively consistent across scenarios. This consistency indicates that the MPC controllers are robust and effective across varying operating conditions and scenarios, whereas the MPCC controllers come with a higher and more variable computational cost.

VII. Discussion

In this section, the key findings are discussed, and a generalized framework is proposed. Thereafter, the limitations of this work are highlighted, and based on that, future research suggestions are made.

A. Impact of Prediction Horizon

The computational performance of hybrid MPC controllers during the DLC maneuver is analyzed for different prediction horizons, revealing a trade-off between model complexity and tracking accuracy. As Fig. 4 shows, the MPC controllers exceed the performance of the MPCC ones in terms of accuracy as well as computation speed. In order to provide a fair comparison between both control structures, the same prediction horizon needs to be employed that has satisfactory performance in both tracking and computation demand for both frameworks. The most suitable prediction horizon for tracking, regarding acceptable accuracy for lower computation times, is 5 or 6; for these horizons, both the relative errors and the median computation time are low for all controllers. Given that an increase in prediction horizon from 5 to 6 results in a significant increase in computation time while tracking performance across all controllers remains in the same region, it is chosen to employ a prediction horizon of $N_\mathrm{p} = 5$ for the scenarios. Choosing a prediction horizon of $N_\mathrm{p} = 5$ does mean that the prediction horizon length is only 1s, which impacts the tracking accuracy of the controllers.

B. Robustness and Variability

In Scenario 1, both the friction coefficient and velocity align with the values utilized in the approximations. Therefore, this scenario specifically highlights the controllers' ability to

track different levels of curvature. Fig. 5 demonstrates that increased model complexity directly implies more accurate tracking due to the more accurate representation of the lateral tire force models. MPC outperforms MPCC counterparts in tracking performance, which is especially evident as trajectory curvature increases, highlighting MPC's robustness against changes in reference trajectories. However, it was expected that MPCC would outperform MPC in terms of tracking, as found in literature [12]. The deviation in results can be explained by the ability of MPC to deploy a more efficient tracking strategy within the same short prediction horizon, in contrast to the more complex MPCC formulation.

In Fig. 7, higher approximation complexity generally correlates with improved tracking performance during friction uncertainty, although exceptions are observed at $\mu = 0.9$ for MPC7 and MPCC7, indicating nuanced dependencies. Increased model complexity enhances robustness against friction uncertainty, although both MPC and MPCC frameworks exhibit similar overall tracking performance. MPCC shows better positional tracking performance in Fig. 8 for low and high friction coefficients, indicating higher robustness against friction uncertainties, as also shown in the relative errors in Fig. 7. This is because MPCC can more effectively enforce and respect the constraints related to the vehicle's position and velocity, especially in low and high friction conditions.

Fig. 9 reveals a trend of decreasing mean relative errors with increased approximation complexity within each framework, except for MPCC1 and MPCC7 at $v_{\mathrm{x}} = 20$m/s. Higher desired velocities lead to significantly higher tracking errors across all controllers due to the quadratic dependency of drag force on velocity. In Fig. 10, MPCC7 demonstrates similar positional tracking performance compared to MPC7 under varying velocities, except at $v_{\mathrm{x}} = 20$m/s, again underscoring the tracking capabilities of MPC.

Analysis in Fig. 11 shows varying performance trends across different road friction coefficients. MPC1 exhibits the lowest feasibility at $\mu = 0.5$ due to a large number of infeasibilities, while MPC3 shows the highest resistance. The infeasibilities of MPC1 can be explained by the oversimplification of the tire model, which results in the inability of the controller to find feasible results due to the large deviation between the plant and the prediction model. MPC3 is significantly better than the others due to the simple yet effective representation of the tire model, which also explains the large percentage of practically infeasible results. Feasibility improves at $\mu = 0.6$ and $\mu = 0.7$ for all controllers, with MPC consistently outperforming MPCC in overall feasibility percentages given in Table V, indicating greater robustness against infeasibility challenges. However, MPC carries a risk of practically infeasible results compared to MPCC. This difference is related to the cost function of the frameworks as MPC might solve more problems feasibly by allowing slight violations or by using a less strict cost function, but this can lead to practically infeasible solutions, like oscillations or control actions that are not smooth or practical in a real-world scenario. MPCC often integrates constraints directly into the optimization problem, focusing on the reference trajectory and strict adherence to constraints. This means MPCC results are either feasible or clearly infeasible, with little room for impractical solutions as the results clearly show.

C. Interpretation of Computational Performance

Computational demands were compared across scenarios varying in curvature, friction coefficients, and desired velocities, revealing that MPC controllers consistently demonstrated superior computational efficiency compared to MPCC controllers, as was confirmed by Fig. 12. This observation aligns with previous findings [10] and highlights MPC controllers' ability to achieve lower median computation times and reduced variability, as indicated by narrower interquartile ranges and shorter whiskers. The lower computation time of MPC controllers is directly attributed to differences in the formulation of their cost functions compared to the more complex adjustments in MPCC, which builds upon the MPC framework.

Furthermore, an increase in computational demand was observed with increased hybrid model complexity. This trend reflects the anticipated greater computational resources required for more intricate representations in higher-level model approximations and frameworks. The observed increase in computational demand due to increased complexity in approximations and frameworks underscores the trade-off between model complexity and computational efficiency.

D. Generalized Framework

The proposed hybridization framework can be implemented in AV applications in emergency evasive maneuvers to improve computational efficiency and tracking performance. Based on the discussed simulation results for different scenarios across all controllers, the following guidelines need to be considered:

1) The general rule of thumb for guaranteeing high tracking performance is to increase the hybridization complexity. It has been shown over a variety of scenarios that high-complexity approximations have superior tracking performance over low-complexity approximations. However, low complexity approximations offer the benefit of low computational demand. Therefore, there is no single solution for this trade-off in computational demand versus tracking performance. Instead, the level of hybridization complexity is highly dependent on the scenario, which should be taken into account. Given a highly aggressive scenario, the controller requires a hybridized model that accurately describes the nonlinear model such that the approximation errors are minimized. However, a lower complexity approximation should be chosen if a sub-optimal solution is preferred over high computational demand. Similar choices should be made in scenarios with model uncertainty by considering the aforementioned trade-off. Lower complexity does provide more robustness against infeasibilities, especially for low friction coefficients. The range of 1 to 7 local modes is already wide enough, and employing more local modes will not improve the tracking performance significantly. However, it will impact the computational demand.

2) For scenarios where aggressive maneuvers are considered while no uncertainty in the model is present, MPC controllers offer superior performance to MPCC in tracking as well as computational demand. Increasing the aggressiveness of the scenario increases the need for fast control, where MPC outperforms the MPCC controllers. Moreover, MPC is able to exploit the vehicle model by performing similar scenarios with higher lateral accelerations while decreasing the relative tracking errors, indicating that control is less conservative than MPCC. However, if specific limits are given to the lateral accelerations, MPCC can offer similar performance, albeit at the expense of computational demand.
3) When considering scenarios with uncertainties in the prediction model, MPCC offers more robustness in terms of tracking performance. Although relative errors are similar with respect to MPC for high levels of complexity, the MPCC controllers have better trajectory tracking results. For these scenarios, MPC controllers offer more robustness against infeasibilities. Although MPC controllers do suffer from practical infeasibilities with respect to the MPCC controllers, MPC has higher feasibility in practice for all low friction scenarios, indicating higher limits of control. The choice between MPC and MPCC in these scenarios depends on the goal of the controller. If high tracking accuracy is preferred over computational demand and feasibility, then MPCC should be chosen. If the emphasis is on providing feasible results at the highest limits of control while tracking a second priority, MPC is able to do so while guaranteeing lower computational demands.

Employing the guidelines outlined above, the suitable trade-off in model complexity and framework selection can be specifically tailored to different applications across diverse AV control scenarios. This adaptive approach ensures optimal trade-offs between computational efficiency and control precision, which is vital for control in complex, high-speed emergency maneuvers.

E. Limitations

The main limitation of the proposed controllers is the parametric approximations of the hybridizations. This approach does not account for changes in lateral tire model characteristics due to friction, longitudinal force, or velocity variations. As a result, the effectiveness of these hybrid models in dynamic and variable driving conditions may be constrained. Additionally, the approximation assumes a fixed velocity for the drag force, which may not accurately represent real-world driving scenarios and could lead to discrepancies between the prediction and the plant model.

The use of a low prediction horizon and large step size contributes to less accurate vehicle control and trajectory tracking. This limitation is evident in the DLC maneuver, which is not tracked accurately, highlighting the need for improvements in this area. Increasing the horizon should theoretically improve tracking. However, at this speed, the step size is actually too large to guarantee proper tracking, even for a high prediction horizon. The real solution would be to use a smaller step size while increasing the prediction horizon. For example, a step size of 0.05s and $N_\mathrm{p} = 20$ would theoretically provide the same 1s prediction horizon but significantly more accuracy. However, the current solver and the current model are unsuitable for scaling up this way due to computational complications.

Moreover, increasing the complexity of the control approach significantly impacts computation time. This rise in complexity can become so severe that it limits the ability to extend the prediction horizon. Consequently, the investigation in scenarios requiring longer prediction horizons may be limited, underscoring the trade-off between model complexity and computational feasibility. Repeating this analysis with different N_p values could provide a better understanding and lead to more conclusive observations.

Another significant limitation is the computational demand, which exceeds real-time feasibility limits. The controllers' high computational requirements have not been thoroughly tested for real-time feasibility, indicating that the controllers may not yet be practical for real-time applications without further optimization and testing.

Finally, the controllers lack further tests for real-time validation with higher-fidelity plant models. High-fidelity models can provide more accurate simulations of vehicle dynamics, which are crucial for validating control strategies in realistic conditions. The absence of such tests suggests that the current results might not fully capture the complexities of real-world vehicle control.

F. Future Work

The recommendations for future work are (i) to approximate the lateral tire forces by considering varying road friction coefficients; (ii) to increase the prediction horizon and decrease the step size for the simulations to improve tracking results; (iii) to add object avoidance to the tracking problem; (iv) to increase the fidelity of the nonlinear plant model and perform simulations to evaluate real-time performance; (v) to create an MPC framework with MPCC as a backup for robustness to practical infeasibilities.

VIII. Conclusion

This paper presented a comparative analysis of hybridized model predictive controllers for collision avoidance during emergency evasive maneuvers, focusing on the effect of hybridization and model complexity on computational demand and tracking performance. It highlighted the nuanced relationship between model complexity, tracking performance, feasibility, and computational efficiency in AV control systems, providing valuable insights for optimizing control strategies in variable driving scenarios by presenting general guidelines. The following conclusions can be drawn regarding the impact of model complexity and the comparative performance of MPC and MPCC controllers:

- Increasing model complexity generally enhances tracking performance while increasing computational demand, as observed in all scenarios (Fig. 5, Fig. 7, Fig. 9).

Controllers with higher complexity, such as MPC7 and MPCC7, exhibit lower relative tracking errors across different scenarios but result in higher computation times, confirming the aforementioned trade-off.

- Higher framework complexity leads to increased computational demand (Fig. 12). MPC controllers consistently demonstrate lower median computation times compared to MPCC controllers across all scenarios, indicating their computational efficiency. For example, in Scenario 1, the median computation time of MPCC is twice the computation time of MPC controllers (0.1535s versus 0.3037s).
- MPC controllers provide more robust tracking performance in Scenario 1 (Fig. 5). They consistently show lower mean and maximum relative errors with respect to MPCC controllers, which is especially evident at higher complexity levels.
- MPC and MPCC controllers offer similar robustness to model uncertainty considering the same model complexity in Scenario 2 and 3 (Fig. 7, Fig. 9).
- MPC controllers exhibit higher robustness against infeasible results (Fig. 11). For instance, at low friction coefficients (e.g., $\mu = 0.5$), MPC has 71.15% feasible results, whereas MPCC only has 29.41%. However, MPC controllers do suffer from practical infeasibilities, whereas MPCC controllers do not (Table V).

Acknowledgments

The author would like to thank T. van den Boom, B. Shyrokau, A. Bertipaglia, and L. Gharavi for their supervision and critical insights and O. Siebinga for his useful feedback on this work.

References

[1] P. Stano, U. Montanaro, D. Tavernini, M. Tufo, G. Fiengo, L. Novella, and A. Sorniotti, "Model Predictive Path Tracking Control for Automated Road Vehicles: A Review," *Annual Reviews in Control*, 12 2022.

[2] A. Sorniotti, P. Barber, and S. De Pinto, "Path Tracking for Automated Driving: A Tutorial on Control System Formulations and Ongoing Research," *Automated Driving: Safer and More Efficient Future Driving*, pp. 71–140, 1 2016.

[3] N. H. Amer, H. Zamzuri, K. Hudha, and Z. A. Kadir, "Modelling and Control Strategies in Path Tracking Control for Autonomous Ground Vehicles: A Review of State of the Art and Challenges," *Journal of Intelligent and Robotic Systems: Theory and Applications*, vol. 86, no. 2, pp. 225–254, 5 2017.

[4] D. Lam, C. Manzie, and M. C. Good, "Model Predictive Contouring Control," *Proceedings of the IEEE Conference on Decision and Control*, pp. 6137–6142, 2010.

[5] A. Rupenyan, M. Khosravi, and J. Lygeros, "Performance-based Trajectory Optimization for Path Following Control Using Bayesian Optimization," *Proceedings of the IEEE Conference on Decision and Control*, vol. 2021-December, pp. 2116–2121, 2021.

[6] B. Brito, B. Floor, L. Ferranti, and J. Alonso-Mora, "Model Predictive Contouring Control for Collision Avoidance in Unstructured Dynamic Environments," *IEEE Robotics and Automation Letters*, vol. 4, no. 4, pp. 4459–4466, 10 2019.

[7] L. Ferranti, B. Brito, E. Pool, Y. Zheng, R. M. Ensing, R. Happee, B. Shyrokau, J. F. Kooij, J. Alonso-Mora, and D. M. Gavrila, "SafeVRU: A Research Platform for the Interaction of Self-driving Vehicles with Vulnerable Road Users," *IEEE Intelligent Vehicles Symposium, Proceedings*, vol. 2019-June, pp. 1660–1666, 6 2019.

[8] W. Schwarting, J. Alonso-Mora, L. Paull, S. Karaman, and D. Rus, "Safe Nonlinear Trajectory Generation for Parallel Autonomy with a Dynamic Vehicle Model," *IEEE Transactions on Intelligent Transportation Systems*, vol. 19, no. 9, pp. 2994–3008, 9 2018.

[9] A. Liniger, A. Domahidi, and M. Morari, "Optimization-based Autonomous Racing of 1:43 Scale RC Cars," *Optimal Control Applications and Methods*, vol. 36, no. 5, pp. 628–647, 9 2015.

[10] A. Romero, S. Sun, P. Foehn, and D. Scaramuzza, "Model Predictive Contouring Control for Time-Optimal Quadrotor Flight," *IEEE Transactions on Robotics*, vol. 38, no. 6, pp. 3340–3356, 12 2022.

[11] J. Ji, X. Zhou, C. Xu, and F. Gao, "CMPCC: Corridor-Based Model Predictive Contouring Control for Aggressive Drone Flight," *Springer Proceedings in Advanced Robotics*, vol. 19, pp. 37–46, 2021.

[12] A. Bertipaglia, M. Alirezaei, R. Happee, and B. Shyrokau, "Model Predictive Contouring Control for Vehicle Obstacle Avoidance at the Limit of Handling," *28th IAVSD International Symposium on Dynamics of Vehicles on Roads and Tracks*, 8 2023.

[13] M. Metzler, D. Tavernini, P. Gruber, and A. Sorniotti, "On Prediction Model Fidelity in Explicit Nonlinear Model Predictive Vehicle Stability Control," *IEEE Transactions on Control Systems Technology*, vol. 29, no. 5, pp. 1964–1980, 9 2021.

[14] J. Subosits and J. C. Gerdes, "Impacts of Model Midelity on Trajectory Optimization for Autonomous Vehicles in Extreme Maneuvers," *IEEE Transactions on Intelligent Vehicles*, 2021.

[15] J. Liu, P. Jayakumar, J. L. Stein, and T. Ersal, "A Study on Model Fidelity for Model Predictive Control-based Obstacle Avoidance in High-speed Autonomous Ground Vehicles," *Vehicle System Dynamics*, vol. 54, no. 11, pp. 1629–1650, 11 2016.

[16] V. A. Laurense and J. Christian Gerdes, "Long-Horizon Vehicle Motion Planning and Control through Serially Cascaded Model Complexity," *IEEE Transactions on Control Systems Technology*, vol. 30, no. 1, pp. 166–179, 1 2022.

[17] N. Chowdhri, L. Ferranti, F. S. Iribarren, and B. Shyrokau, "Integrated Nonlinear Model Predictive Control for Automated Driving," *Control Engineering Practice*, vol. 106, p. 104654, 1 2021.

[18] P. Falcone, F. Borrelli, J. Asgari, H. E. Tseng, and D. Hrovat, "Predictive Active Steering Control for Autonomous Vehicle Systems," *IEEE Transactions on Control Systems Technology*, vol. 15, no. 3, pp. 566–580, 5 2007.

[19] J. Funke, M. Brown, S. M. Erlien, and J. C. Gerdes, "Collision Avoidance and Stabilization for Autonomous Vehicles in Emergency Scenarios," *IEEE Transactions on Control Systems Technology*, vol. 25, no. 4, pp. 1204–1216, 7 2017.

[20] W. Y. Choi, D. J. Kim, C. M. Kang, S. H. Lee, and C. C. Chung, "Autonomous Vehicle Lateral Maneuvering by Approximate Explicit Predictive Control," *Proceedings of the American Control Conference*, vol. 2018-June, pp. 4739–4744, 8 2018.

[21] X. Sun, Y. Cai, S. Wang, X. Xu, and L. Chen, "Optimal Control of Intelligent Vehicle Longitudinal Dynamics via Hybrid Model Predictive Control," *Robotics and Autonomous Systems*, vol. 112, pp. 190–200, 2 2019.

[22] K. Liu, J. Gong, A. Kurt, H. Chen, and U. Ozguner, "Dynamic Modeling and Control of High-speed Automated Vehicles for Lane Change Maneuver," *IEEE Transactions on Intelligent Vehicles*, vol. 3, no. 3, pp. 329–339, 9 2018.

[23] T. Novi, A. Liniger, R. Capitani, and C. Annicchiarico, "Real-time Control for At-limit Handling Driving on a Predefined Path," *International Journal of Vehicle Mechanics and Mobility*, vol. 58, no. 7, pp. 1007–1036, 7 2019.

[24] Y. Li, J. Fan, Y. Liu, and X. Wang, "Path Planning and Path Tracking for Autonomous Vehicle Based on MPC with Adaptive Dual-Horizon-Parameters," *International Journal of Automotive Technology*, vol. 23, no. 5, pp. 1239–1253, 10 2022.

[25] M. Rokonuzzaman, N. Mohajer, S. Nahavandi, and S. Mohamed, "Model Predictive Control with Learned Vehicle Dynamics for Autonomous Vehicle Path Tracking," *IEEE Access*, vol. 9, pp. 128 233–128 249, 2021.

[26] E. Asarin, T. Dang, and A. Girard, "Hybridization Methods for the Analysis of Nonlinear Systems," *Acta Informatica*, vol. 43, no. 7, pp. 451–476, 2 2007.

[27] Q. Cui, R. Ding, C. Wei, and B. Zhou, "A Hierarchical Framework of Emergency Collision Avoidance amid Surrounding Vehicles in Highway Driving," *Control Engineering Practice*, vol. 109, p. 104751, 4 2021.

[28] X. He, Y. Liu, C. Lv, X. Ji, and Y. Liu, "Emergency Steering Control of Autonomous Vehicle for Collision Avoidance and Stabilisation," *Vehicle System Dynamics*, vol. 57, no. 8, pp. 1163–1187, 8 2018.

[29] Q. Cui, R. Ding, X. Wu, and B. Zhou, "A New Strategy for Rear-end Collision Avoidance via Autonomous Steering and Differential Braking in Highway Driving," *Vehicle System Dynamics*, vol. 58, no. 6, pp. 955–986, 6 2019.

[30] K. Zhang, J. Sprinkle, and R. G. Sanfelice, "Computationally Aware Control of Autonomous Vehicles: A Hybrid Model Predictive Control Approach," *Autonomous Robots*, vol. 39, no. 4, pp. 503–517, 12 2015.
[31] F. Borrelli, P. Falcone, T. Keviczky, J. Asgari, and D. Hrovat, "MPC-based Approach to Active Steering for Autonomous Vehicle Systems," *International Journal of Vehicle Autonomous Systems*, vol. 3, no. 2-4, pp. 265–291, 2005.
[32] T. Besselmann and M. Morari, "Hybrid Parameter-varying Model Predictive Control for Autonomous Vehicle Steering," *European Journal of Control*, vol. 14, no. 5, pp. 418–431, 1 2008.
[33] D. Bernardini, S. Di Cairano, A. Bemporad, and H. E. Tseng, "Drive-by-wire Vehicle Stabilization and Yaw Regulation: A Hybrid Model Predictive Control Design," *Proceedings of the IEEE Conference on Decision and Control*, pp. 7621–7626, 2009.
[34] W. Liu, J. Zhang, D. Sun, and H. Hu, "Piecewise Affine Based Model Predictive Trajectory Tracking Control with Stability Guarantees for Autonomous Ground Vehicles," *2022 China Automation Congress (CAC)*, pp. 3664–3670, 3 2023.
[35] T. Fu, H. Jing, H. Zhou, and Z. Liu, "Mixed Logical Dynamic based Path-Tracking Model Predictive Control for Autonomous Vehicles," *IEEE Conference on Intelligent Transportation Systems, Proceedings (ITSC)*, pp. 189–196, 2022.
[36] L. Gharavi, B. De Schutter, and S. Baldi, "Efficient MPC for Emergency Evasive Maneuvers, Part I: Hybridization of the Nonlinear Problem," *IEEE Transactions on Intelligent Vehicles*, vol. 0, no. 0, 10 2023.
[37] ——, "Efficient MPC for Emergency Evasive Maneuvers, Part II: Comparative Assessment for Hybrid Control," *IEEE Transactions on Intelligent Vehicles*, vol. 00, no. 0, 2023.
[38] L. Gharavi, A. Dabiri, J. Verkuijlen, B. De Schutter, S. Baldi, and S. Member, "Proactive Emergency Collision Avoidance for Automated Driving in Highway Scenarios," *IEEE Transactions on Control Systems Technology, Special Issue*, 10 2023.
[39] A. Szucs, M. Kvasnica, and M. Fikar, "Optimal Piecewise Affine Approximations of Nonlinear Functions Obtained from Measurements," *IFAC Proceedings Volumes*, vol. 45, no. 9, pp. 160–165, 1 2012.
[40] Y. Koren and C. Lo, "Advanced Controllers for Feed Drives," *CIRP Annals*, vol. 41, no. 2, pp. 689–698, 1992.
[41] H. Pacejka, *Tire and Vehicle Dynamics*, 2nd ed. Butterworth-Heinemann, 12 2005.
[42] Gurobi Optimization LLC, "Gurobi Optimizer Reference Manual," 2024.

3
Discussion

This chapter elaborates on the proposed generalized framework and discusses the advantages, limitations, societal impact, and future work suggestions related to the proposed hybridization framework. The comparison benchmark provides valuable insights into hybridization complexity and hybrid model predictive approaches through comparative analysis but faces limitations in computational demand and real-world applicability. The societal implications of these advancements are explored, and recommendations for future research are outlined to address the benchmark and framework limitations and refine control strategies for safer and more efficient AVs further.

3.1. Generalized Framework

The proposed hybridization framework presents a versatile approach for enhancing computational efficiency and tracking performance in AV applications, particularly in emergency evasive maneuvers. To effectively implement this framework, several key considerations must be taken into account to ensure optimal performance across diverse scenarios.

3.1.1. Tailoring Hybridization Complexity to Scenario Requirements

A fundamental aspect to address is the complexity of hybridization, which directly influences tracking performance and computational demand. Generally, augmenting hybridization complexity enhances tracking accuracy by capturing intricate nonlinear dynamics more effectively. However, this comes with increased computational overhead. In scenarios demanding precise trajectory tracking, such as unpredictable road conditions, opting for high-complexity hybridized models is paramount to minimize approximation errors with respect to the reference trajectory. Conversely, low-complexity hybridizations may be more beneficial in scenarios such as sudden obstacle avoidance due to lower precision requirements or constrained computational resources. Furthermore, lower complexity models offer enhanced robustness against infeasibilities, particularly in scenarios characterized by low road friction coefficients.

3.1.2. Adapting to Maneuver Characteristics

Another crucial consideration is adapting the hybridization framework to the specific characteristics of the maneuver scenario. Different maneuvers may necessitate varying levels of tracking accuracy and computational efficiency. For instance, aggressive maneuvers devoid of uncertainties typically require precise trajectory tracking, favoring high-complexity hybridized models. Here, MPC controllers showcase superior performance in both tracking accuracy and computational efficiency compared to MPCC. Conversely, in scenarios featuring uncertainties in the prediction model, such as variations in road friction or environmental conditions, MPCC emerges as a more robust choice for trajectory tracking. Despite potential challenges with infeasibilities, MPCC controllers exhibit superior performance in uncertain scenarios, yielding enhanced trajectory tracking results compared to MPC. MPC controllers could be employed if robustness to feasibilities is of importance.

3.1.3. Aligning Framework Selection with Control Objectives

The selection between MPC and MPCC should align with the controller's specific objectives. MPCC is favored for scenarios demanding high tracking accuracy in the presence of uncertainties, while MPC is more suitable for scenarios emphasizing computational efficiency. By carefully assessing the characteristics of each maneuver scenario and the desired trade-off between tracking accuracy and computational demand, practitioners can effectively tailor the hybridization framework to achieve optimal performance in AV control.

Adhering to these guidelines allows for the customization of the appropriate trade-off in model complexity and framework selection for different applications in AV control scenarios. This adaptive approach ensures an optimal balance between computational efficiency and control precision, crucial for effective control in complex, high-speed emergency maneuvers.

3.2. Advantages of the Comparison Benchmark

The comparison benchmark provides valuable insights into the complexities of hybridization. By exploring various levels of hybridization complexity, the benchmark helps in understanding how different approaches impact the performance of vehicle control systems during emergency evasive maneuvers. This understanding is crucial for optimizing the balance between computational efficiency and control accuracy, ensuring that the most effective solutions are identified for real-world applications.

In addition to shedding light on hybridization complexity, the comparison benchmark offers detailed insights into hybrid MPCC. It examines the performance of MPCC when integrated with hybrid models, highlighting the strengths and weaknesses of this approach. This analysis is particularly important for researchers and practitioners aiming to develop robust and efficient control strategies for AVs.

The comparison benchmark stands out for its clear comparative analysis. Systematic comparisons of different hybridized models and their corresponding control formulations comprehensively evaluate their performance. This clarity helps in identifying the most suitable models for various driving scenarios, facilitating the development of more effective control systems.

The benchmark also underscores the correlation between increased complexity and computational demand. It demonstrates how increasing the complexity of the approximation can enhance tracking accuracy but at the cost of higher computational demand. As the complexity of the control approach rises, so does the computational burden. This finding highlights the importance of optimizing control strategies to achieve the best possible performance without overwhelming the computational capabilities of the vehicle's control system.

The comparison benchmark provides these insights and serves as a valuable tool for advancing the field of vehicle control systems. It can help researchers and developers navigate the complexities of hybridization, MPCC, and computational trade-offs, ultimately contributing to the development of safer and more efficient AVs.

3.3. Limitations of the Comparison Benchmark

One key limitation of the comparison benchmark is that the hybridizations are approximated parametrically. This limitation means that the hybrid models do not account for changes in lateral tire model characteristics due to friction, longitudinal force, or velocity variations. As a result, the effectiveness of these hybrid models in dynamic and variable driving conditions may be constrained. Additionally, the benchmark assumes a fixed velocity for the drag force, which may not accurately represent real-world driving scenarios, which could lead to discrepancies between the prediction and the plant model.

The controller's low prediction horizon and large step size contribute to less accurate vehicle control and trajectory tracking. This means that the DLC is not executed properly, highlighting the need for improvements in this area. Additionally, increasing the complexity of the control approach significantly impacts computation time. This rise in complexity can become so severe that it limits the ability to

extend the prediction horizon. Consequently, the benchmark's investigation in scenarios requiring longer prediction horizons may be limited, underscoring the trade-off between model complexity and computational feasibility. Repeating this analysis with different N_p values could provide a better understanding and lead to more conclusive observations.

Another significant limitation is the computational demand, which exceeds the real-time feasibility limits. The controllers' high computational requirements have not been thoroughly tested for real-time feasibility. This gap indicates that the frameworks may not yet be practical for real-time applications without further optimization and testing.

Finally, the benchmark lacks further tests for real-time validation with higher-fidelity plant models. High-fidelity models can provide more accurate simulations of vehicle dynamics, which are crucial for validating control strategies in realistic conditions. The absence of such tests suggests that the benchmark's current results might not fully capture the complexities of real-world vehicle control.

3.4. Societal Impact

The advancements in hybridization complexity for AV control presented in this thesis have significant implications for society. Enhancing road safety is one of the most immediate and significant societal impacts of improved AV control. Emergency evasive maneuvers are critical in preventing accidents, particularly in high-risk scenarios such as sudden obstacle appearance or adverse weather conditions. By optimizing the hybridization complexity in model predictive frameworks, AVs have the potential to execute these maneuvers more accurately and reliably, reducing the likelihood of collisions and associated injuries or fatalities. This advancement directly supports the vision of mitigating the human error of the road. The ability of AVs to perform emergency maneuvers more effectively can also lead to improved traffic management. By avoiding accidents, which often cause significant traffic disruptions, AVs can help maintain smoother traffic flow.

The economic benefits of improved AV control are multifaceted. Reduced accident rates translate into lower costs for emergency response, healthcare, and vehicle repairs. Moreover, enhanced traffic management leads to reduced congestion, which can decrease fuel consumption and associated costs. For the automotive industry, developing and deploying vehicles with automated emergency control capabilities can provide a competitive edge, driving innovation and economic growth.

The advancements presented in this research have the potential to accelerate the adoption of AVs. Public trust in automated technology is crucial for its widespread acceptance. Demonstrating that AVs can handle emergency situations with high precision and reliability can increase consumer confidence. As AVs become more prevalent, the transportation landscape will shift towards increased automation, with potential benefits including reduced traffic congestion, lower emissions, and enhanced mobility for individuals unable to drive due to age or disability.

The research on hybridization complexity for AV control in emergency evasive maneuvers holds significant promise for societal advancement. By enhancing road safety and mitigating human errors on the road, improving traffic management, generating economic benefits, and promoting the adoption of autonomous vehicles, these technological advancements contribute to the creation of a safer and more efficient transportation system. As the field continues to evolve, ongoing research and collaboration among engineers, policymakers, and society at large will be essential to fully realize the benefits of AV technology.

3.5. Future Work Suggestions

The recommendations for future work based on this study include several key areas that could enhance the effectiveness and applicability of the hybridized controllers for emergency evasive maneuvers. One important direction is to approximate the lateral tire forces by considering varying road friction coefficients. This enhancement would improve the model's accuracy and reliability, allowing for more precise control in diverse road friction conditions by avoiding model uncertainty. By accounting for

different friction levels, the controllers can better handle the variability encountered in real-world driving scenarios, leading to safer and more robust performance.

Another direction of future research involves increasing the prediction horizon as well as decreasing the step size for simulations. These changes can significantly improve control precision by providing more detailed and accurate predictions of vehicle behavior over longer periods. This increased foresight allows the controller to make more informed decisions, enhancing its ability to effectively navigate complex and dynamic driving environments.

In addition to enhancing the control algorithms, adding object avoidance capabilities to the tracking problem is crucial for comprehensive safety measures. Current models primarily focus on maintaining a collision-free trajectory by tracking the reference itself; however, incorporating object avoidance would enable the vehicle to respond to obstacles, further reducing the risk of accidents and improving the control algorithm.

Other recommended areas for future work include increasing the fidelity of the nonlinear plant model and performing simulations in IPG CarMaker. High-fidelity models provide a more accurate representation of the vehicle dynamics, leading to better control performance. Advanced simulation platforms like IPG CarMaker allow for realistic testing and validation of the controllers under various scenarios, ensuring that they perform reliably in real-world conditions. This step is essential for transitioning from theoretical models to practical applications.

Lastly, developing an MPCC framework with MPC as a backup can enhance robustness against infeasibilities. In scenarios where the primary controller encounters issues, having a secondary control strategy with increased robustness to infeasibilities ensures that the vehicle can maintain safe operation. This dual-framework approach combines the strengths of both MPC and MPCC, providing a more resilient and adaptive control system. By integrating these advancements, the hybridization framework can be further refined to meet the demands of emergency evasive maneuvers in AVs, ensuring higher levels of safety and efficiency.

By focusing on these areas, future research can build on this study's findings to develop more robust, precise, and reliable controllers for AVs. These advancements will be critical for improving the overall safety and performance of AVs and fostering greater public trust and acceptance of this transformative technology.

4

Conclusion

The hybridization framework introduced in this research is a comprehensive approach to addressing model approximation problems in autonomous vehicle (AV) control systems, particularly for emergency evasive maneuvers. This framework begins with defining four hybridized models by approximating the lateral tire force models for both the front and the rear tires. These hybrid tire approximations are then integrated into both Model Predictive Control (MPC) and Model Predictive Control with Constraints (MPCC) frameworks, resulting in hybrid MPC and MPCC controllers with varying degrees of hybridization complexity. The subsequent analysis of these hybridized models and their corresponding MPC formulations offers a comparative benchmark that evaluates the computational demand and tracking performance. This comparison benchmark provides valuable insights into optimizing computational performance across diverse MPC applications by assessing different hybridization approaches.

The findings from this study indicate that the complexity of hybridization substantially influences the tracking performance and computational efficiency of the hybrid controllers. High-complexity models excel in tracking performance, capturing intricate nonlinear dynamics and delivering superior accuracy. However, this comes at the expense of increased computational demand. On the other hand, low-complexity models offer reduced computational demands but may compromise on tracking accuracy. This trade-off suggests that the level of hybridization complexity should be carefully tailored to meet the specific requirements of each scenario, balancing the need for precise control with computational feasibility. For instance, high-complexity models are better suited for scenarios requiring precise trajectory tracking in unpredictable road conditions, while low-complexity models are more appropriate for scenarios with lower precision requirements or constrained computational resources.

Throughout the study, MPC controllers consistently demonstrated lower median computation times compared to MPCC controllers across all tested scenarios, highlighting their computational efficiency. In some cases, the median computation time of MPCC was observed to be twice that of MPC controllers. This significant difference underscores the advantage of MPC controllers in terms of computational efficiency, making them a preferable choice for real-time applications where quick response times are critical. Additionally, MPC controllers exhibited more robust tracking performance in certain scenarios, showing lower mean and maximum relative errors compared to MPCC controllers, especially at higher complexity levels. This robustness in tracking performance further enhances their suitability for high-speed and dynamic driving scenarios.

When considering model uncertainty, both MPC and MPCC controllers demonstrated similar robustness, suggesting that either framework can effectively handle varying conditions. However, MPC controllers exhibited higher robustness against infeasible results, particularly at low friction coefficients. This robustness is crucial for ensuring reliable control under varying road conditions, enhancing the overall safety and performance of AV systems. Although MPC controllers suffered from practical infeasibilities that MPCC controllers did not encounter, their overall robustness and computational efficiency make them a strong candidate for real-time AV control applications.

Overall, this study provides essential guidelines for selecting and optimizing model predictive control frameworks in AV systems. The insights gained from this research can significantly inform the development of more effective and reliable automated driving systems, capable of handling the complexities of real-world driving scenarios. Balancing tracking accuracy and computational efficiency is key to advancing these control strategies, ensuring both safety and performance in high-speed automated driving.

A

Hybrid Approximations of Nonlinearities

This section details the hybridization of the nonlinear lateral tire models and other nonlinear elements of the single-track vehicle model. Employing 1-D and 2-D approximations, single-variable and bivariate terms can be approximated.

A.1. Lateral Tire Forces

Four hybrid approximations are constructed separately for the front and rear lateral tire models. A piecewise affine (PWA) approximation for the lateral tire force models is obtained using nonlinear optimization, as explained in chapter 2. For the approximations, it is assumed that the road friction, the longitudinal velocity, and the longitudinal force are fixed as follows:

$$\mu_\mathrm{f} = 0.8, \quad \mu_\mathrm{r} = 0.9, \quad v_\mathrm{x} = 17.5\mathrm{m/s}, \quad F_\mathrm{x} = 0\mathrm{N}. \tag{A.1}$$

The four hybrid approximations differ in the number of local modes that are used to describe the nonlinear tire force models, with configurations of 1, 3, 5, and 7 local modes being evaluated. Optimizations are performed to find local modes for both tire force equations for all configurations. Each of the local modes is bounded by a lower and an upper bound on the tire slip angle, and each local mode is described by a linear equation. The following PWA approximations describe the approximations of the front and rear lateral tire forces depending on the number of local modes n:

$$F_{\mathrm{y},i}(\alpha_i) = \begin{cases} a_{i,1}\alpha_i + c_{i,1} & \text{for} \quad \alpha_i \in [r_{i,0}, r_{i,1}] \\ \quad \vdots & \qquad\qquad\qquad\qquad \text{for } i \in \{\mathrm{f/r}\} \\ a_{i,n}\alpha_i + c_{i,n} & \text{for} \quad \alpha_i \in [r_{i,n-1}, r_{i,n}] \end{cases}$$

which depends on the tire slip angle α_j and the optimized variables a_i (the slope), c_i (the offset), and r_i (the breakpoints). Using MATLAB's `fmincon` function with the interior-point optimization algorithm and following the 1-D approximation procedure outlined by Szucs et al. [47], local modes for both tire force equations in all configurations were determined by optimizing slopes, offsets, and breakpoints. The resulting approximations for the front and the rear tire lateral forces are illustrated in Figure A.1. These approximations will be used for the hybrid prediction models in this study.

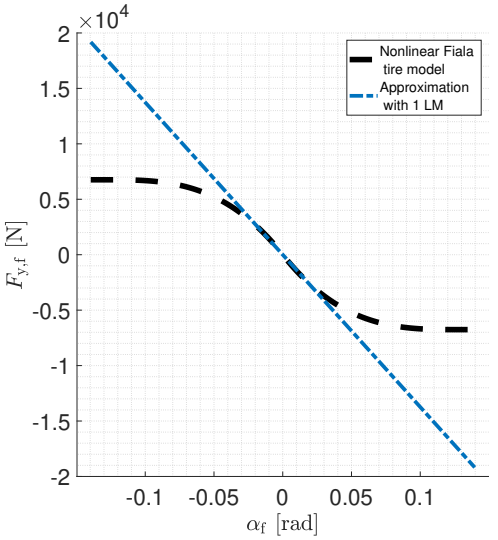

(a) PWA approximation of $F_{y,f}$ with 1 local mode.

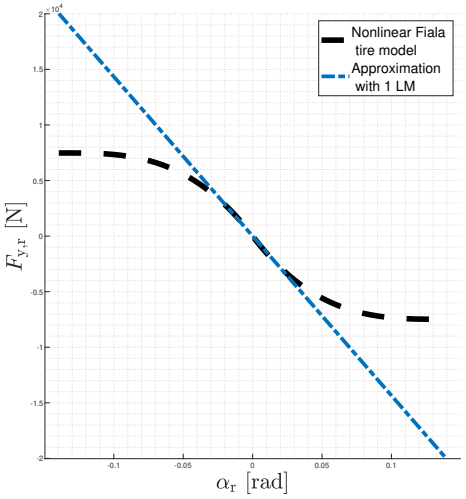

(b) PWA approximation of $F_{y,r}$ with 1 local mode.

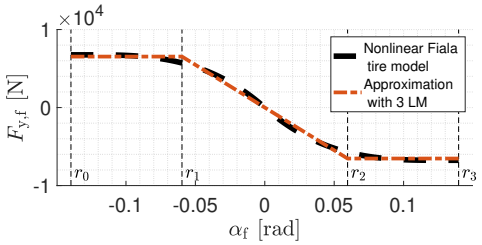

(c) PWA approximation of $F_{y,f}$ with 3 local modes.

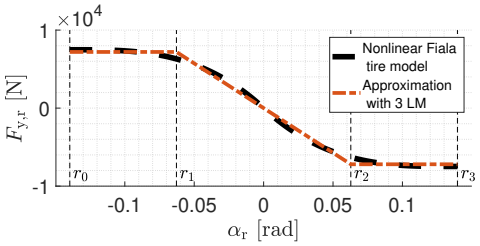

(d) PWA approximation of $F_{y,r}$ with 3 local modes.

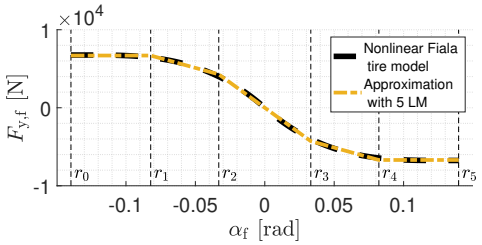

(e) PWA approximation of $F_{y,f}$ with 5 local modes.

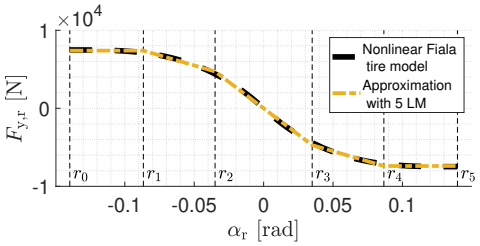

(f) PWA approximation of $F_{y,r}$ with 5 local modes.

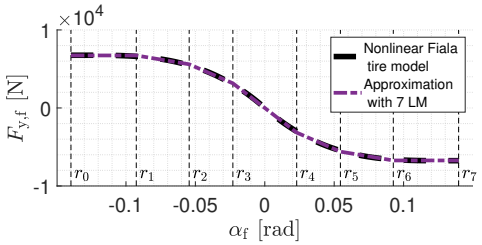

(g) PWA approximation of $F_{y,f}$ with 7 local modes.

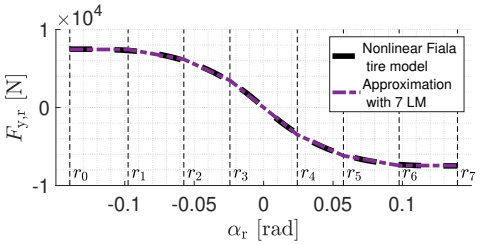

(h) PWA approximation of $F_{y,r}$ with 7 local modes.

Figure A.1: PWA approximations of the front and rear lateral tire forces with breakpoints r_i.

A.2. Trigonometric Functions

Similar to the lateral tire force approximations, the trigonometric non-linearities related to the vehicle model can also be hybridized by 1-D PWA approximations. The trigonometric functions all depend on the yaw angle and are visualized in Figure A.2.

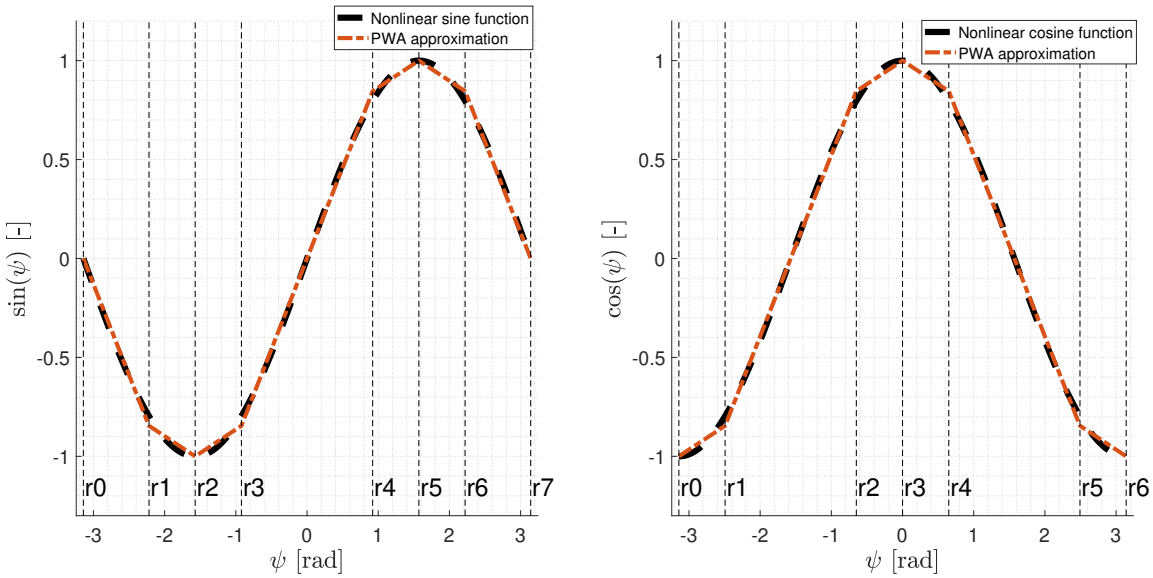

(a) PWA approximation of the sine function with 7 local modes.

(b) PWA approximation of the cos function with 6 local modes.

Figure A.2: PWA approximation of trigonometric nonlinearities with breakpoints r_i.

A.3. Bivariate Terms

The method of Kvasnica et al. [48] can be employed for the bivariate terms by approximating 2-D functions. This method will be briefly explained here. First and foremost, the realization that needs to be made is that a bivariate term can be rewritten as:

$$f(z_1, z_2) = z_1 z_2 = \frac{1}{4}\left(y_1^2 + y_2^2\right) \tag{A.2}$$

where

$$y_1 = (z_1 + z_2), \quad y_2 = (z_1 - z_2) \tag{A.3}$$

In order to make an accurate approximation of this bivariate term and to avoid the multiplication of two separate PWA approximations, the terms are divided according to Equation A.2 and A.3. Thereafter, the bounds of y_1 and y_2 are determined as follows:

$$\begin{aligned}
\underline{y}_1 &= \min\{f_1(z_1) + f_2(z_2) | [z_1, z_2]^T \in \mathcal{Z}\} \\
\overline{y}_1 &= \max\{f_1(z_1) + f_2(z_2) | [z_1, z_2]^T \in \mathcal{Z}\} \\
\underline{y}_2 &= \min\{f_1(z_1) - f_2(z_2) | [z_1, z_2]^T \in \mathcal{Z}\} \\
\overline{y}_2 &= \max\{f_1(z_1) - f_2(z_2) | [z_1, z_2]^T \in \mathcal{Z}\}
\end{aligned}$$

These bounds are used to describe the regions for which y^1 and y^2 will be approximated by again making use of 1-D approximation techniques with an appropriate number of local modes depending on the desired accuracy. In doing so, $f(z_1, z_2)$ is approximated by a 2-D hybrid function with a total number of local modes equal to the product of the number of local modes for each individual approximation. In Figure A.3, approximations of the bivariate terms related to the kinematics of the nonlinear vehicle model are visualized and compared to the original nonlinear representations.

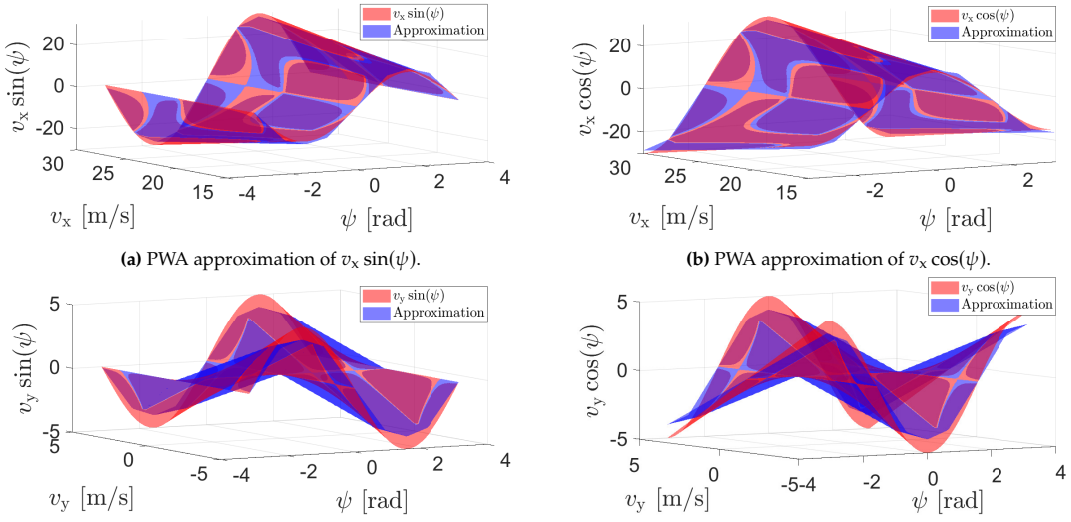

(a) PWA approximation of $v_x \sin(\psi)$.

(b) PWA approximation of $v_x \cos(\psi)$.

(c) PWA approximation of $v_y \sin(\psi)$.

(d) PWA approximation of $v_y \cos(\psi)$.

Figure A.3: PWA approximations of the bivariate terms.

A.4. Alternative Approach for Nonlinear Terms

This study will not employ the hybridization methods for approximating trigonometric functions and bivariate terms as explained in section A.2 and A.3. Instead, an alternative method using over- and under-approximations to create piecewise linear (PWL) approximations will be utilized to approximate nonlinear elements other than the lateral tire forces. This approach simplifies handling complex nonlinear functions by breaking them into manageable linear segments, where the ratio between the over- and under-approximations can be tuned accordingly. Additional tuning parameters for this method include the length and number of segments. The findings from the approximation of trigonometric functions and bivariate terms in section A.2 and A.3 will inform the choice of segment lengths and the number of segments, ensuring that the approximations are both precise and computationally feasible. By using PWL approximations, the characteristics of these non-linearities can be effectively captured while keeping the approximations tractable for real-time applications.

B

Open-Loop Validation

This section compares the hybrid models with the nonlinear model in open-loop simulations to validate the hybrid approximations of the lateral tire forces. To ensure driving up to the limits of handling, the sine-with-dwell test will be implemented as a maneuver. First, the sine-with-dwell maneuver will be explained, followed by the open-loop simulations.

B.1. Sine-with-Dwell Maneuver

The open-loop simulations validate the behavior of the hybrid models compared to the nonlinear model, ensuring its accuracy in representing the vehicle's dynamics, especially at handling limits. A standardized test known as the sine-with-dwell maneuver is employed to achieve this. This maneuver involves subjecting the vehicle to a trajectory similar to what might occur during evasive maneuvers by a human driver. In autonomous vehicle testing, the sine-with-dwell maneuver assesses dynamic performance and control capabilities under varying conditions. Engineers can evaluate a vehicle's performance under challenging conditions by carefully controlling parameters like frequency, dwell time, and amplitude. The maneuver allows trajectory tracking, stability, and response evaluation during dynamic maneuvers and stationary or low-speed scenarios. The test involves bringing the vehicle to a speed slightly above 80 km/h and allowing it to coast before a robotic system applies a sinusoidal steering input with specified characteristics. This input includes a frequency of 0.7 Hz and a dwell time of 0.5 seconds, which is crucial for evaluating the vehicle's response at critical points in the maneuver. The sine-with-dwell maneuver ensures driving up to the limits of handling, making this maneuver particularly suitable for validating different hybrid models with respect to the nonlinear model. For the open-loop simulations, the following characteristics are used:

- Discretization step size of 0.05 s
- A total simulation time of 10 s
- The steering angle itself is used as an input instead of the rate of the steering angle
- Constant longitudinal force input of $F_x = 0N$
- Constant longitudinal velocity of $v_x = 22.22$ m/s (80 km/h)

The corresponding steering angle input for the sine-with-dwell maneuver is visualized in Figure B.1a, where it can be observed that the steering maneuver itself only lasts two seconds.

B.2. Validation of Hybrid Approximations

The validation of the hybrid approximations of the lateral tire forces is conducted by making use of the different levels of approximations in Appendix A. To validate the approximations, the open-loop simulations of the hybrid models are compared to the open-loop simulation of the nonlinear model. The nonlinear and hybridized models can be found in chapter 2. The lateral accelerations and the yaw rates of the models during the open-loop simulations will be compared to compare the hybrid models with the nonlinear model. These results are key indicators of a vehicle's dynamic response to steering

inputs, especially in highly nonlinear scenarios. By comparing these parameters, it can be evaluated how well the hybrid model captures the essential dynamics of the vehicle during a demanding maneuver.

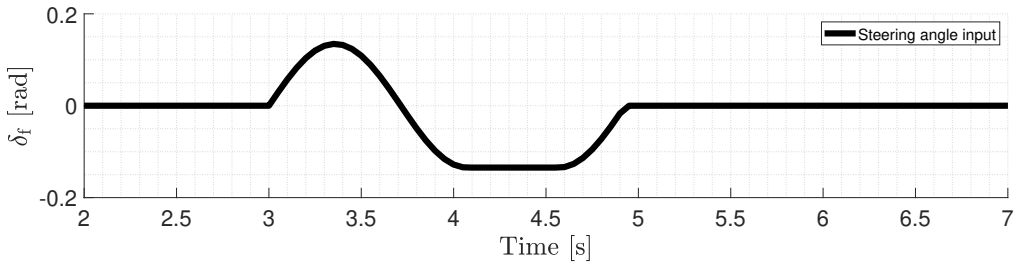

(a) Steering angle input for sine-with-dwell maneuver.

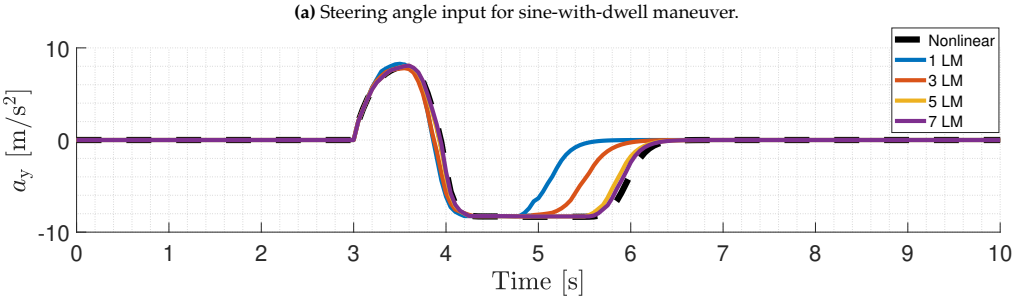

(b) Lateral acceleration of nonlinear and hybrid vehicle models in open-loop sine-with-dwell maneuver.

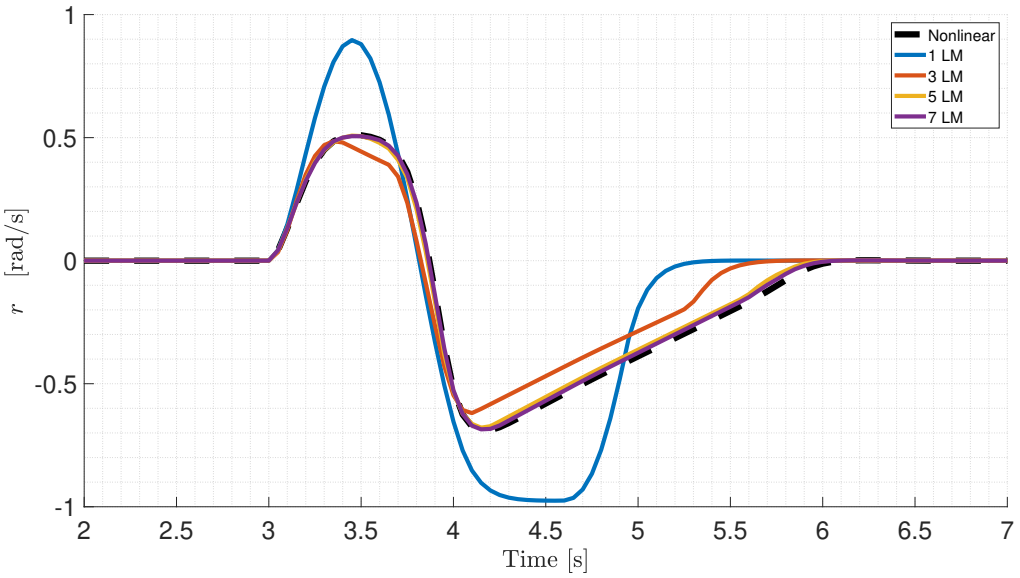

(c) Yaw rate of nonlinear and hybrid vehicle models in open-loop sine-with-dwell maneuver.

Figure B.1: Open-loop simulations of the sine-with-dwell maneuver.

In Figure B.1, the open-loop results of all vehicle models are shown for the sine-with-dwell steering angle input. It can be observed in Figure B.1b that the lateral acceleration of the nonlinear vehicle model is in the highly nonlinear regime above 8 m/s^2, indicating vehicle operation near the limits of handling. The hybrid models all experience lateral accelerations in the same region as the nonlinear model, and a similar trajectory can be observed. However, the influence of the complexity of hybridization is evident. For the first segment between 3 and 4.5 seconds, it can already be observed that increased hybridization complexity results in more similar lateral accelerations to the nonlinear vehicle model, whereas low complexity hybridizations deviate from this visibly before all reaching similar maximum lateral accelerations at around 4.5 s. In the second segment, between 4.5 and 6.5 seconds, the differences between the different levels of hybridization become even more pronounced. The higher the hybridization

complexity, the more accurately the nonlinear behavior is replicated.

In Figure B.1c, the yaw rates of all models during the open-loop simulation are visualized. It can be observed that similar differences arise with respect to the complexity of hybridization. The higher the level of complexity, the closer the yaw rate trajectories approach the nonlinear yaw rate trajectory. Especially the approximations with 5 or 7 local modes are very similar, whereas the approximation with only 3 local modes deviates more from the nonlinear model. The hybrid vehicle model incorporating the linear tire model exhibits substantial deviations from the nonlinear results, primarily attributable to the model's single local mode, which does not adequately represent the nonlinear characteristics of the lateral tire force model.

Based on the open-loop simulation results, it can be confirmed that the complexity of the approximations plays a significant role in determining the extent to which the nonlinear behavior can be replicated. Increased complexity results in a more accurate representation of the nonlinear vehicle model, as could be expected, whereas the linear tire model shows significant deviations in results from the nonlinear model. Moreover, it needs to be noted that in this open-loop simulation case, velocity across all models remains almost the same, and no longitudinal force is applied. Moreover, road friction is the same in all cases, indicating that the lateral tire force model approximations operate in the same regions as the nonlinear lateral tire model. With varying road conditions and applied braking or accelerating, the nonlinear lateral tire model will deviate from the hybrid models. Therefore, these open-loop simulations can validate that high-level hybrid approximations demonstrate near-identical behavior to the nonlinear model under specific conditions in nonlinear driving scenarios.

C

Sensitivity Analysis

This section elaborates on the sensitivity analysis employed for the MPC and MPCC frameworks. The highest complexity models are used to account for the most nonlinear model elements in tuning the weights for both frameworks. First, the general step-by-step approach for this analysis is explained. Thereafter, the analysis for the MPC with seven local modes and the MPCC with seven local modes will be visualized and discussed.

C.1. General Approach

Both the MPC and the MPCC have a total of five different elements in the cost function, as can be observed in chapter 2. For MPC, the cost function is given as

$$J_k = \sum_{i=1}^{N_\mathrm{p}} \left(\|\Delta \mathrm{Y}_{k+i}\|_1^{q_{\Delta \mathrm{Y}}} + \|\Delta \psi_{k+i}\|_1^{q_{\Delta \psi}} + \|\Delta v_{\mathrm{x},k+i}\|_1^{q_{\Delta v_\mathrm{x}}} + \left\|\dot{\delta}_{\mathrm{f},k+i}\right\|_1^{q_{\dot{\delta}_\mathrm{f}}} + \left\|\dot{F}_{\mathrm{x},k+i}\right\|_1^{q_{\dot{F}_\mathrm{x}}} \right), \tag{C.1}$$

where the corresponding weights for the MPC frameworks are the cost for deviation of the lateral position $q_{\Delta Y}$, the cost for deviation of the heading $q_{\Delta \psi}$, the cost for deviation of the longitudinal velocity $q_{\Delta v_\mathrm{x}}$, and the cost for the inputs of the steering angle rate $q_{\dot{\delta}_\mathrm{f}}$ and the total longitudinal force rate $q_{\dot{F}_\mathrm{x}}$. Similarly, for MPCC, the cost function is given as

$$J_k = \sum_{i=1}^{N_\mathrm{p}} \left(\|\hat{\epsilon}^\mathrm{c}(x_{k+i}, \theta_{k+i})\|_1^{q_{\hat{\epsilon}^\mathrm{c}}} + \left\|\hat{\epsilon}^\mathrm{l}(x_{k+i}, \theta_{k+i})\right\|_1^{q_{\hat{\epsilon}^\mathrm{l}}} + \|\Delta v_{\mathrm{x},k+i}\|_1^{q_{\Delta v_\mathrm{x}}} + \left\|\dot{\delta}_{\mathrm{f},k+i}\right\|_1^{q_{\dot{\delta}_\mathrm{f}}} + \left\|\dot{F}_{\mathrm{x},k+i}\right\|_1^{q_{\dot{F}_\mathrm{x}}} \right). \tag{C.2}$$

where instead of costs for the deviation of the lateral position and the heading angle, the MPCC frameworks utilize costs related to the contouring error $q_{\hat{\epsilon}^\mathrm{c}}$ and the lag error $q_{\hat{\epsilon}^\mathrm{l}}$.

For both frameworks, an initial manual tuning process was carried out to evaluate the effect of the different cost elements on the cost functions. Based on this manual tuning, an initial value and suitable ranges for the weights have been selected. Since it is not possible to evaluate all weights for all combinations with an appropriate step size, it is chosen to divide the sensitivity analysis into separate steps by evaluating combinations of weights. The first combination is related to the positional tracking of the frameworks. The weight terms related to the lateral position and heading will be evaluated for the MPC frameworks, while fixed values for the other weights will be used based on the manual tuning process. For the MPCC frameworks, the weights related to the contouring and the lag error will be considered. After the analysis of the first combination of weights, the resulting values of the weights will be fixed for the next combination. The next combination is related to the longitudinal velocity and the total longitudinal force rate input, which are directly related. For the final step, the steering rate input will be evaluated separately using the results of the previous combinations to fix the values for these weights. The general approach for the sensitivity analysis is as follows:

1. Evaluating the combinations of $q_{\Delta \mathrm{Y}}$ and $q_{\Delta \psi}$ (MPC) or $q_{\hat{\epsilon}^\mathrm{c}}$ and $q_{\hat{\epsilon}^\mathrm{l}}$ (MPCC) for fixed values of the other weights based on the manual tuning

2. Evaluating the combination of $q_{\Delta v_x}$ and $q_{\dot{F}_x}$ for fixed other weights, where $q_{\Delta Y}$ and $q_{\Delta\psi}$ (MPC) or $q_{\hat{e}^c}$ and $q_{\hat{e}^l}$ (MPCC) are based on the results of step 1
3. Evaluating the effect of $q_{\dot{\delta}_f}$ for fixed other weights based on the results of both steps 1 and 2

After the above steps, a final tuning is obtained that can be used for each specific framework. However, the results of these steps do not give one global minimum for which the framework is best. Instead, each step consists of two phases. For both phases, relevant KPIs are considered to properly evaluate the effects of the weights. The KPIs that are considered for the first phase are median computation time per step and the RMSE of X, Y, ψ, v_x. The RMS of the inputs are not considered in this phase of the sensitivity analysis. A combined result is obtained by normalizing and scaling the KPIs according to priority. Since the combined result consists of numerous local minima, it is chosen to select the five tunings for which the combined result is the lowest. Although this does not guarantee the global minimum for each evaluation, it does give a comprehensive and structured approach to finding a suitable tuning. The five minima are then compared in the second phase, and both time-based simulations and new KPIs are considered to select the optimal solution. These KPIs are the maximum absolute derivative of the longitudinal velocity $\max|dv_x|$, the maximum absolute inputs $\max|\dot{\delta}_f|$ and $\max|\dot{F}_x|$, and the maximum and median computation time per time. Since the first phase focused on KPIs related to tracking, and the five minima are already found to have reasonable results in that respect, this phase focuses on the effect of the inputs. Both the normalized KPIs and the time-domain trajectories are compared, and a final choice can be made on the most suitable tuning for that specific combination. This process is repeated for all steps, and the result is a local optimal tuning for the framework. In the next sections, both the MPC and the MPCC with seven local modes will be tuned so that the resulting tuning for both frameworks can also be employed for the controllers with lower complexity approximations. It should be noted that the resulting tunings are not optimal, representing local minima rather than the global optimum. These tunings are determined through an analysis utilizing relevant KPIs to identify the most suitable settings. While they may not achieve the highest possible performance, careful consideration is given to both KPIs and subjective preferences when selecting the best tuning.

C.2. MPC

This section provides a sensitivity analysis of the MPC controllers by evaluating MPC7.

C.2.1. Tuning of $q_{\Delta Y}$ versus $q_{\Delta\psi}$

The first step is to evaluate the combinations of $q_{\Delta Y}$ and $q_{\Delta\psi}$ for fixed $q_{\Delta v_x}$, $q_{\dot{\delta}_f}$, and $q_{\dot{F}_x}$. Based on manual tuning, the following weights and ranges are considered:

$q_{\Delta Y}$	$q_{\Delta\psi}$	$q_{\Delta v_x}$	$q_{\dot{\delta}_f}$	$q_{\dot{F}_x}$
0:0.1:10	0:0.3:30	0.8	4.5	3.00e-05

Based on the ranges of $q_{\Delta Y}$ and $q_{\Delta\psi}$, a total of 10201 combinations are simulated. The results are visualized for all KPIs in Figure C.1. In the sensitivity analysis plots, the color scale serves as a visual aid to interpret the KPIs depicted. Dark blue regions correspond to lower KPI values, which are typically desirable as they signify optimal system performance. Conversely, regions colored yellow indicate significantly elevated KPI values, often indicating infeasible or undesirable system states. This color scheme remains consistent across all sensitivity analysis plots, considering a combination of two weights. As can be observed, the effect of $q_{\Delta Y}$ and $q_{\Delta\psi}$ varies per KPI. For KPIs related to the input, lower values of $q_{\Delta\psi}$ are desired, whereas KPIs related to the tracking of the position require the opposite. In order to find local optima for the tuning that takes into account multiple KPIs, a selection of KPIs are normalized and scaled. The KPIs related to the median computation time per step and the RMSE of X, Y, ψ, v_x are normalized. The scaling of these KPIs is as follows:

$$0.1\hat{X}_{\text{RMSE}} + 0.7\hat{Y}_{\text{RSME}} + 0.1\hat{\psi}_{\text{RMSE}} + 0\hat{v}_{x,\text{RMSE}} + 0.1\hat{T}_{\text{median}} \tag{C.3}$$

It should be noted that the scaling of $\hat{v}_{x,\text{RMSE}}$ in this step is zero. The author made this decision to prioritize this specific KPI in the subsequent step, which will incorporate weights associated with

longitudinal velocity and total longitudinal force. The combined result is visualized in Figure C.2, and the five minima with the lowest overall value are given as follows:

	Minimum 1	Minimum 2	Minimum 3	Minimum 4	Minimum 5
Value	0.34851	0.34977	0.34992	0.35128	0.35263
$q_{\Delta Y}$	8.1	2.4	8	2.8	8.5
$q_{\Delta\psi}$	11.7	9.3	12.3	9.3	20.4

The tunings corresponding to these five minima are evaluated using time domain analysis. Additionally, a new set of KPIs is employed to assess the outcomes of these five tunings in detail. These KPIs are the maximum absolute derivative of the longitudinal velocity $\max|dv_x|$, the maximum absolute inputs $\max|\dot{\delta}_f|$ and $\max|\dot{F}_x|$, and the maximum and median computation time per time. To ensure proper evaluation in the visualization, these KPIs have been normalized. In Figure C.3, the time domain results are visualized, and in Figure C.4, the normalized KPIs are given for each minimum. The average of the normalized KPIs for each minimum is given as follows:

	Minimum 1	Minimum 2	Minimum 3	Minimum 4	Minimum 5
Average	0.88167	0.69538	0.94272	0.83479	0.78567

Based on the analysis of the results, Minimum 2 emerges as the most optimal among all identified minima. Although the time-domain analysis indicates minimal deviations between the various minima, the normalized KPIs present a different perspective. Across all KPIs, Minimum 2 exhibits consistently low scores, indicating reduced utilization of input while maintaining precise velocity tracking. Furthermore, it demonstrates relatively low computational demands. This means that for the tuning of the MPC, the values of $q_{\Delta Y}$ and $q_{\Delta\psi}$ are found:

$$q_{\Delta Y} = 2.4, \quad q_{\Delta\psi} = 9.3 \tag{C.4}$$

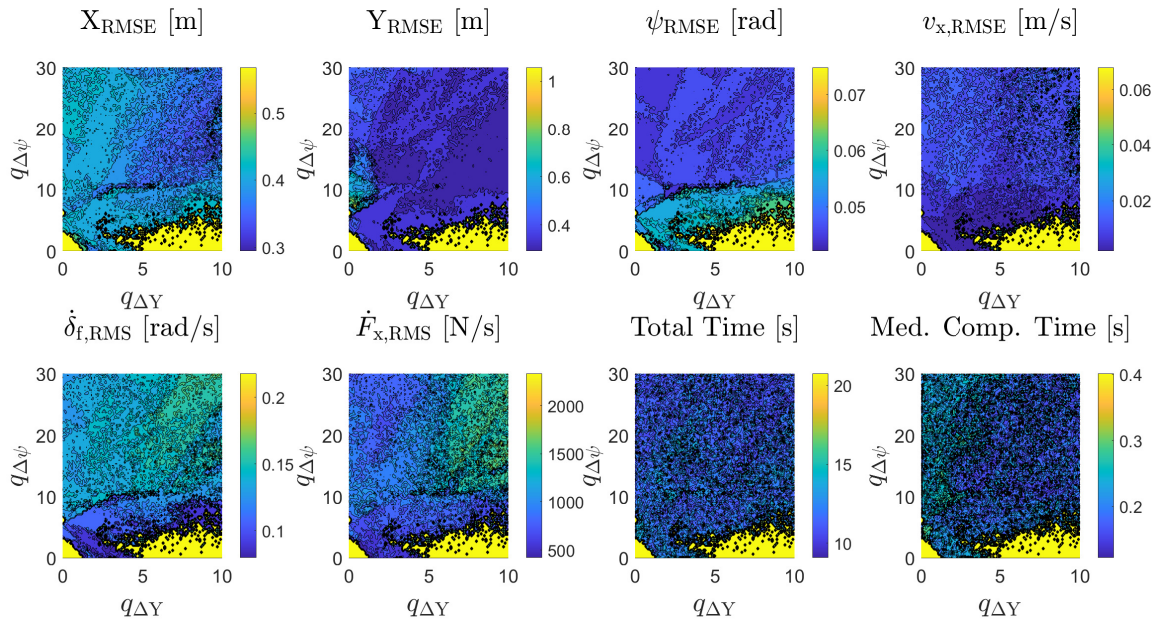

Figure C.1: MPC: KPIs for weights $q_{\Delta Y}$ versus $q_{\Delta\psi}$.

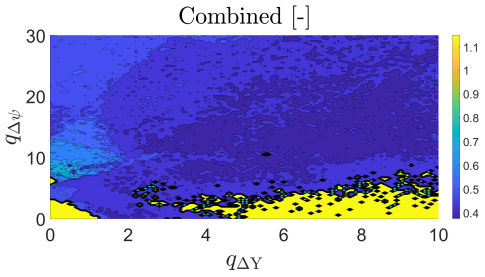

Figure C.2: MPC: Combination of KPIs weights $q_{\Delta Y}$ versus $q_{\Delta\psi}$.

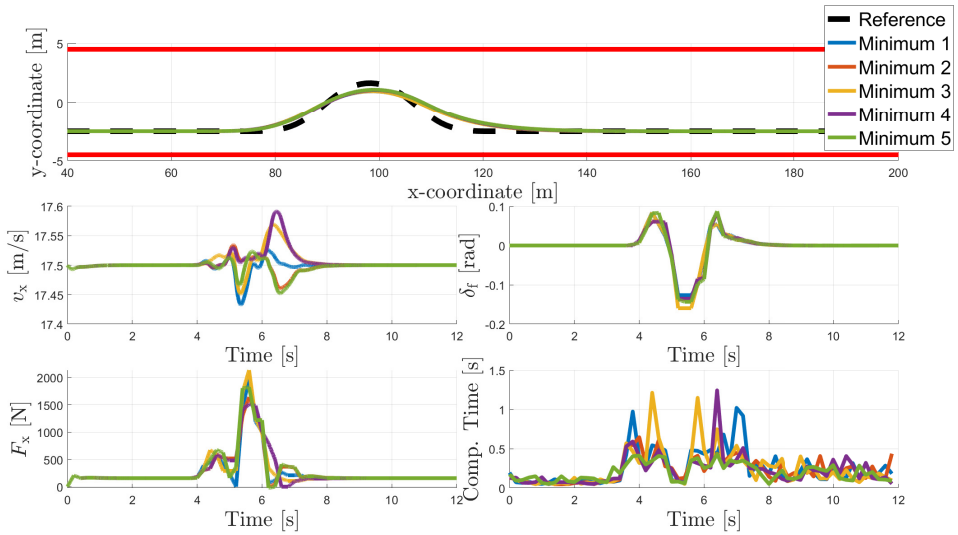

Figure C.3: MPC: Time-domain simulations of five minima for weights $q_{\Delta Y}$ versus $q_{\Delta\psi}$.

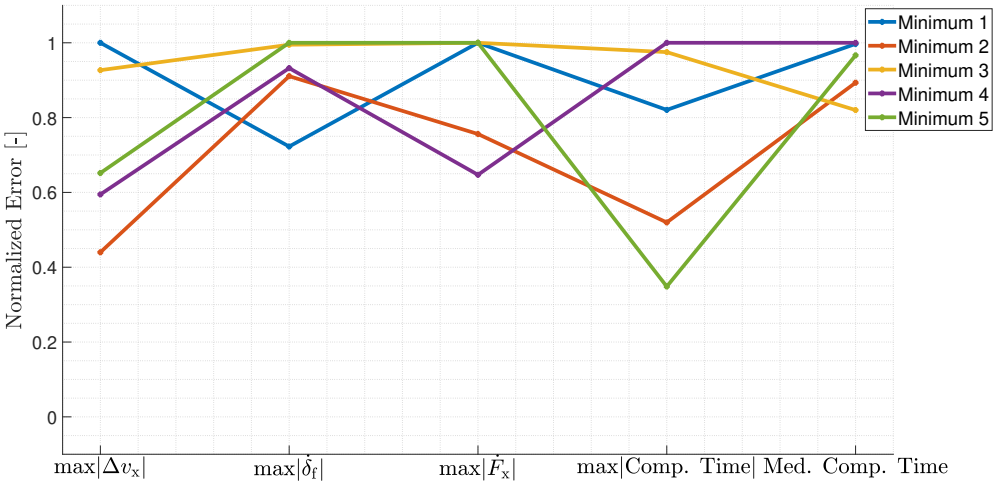

Figure C.4: MPC: Normalized KPIs of five minima for weights $q_{\Delta Y}$ versus $q_{\Delta\psi}$.

C.2.2. Tuning of $q_{\Delta v_x}$ versus $q_{\dot{F}_x}$

The next combination of weights that will be considered is the combination of $q_{\Delta v_x}$ and $q_{\dot{F}_x}$. The following range of tunings is now employed:

$q_{\Delta Y}$	$q_{\Delta\psi}$	$q_{\Delta v_x}$	q_{δ_f}	$q_{\dot{F}_x}$
2.4	9.3	0:0.025:1.5	4.5	0:1e-6:5e-5

Based on these ranges, a total of 3111 simulations are executed. The results are visualized in Figure C.5, where it can be perceived that there is a large variation for suitable tunings when considering each KPI individually. The scaling of the KPIs is as follows:

$$0.1\hat{X}_{\text{RMSE}} + 0.7\hat{Y}_{\text{RSME}} + 0.1\hat{\psi}_{\text{RMSE}} + 0.2\hat{v}_{x,\text{RMSE}} + 0.1\hat{T}_{\text{median}} \tag{C.5}$$

The scaling of $\hat{v}_{x,\text{RMSE}}$ in this step is not zero since the weights are associated with longitudinal velocity and total longitudinal force, which directly impact the velocity. The combined result is visualized in Figure C.6, and the five minima with the lowest overall value are given as follows:

	Minimum 1	Minimum 2	Minimum 3	Minimum 4	Minimum 5
Value	0.42482	0.42916	0.42932	0.4296	0.43139
$q_{\Delta Y}$	0.725	0.825	0.825	0.8	0.425
$q_{\Delta\psi}$	2.3e-05	2e-05	1.7e-05	1.1e-05	3e-06

These minima are evaluated in time domain simulations, and the results can be found in Figure C.7 and C.8. The average of the normalized KPIs are:

	Minimum 1	Minimum 2	Minimum 3	Minimum 4	Minimum 5
Average	0.85857	0.85174	0.74822	0.83741	0.8561

In Figure C.7, Minimum 5 experiences chattering in the longitudinal force rate input, resulting in undesired oscillating behavior for the longitudinal velocity. For the other minima, no significant deviations are found. In Figure C.8, Minimum 3 shows the overall best potential by scoring low on all KPIs. This is confirmed by the average of the normalized KPIs. Therefore, the weights of Minimum 3 are adapted for the MPC:

$$q_{\Delta v_x} = 0.825, \quad q_{\dot{F}_x} = 1.7e-05 \tag{C.6}$$

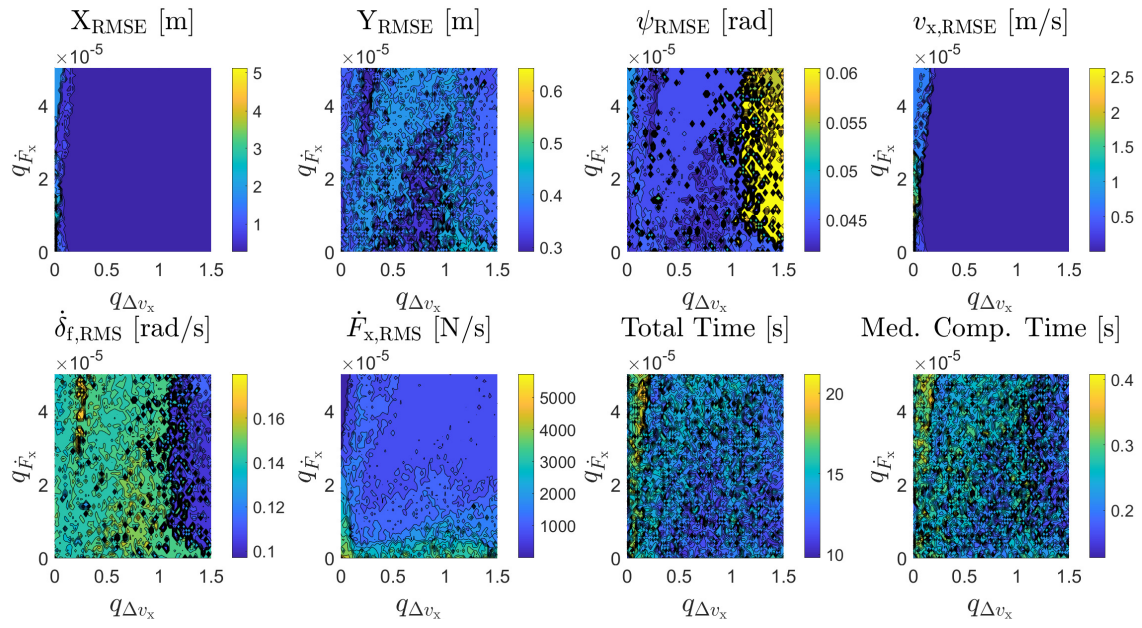

Figure C.5: MPC: KPIs for weights $q_{\Delta v_x}$ versus $q_{\dot{F}_x}$.

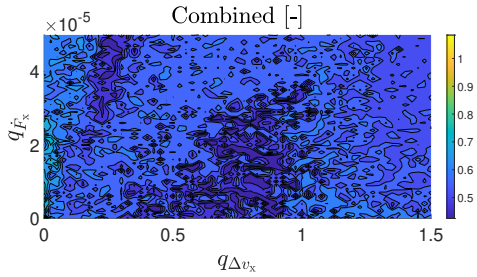

Figure C.6: MPC: Combination of KPIs for weights $q_{\Delta v_x}$ versus $q_{\dot{F}_x}$.

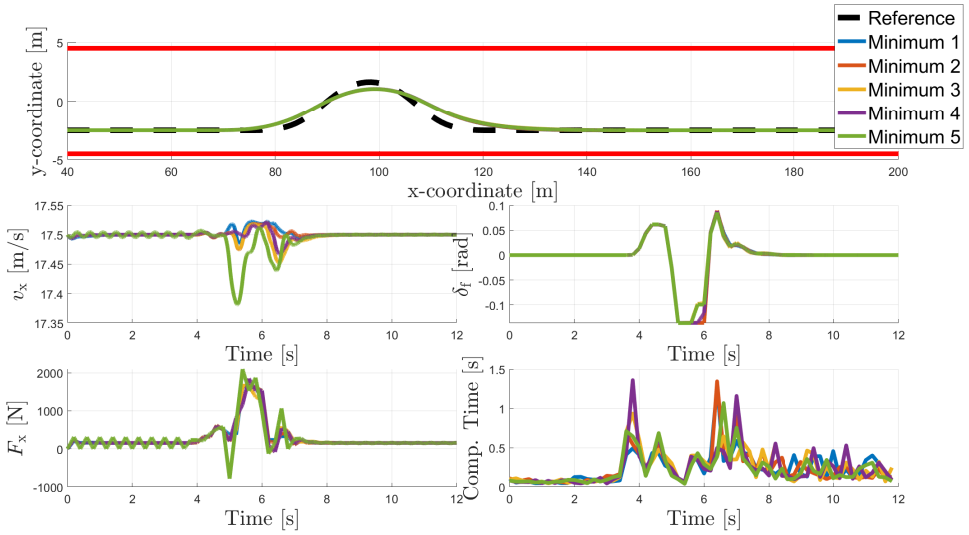

Figure C.7: MPC: Time-domain simulations of five minima for weights $q_{\Delta v_x}$ versus $q_{\dot{F}_x}$.

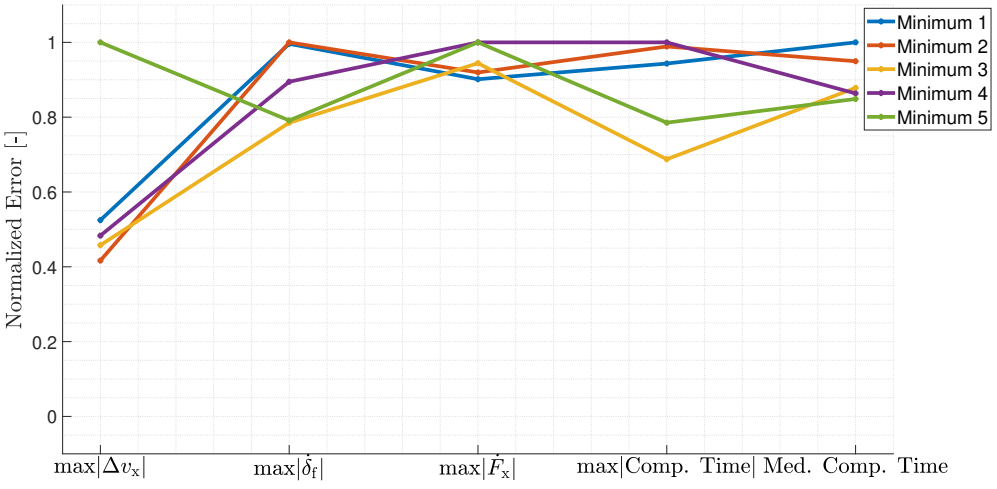

Figure C.8: MPC: Normalized KPIs of five minima for weights $q_{\Delta v_x}$ versus $q_{\dot{F}_x}$.

C.2.3. Tuning of $q_{\dot{\delta}_f}$

The final step in the sensitivity analysis related to MPC is to analyze the effect of the weight $q_{\dot{\delta}_f}$. This is done by evaluating the following range of tunings:

$q_{\Delta Y}$	$q_{\Delta\psi}$	$q_{\Delta v_x}$	$q_{\dot{\delta}_f}$	$q_{\dot{F}_x}$
2.4	9.3	0.825	0:0.025:5	1.7e-5

In Figure C.9, the KPIs with respect to the range of $q_{\dot{\delta}_f}$ are illustrated. Since only the weight $q_{\dot{\delta}_f}$ is evaluated, the corresponding figures contain line plots. To find a combined optimum, the following scaling of the KPIs is employed:

$$0.3\hat{X}_{\text{RMSE}} + 0.7\hat{Y}_{\text{RSME}} + 0.1\hat{\psi}_{\text{RMSE}} + 0.1\hat{v}_{x,\text{RMSE}} + 0.2\hat{T}_{\text{median}} \tag{C.7}$$

The combined result is visualized in Figure C.10, and the five minima with the lowest overall value are given as follows:

	Minimum 1	Minimum 2	Minimum 3	Minimum 4	Minimum 5
Value	0.92751	1.0039	1.0197	1.0294	1.0301
$q_{\dot{\delta}_f}$	4.5	3.6	3.2	2.9	3.4

The time domain results are presented in Figure C.11 and C.12, and the average of the normalized KPIs are:

	Minimum 1	Minimum 2	Minimum 3	Minimum 4	Minimum 5
Average	0.8663	0.70079	0.82272	0.83155	0.69261

Based on the result of the normalized KPIs in Figure C.12, it can be concluded that Minimum 5 has the best overall values with respect to the other minima. The lowest average supports this. Therefore, Minimum 5 determines the weight of $q_{\dot{\delta}_f} = 2.9$, and the final tuning for the MPC frameworks becomes:

$q_{\Delta Y}$	$q_{\Delta\psi}$	$q_{\Delta v_x}$	$q_{\dot{\delta}_f}$	$q_{\dot{F}_x}$
2.4	9.3	0.825	2.9	1.7e-5

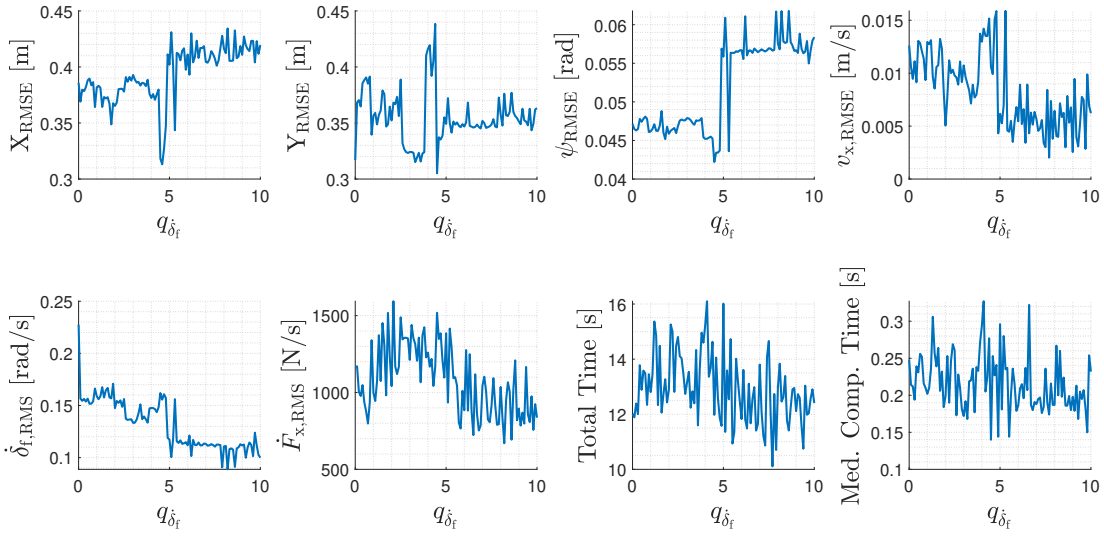

Figure C.9: MPC: KPIs for weight $q_{\dot{\delta}_f}$.

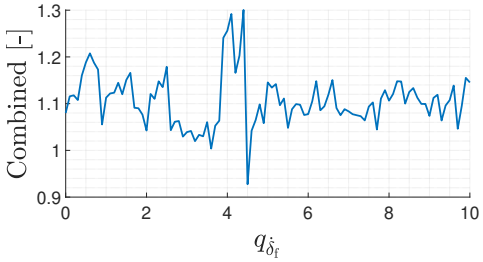

Figure C.10: MPC: Combination of KPIs for weight $q_{\dot{\delta}_f}$.

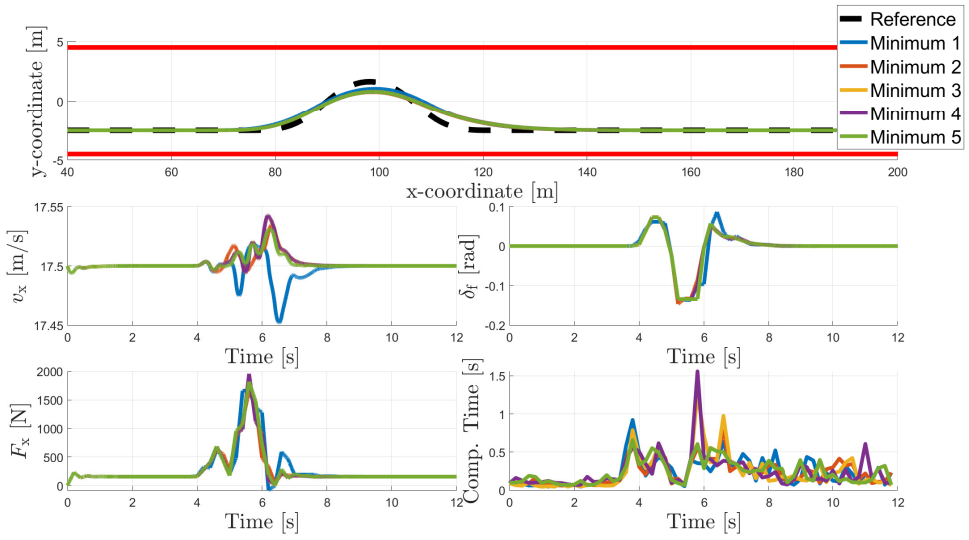

Figure C.11: MPC: Time-domain simulations of five minima for weight $q_{\dot{\delta}_f}$.

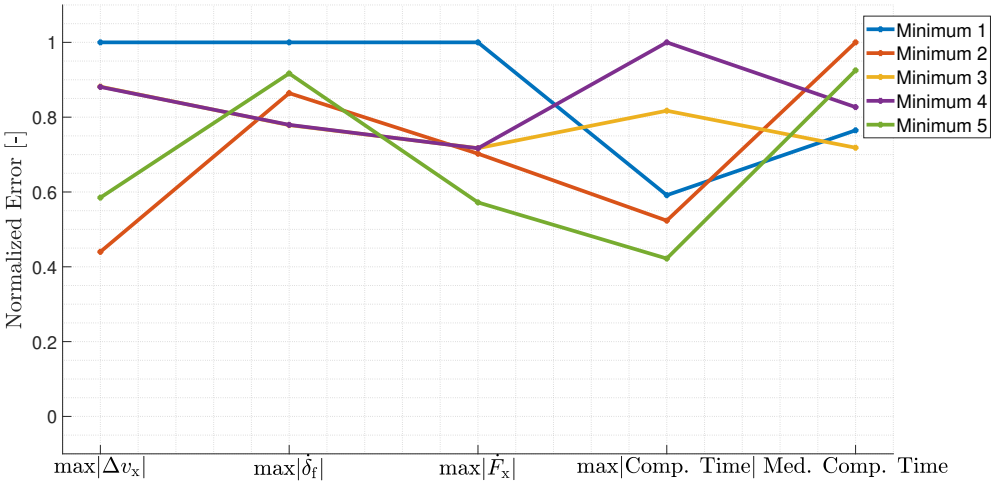

Figure C.12: MPC: Normalized KPIs of five minima for weight $q_{\dot{\delta}_f}$.

C.3. MPCC

This section provides a sensitivity analysis of the MPCC controllers by evaluating MPCC7.

C.3.1. Tuning of $q_{\hat{e}^c}$ versus $q_{\hat{e}^l}$

The first step is to evaluate the combinations of $q_{\hat{e}^c}$ and $q_{\hat{e}^l}$ for fixed $q_{\Delta v_x}$, $q_{\dot{\delta}_f}$, and $q_{\dot{F}_x}$. Based on manual tuning, the following weights and ranges are considered:

$q_{\hat{e}^c}$	$q_{\hat{e}^l}$	$q_{\Delta v_x}$	$q_{\dot{\delta}_f}$	$q_{\dot{F}_x}$
0:0.15:15	0:1e-04:0.05	1	16	2.00e-04

A total of 10201 simulations were conducted. The results are illustrated in Figure C.13, revealing two distinct regions warranting further investigation for optimal tunings. These regions are divided by a stretch of infeasible outcomes, emphasizing the importance of careful deliberation in tuning selection. Given that infeasible outcomes are observed across all KPIs, all scaling settings will ensure avoidance of the infeasible region. The scaling of the relevant normalized KPIs is outlined below:

$$0.1\hat{X}_{\text{RMSE}} + 0.7\hat{Y}_{\text{RSME}} + 0.1\hat{\psi}_{\text{RMSE}} + 0\hat{v}_{x,\text{RMSE}} + 0.1\hat{T}_{\text{median}} \tag{C.8}$$

The combined result is given in Figure C.14, where it can be observed that the same two regions appear and are separated by an unfeasible region. Due to the scaling, the lower region is for higher values of $q_{\hat{e}^c}$. The following five minima are found:

	Minimum 1	Minimum 2	Minimum 3	Minimum 4	Minimum 5
Value	0.12291	0.12325	0.12334	0.12386	0.12387
$q_{\hat{e}^c}$	14.25	9.9	14.25	13.2	10.65
$q_{\hat{e}^l}$	0.019	0.046	0.0475	0.0145	0.0395

The time domain trajectories are presented in Figure C.15 and C.16, and the average normalized KPIs are:

	Minimum 1	Minimum 2	Minimum 3	Minimum 4	Minimum 5
Average	0.85064	0.81389	0.93629	0.79693	0.79193

As can be observed from Figure C.15, Minimum 3 experiences chattering in the steering angle, and it experiences an offset when considering the longitudinal velocity. Moreover, Minimum 2 suffers from overshoot when finishing the DLC maneuver. Since the other minima do not diverge much, the normalized KPIs in Figure C.16 are considered. This figure clearly shows that Minimums 4 and 5 have the best relative results. Therefore, both could be chosen, but Minimum 5 is preferred due to the lower median computation time. The resulting tuning for $q_{\hat{e}^c}$ and $q_{\hat{e}^l}$ then becomes:

$$q_{\hat{e}^c} = 10.65, \quad q_{\hat{e}^l} = 0.0395 \tag{C.9}$$

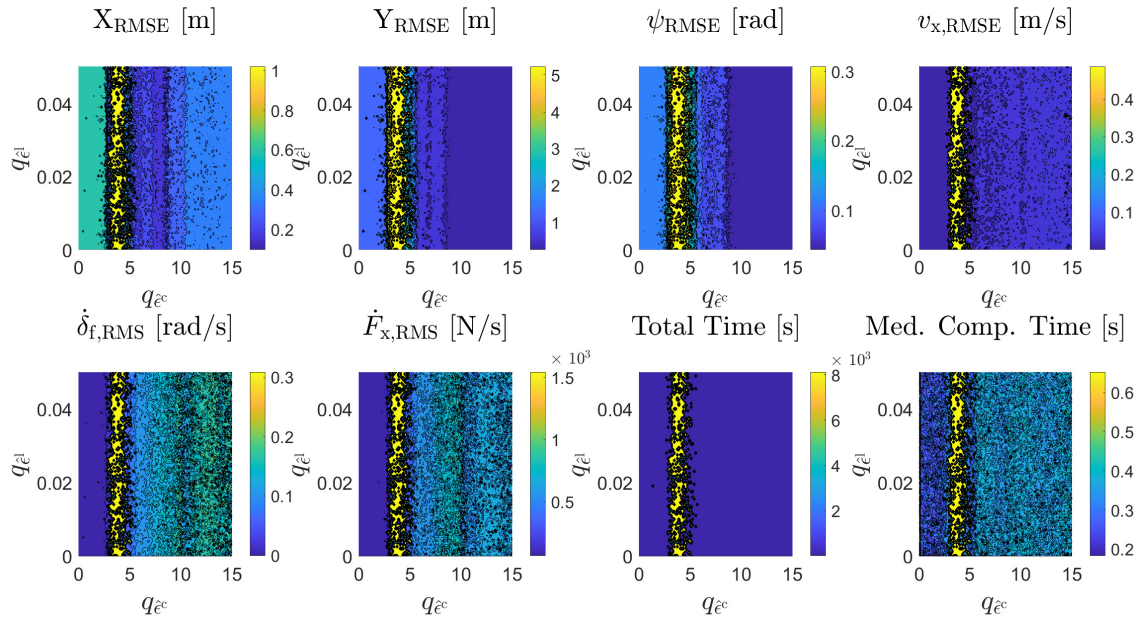

Figure C.13: MPCC: KPIs for weights $q_{\hat{e}^c}$ versus $q_{\hat{e}^l}$.

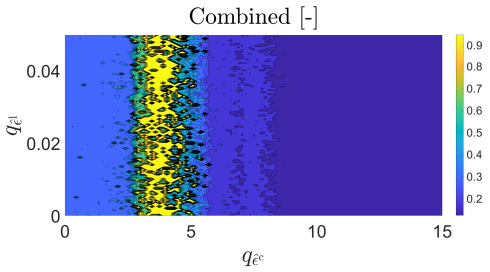

Figure C.14: MPCC: Combination of KPIs for weights $q_{\hat{e}^c}$ versus $q_{\hat{e}^l}$.

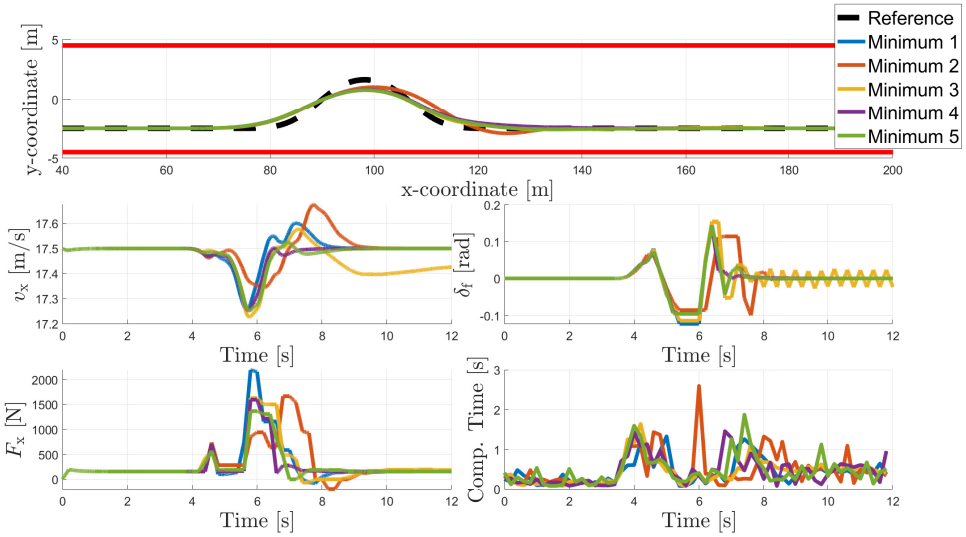

Figure C.15: MPCC: Time-domain simulations of five minima for weights $q_{\hat{e}^c}$ versus $q_{\hat{e}^l}$.

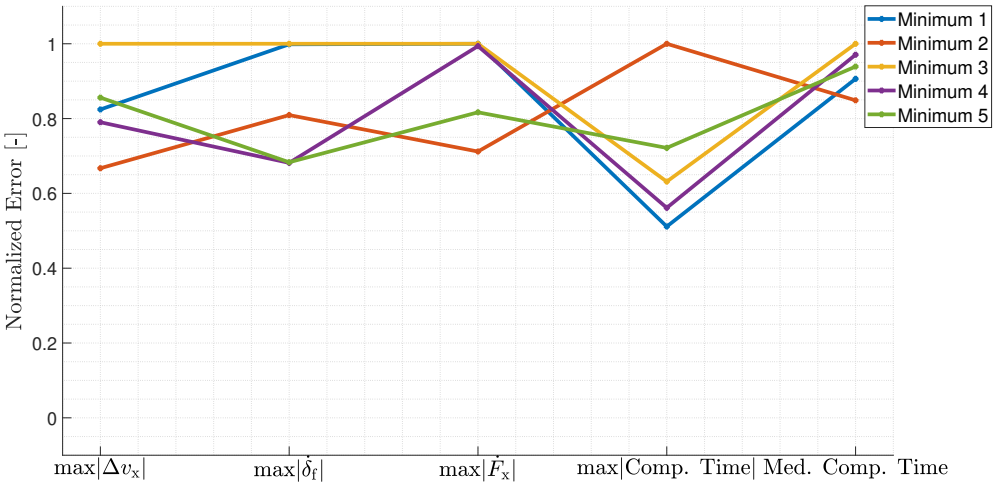

Figure C.16: MPCC: Normalized KPIs of five minima for weights $q_{\hat{e}^c}$ versus $q_{\hat{e}^l}$.

C.3.2. Tuning of $q_{\Delta v_x}$ versus $q_{\dot{F}_x}$

This section evaluates the combinations of $q_{\Delta v_x}$ and $q_{\dot{F}_x}$ for fixed $q_{\hat{\epsilon}^c}$, $q_{\hat{\epsilon}^l}$, and $q_{\dot{\delta}_f}$ based on the results of the previous combination. The following range of weights are considered:

$q_{\hat{\epsilon}^c}$	$q_{\hat{\epsilon}^l}$	$q_{\Delta v_x}$	$q_{\dot{\delta}_f}$	$q_{\dot{F}_x}$
10.65	0.0395	0:0.025:1.5	16	0:1e-5:5e-4

The specified ranges encompass a total of 3111 simulations, with the corresponding KPI results visualized in Figure C.17. A pattern emerges regarding the weights, as evidenced by a division that separates the results into two distinct regions. Since the optimal region differs per KPI, the following scaling is used:

$$0.1\hat{X}_{\text{RMSE}} + 0.7\hat{Y}_{\text{RSME}} + 0.1\hat{\psi}_{\text{RMSE}} + 0.2\hat{v}_{x,\text{RMSE}} + 0.1\hat{T}_{\text{median}} \tag{C.10}$$

Corresponding to this scaling, the combined result is portrayed in Figure C.18, and the five minima are given as:

	Minimum 1	Minimum 2	Minimum 3	Minimum 4	Minimum 5
Value	0.42021	0.42029	0.42257	0.42279	0.423
$q_{\hat{\epsilon}^c}$	1.175	1.275	1.3	1.05	1.25
$q_{\hat{\epsilon}^l}$	3e-05	7e-05	4e-05	1e-05	1.6e-04

It can be observed from the time domain results in Figure C.19 that Minimum 4 experiences chattering in the longitudinal force rate input, which translates to oscillatory behavior for the longitudinal velocity. The other minima have similar time domain trajectories, but in Figure C.20, the normalized KPI results for Minimum 1 show to have the most potential relative to the other minima. This is supported by the average of the normalized KPIs:

	Minimum 1	Minimum 2	Minimum 3	Minimum 4	Minimum 5
Average	0.75134	0.87859	0.91931	0.85306	0.84092

Therefore, the weights of Minimum 1 are used for $q_{\Delta v_x}$ and $q_{\dot{F}_x}$:

$$q_{\Delta v_x} = 1.175, \quad q_{\dot{F}_x} = 3e-05 \tag{C.11}$$

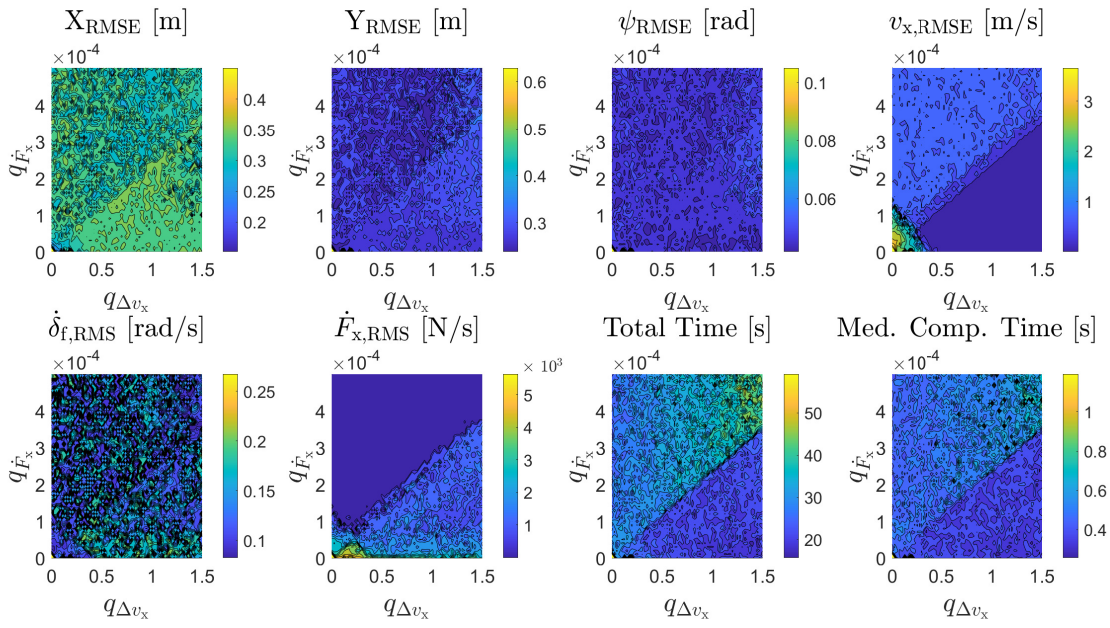

Figure C.17: MPCC: KPIs for weights $q_{\Delta v_x}$ versus $q_{\dot{F}_x}$.

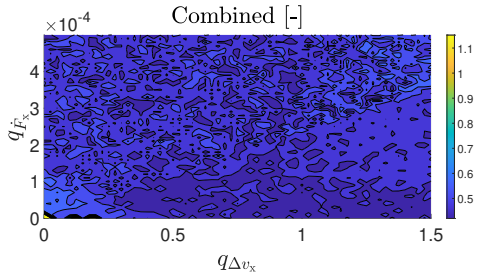

Figure C.18: MPCC: Combination of KPIs for weights $q_{\Delta v_x}$ versus $q_{\dot{F}_x}$.

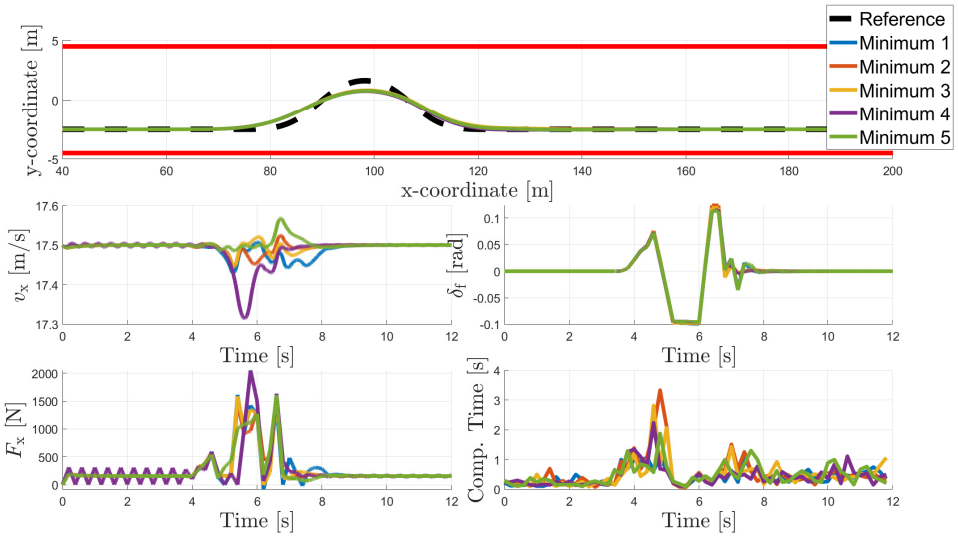

Figure C.19: MPCC: Time-domain simulations of five minima for weights $q_{\Delta v_x}$ versus $q_{\dot{F}_x}$.

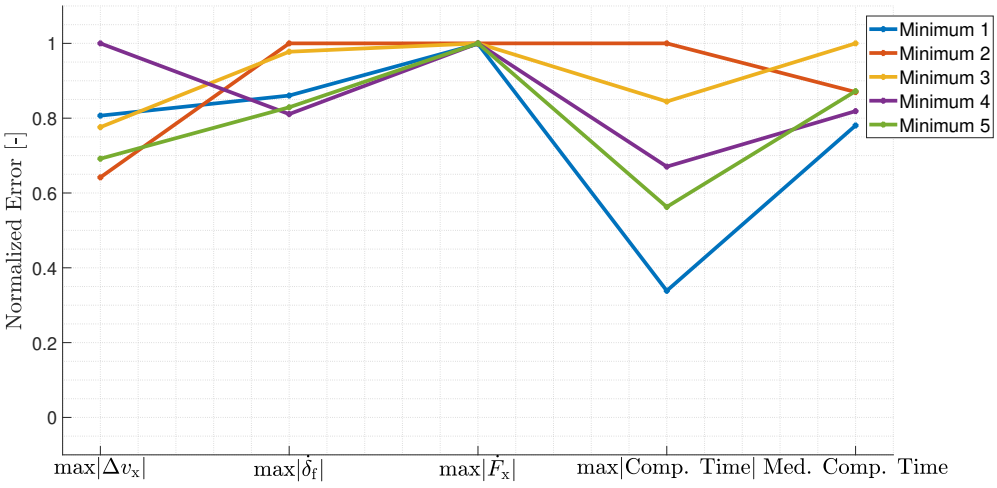

Figure C.20: MPCC: Normalized KPIs of five minima for weights $q_{\Delta v_x}$ versus $q_{\dot{F}_x}$.

C.3.3. Tuning of $q_{\dot{\delta}_\mathrm{f}}$

The final step in the sensitivity analysis for MPCC involves assessing the impact of the weight $q_{\dot{\delta}_\mathrm{f}}$. The following range of tunings are considered:

$q_{\hat{\epsilon}^\mathrm{c}}$	$q_{\hat{\epsilon}^\mathrm{l}}$	$q_{\Delta v_\mathrm{x}}$	$q_{\dot{\delta}_\mathrm{f}}$	$q_{\dot{F}_\mathrm{x}}$
10.65	0.0395	1.175	0:0.2:20	3e-05

In Figure C.21, the KPIs with respect to the range of $q_{\dot{\delta}_\mathrm{f}}$ are illustrated. To find a combined optimum, the following scaling of the KPIs is employed: In Figure C.21, the KPIs across the range of $q_{\dot{\delta}_\mathrm{f}}$ are depicted. To determine a suitable optimum, the following scaling of the KPIs is applied:

$$0.3\hat{\mathrm{X}}_\mathrm{RMSE} + 0.7\hat{\mathrm{Y}}_\mathrm{RSME} + 0.1\hat{\psi}_\mathrm{RMSE} + 0.1\hat{v}_\mathrm{x,RMSE} + 0.2\hat{T}_\mathrm{median} \tag{C.12}$$

The collective outcome is presented in Figure C.22, with the five minima exhibiting the lowest overall values listed below:

	Minimum 1	Minimum 2	Minimum 3	Minimum 4	Minimum 5
Value	0.83862	0.85644	0.86957	0.87501	0.88273
$q_{\dot{\delta}_\mathrm{f}}$	16.4	15.2	15.8	14.8	15.4

The time domain results are displayed in Figure C.23 and C.24. The averages of the normalized key performance indicators (KPIs) are as follows:

	Minimum 1	Minimum 2	Minimum 3	Minimum 4	Minimum 5
Average	0.78296	0.86846	0.97537	0.86166	0.91801

The time domain trajectories exhibit similar behavior across all minima, with no distinct minima showing significant positive or negative characteristics.

Furthermore, the analysis of the normalized key performance indicators (KPIs) in Figure C.24 reveals that Minimum 1 demonstrates the most favorable overall values compared to the other minima. This conclusion is supported by the lowest average value. As a result, Minimum 1 dictates the weight of $q_{\dot{\delta}_\mathrm{f}} = 16.4$, leading to the final tuning for the MPC frameworks as follows:

$q_{\hat{\epsilon}^\mathrm{c}}$	$q_{\hat{\epsilon}^\mathrm{l}}$	$q_{\Delta v_\mathrm{x}}$	$q_{\dot{\delta}_\mathrm{f}}$	$q_{\dot{F}_\mathrm{x}}$
10.65	0.0395	1.175	16.4	3e-5

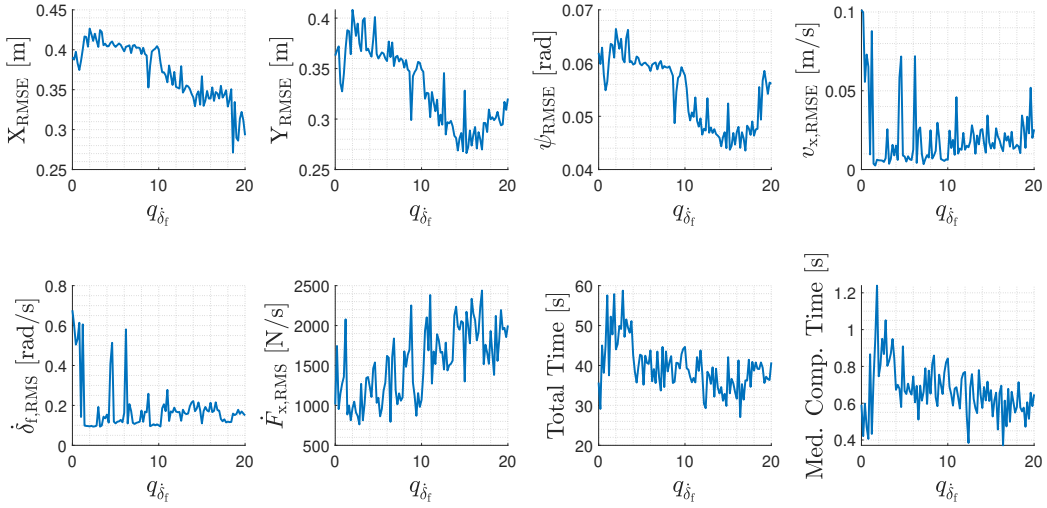

Figure C.21: MPCC: KPIs for weight $q_{\dot{\delta}_\mathrm{f}}$.

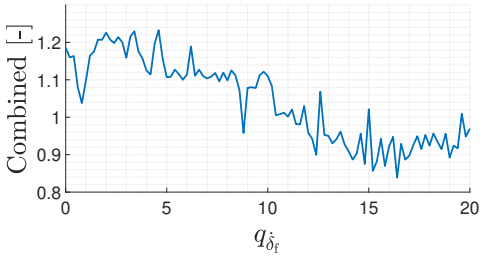

Figure C.22: MPCC: Combination of KPIs for weight $q_{\dot{\delta}_f}$.

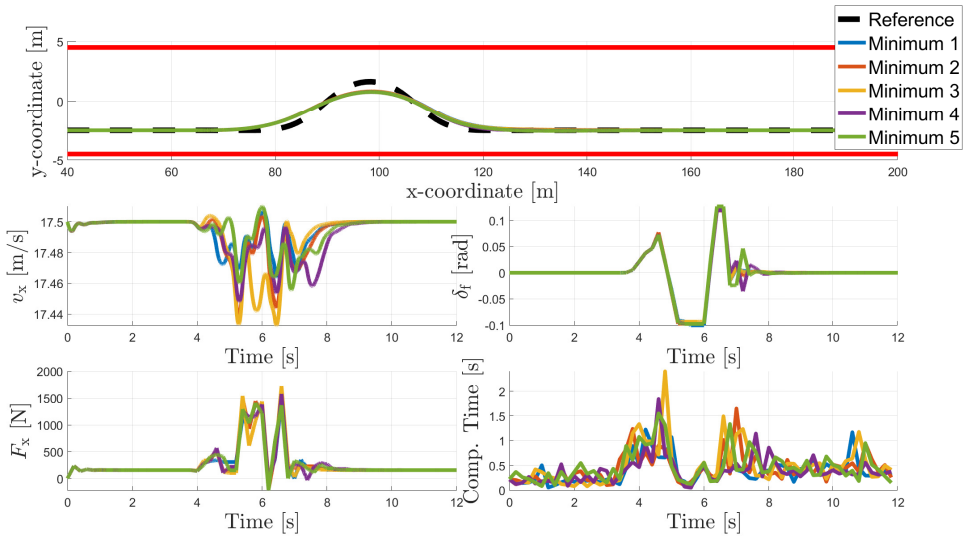

Figure C.23: MPCC: Time-domain simulations of five minima for weight $q_{\dot{\delta}_f}$.

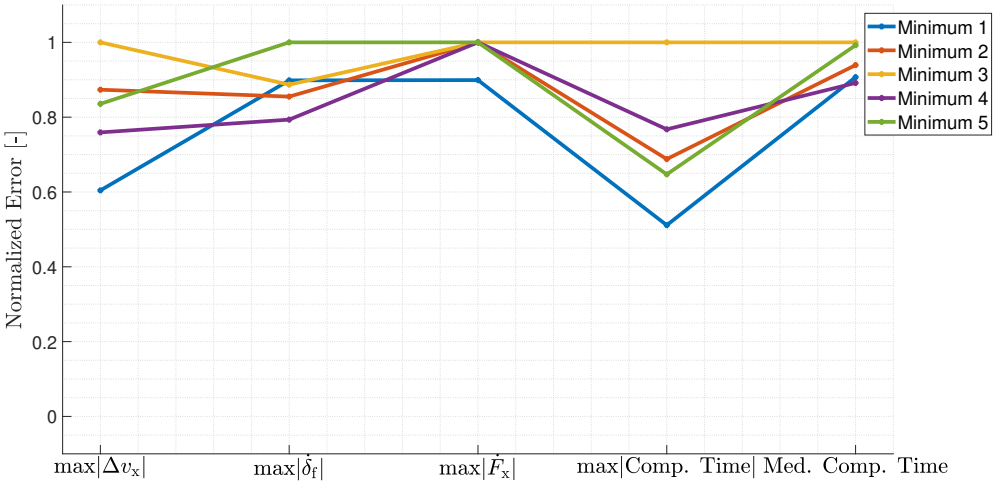

Figure C.24: MPCC: Normalized KPIs of five minima for weight $q_{\dot{\delta}_f}$.

Bibliography

[1] World Health Organization, "Global Status Report on Road Safety 2018," World Health Organization, Geneva, Switzerland, Tech. Rep., 2018.

[2] F. Malin, I. Norros, and S. Innamaa, "Accident Risk of Road and Weather Conditions on Different Road Types," *Accident Analysis & Prevention*, vol. 122, pp. 181–188, 1 2019.

[3] D. J. Fagnant and K. Kockelman, "Preparing a Nation for Autonomous Vehicles: Opportunities, Barriers and Policy Recommendations," *Transportation Research Part A: Policy and Practice*, vol. 77, pp. 167–181, 2015.

[4] SAE International, "Taxonomy and Definitions for Terms Related to Driving Automation Systems for On-Road Motor Vehicles (SAE J3016_202104))," Society of Automotive Engineers, SAE Technical Standards Board; SAE International, Warrendale, PA, USA, Tech. Rep., 2021.

[5] M. Martínez-Díaz, F. Soriguera, and I. Pérez, "Autonomous Driving: A Bird's Eye View," *IET Intelligent Transport Systems*, vol. 13, no. 4, pp. 563–579, 4 2019.

[6] J. Hang, X. Yan, X. Li, K. Duan, J. Yang, and Q. Xue, "An Improved Automated Braking System for Rear-end Collisions: A Study based on a Driving Simulator Experiment," *Journal of Safety Research*, vol. 80, pp. 416–427, 2 2022.

[7] J. Bornholt and M. Heidt, "To Drive or not to Drive - A Critical Review Regarding the Acceptance of Autonomous Vehicles," *ICIS 2019 Proceedings*, vol. 5, 2019.

[8] N. Chowdhri, L. Ferranti, F. S. Iribarren, and B. Shyrokau, "Integrated Nonlinear Model Predictive Control for Automated Driving," *Control Engineering Practice*, vol. 106, p. 104654, 1 2021.

[9] P. Stano, U. Montanaro, D. Tavernini, M. Tufo, G. Fiengo, L. Novella, and A. Sorniotti, "Model Predictive Path Tracking Control for Automated Road Vehicles: A Review," *Annual Reviews in Control*, 12 2022.

[10] A. Sorniotti, P. Barber, and S. De Pinto, "Path Tracking for Automated Driving: A Tutorial on Control System Formulations and Ongoing Research," *Automated Driving: Safer and More Efficient Future Driving*, pp. 71–140, 1 2016.

[11] D. Lam, C. Manzie, and M. C. Good, "Model Predictive Contouring Control," *Proceedings of the IEEE Conference on Decision and Control*, pp. 6137–6142, 2010.

[12] A. Rupenyan, M. Khosravi, and J. Lygeros, "Performance-based Trajectory Optimization for Path Following Control Using Bayesian Optimization," *Proceedings of the IEEE Conference on Decision and Control*, vol. 2021-December, pp. 2116–2121, 2021.

[13] B. Brito, B. Floor, L. Ferranti, and J. Alonso-Mora, "Model Predictive Contouring Control for Collision Avoidance in Unstructured Dynamic Environments," *IEEE Robotics and Automation Letters*, vol. 4, no. 4, pp. 4459–4466, 10 2019.

[14] L. Ferranti, B. Brito, E. Pool, Y. Zheng, R. M. Ensing, R. Happee, B. Shyrokau, J. F. Kooij, J. Alonso-Mora, and D. M. Gavrila, "SafeVRU: A Research Platform for the Interaction of Self-driving Vehicles with Vulnerable Road Users," *IEEE Intelligent Vehicles Symposium, Proceedings*, vol. 2019-June, pp. 1660–1666, 6 2019.

[15] W. Schwarting, J. Alonso-Mora, L. Paull, S. Karaman, and D. Rus, "Safe Nonlinear Trajectory Generation for Parallel Autonomy with a Dynamic Vehicle Model," *IEEE Transactions on Intelligent Transportation Systems*, vol. 19, no. 9, pp. 2994–3008, 9 2018.

[16] A. Liniger, A. Domahidi, and M. Morari, "Optimization-based Autonomous Racing of 1:43 Scale RC Cars," *Optimal Control Applications and Methods*, vol. 36, no. 5, pp. 628–647, 9 2015.

[17] A. Romero, S. Sun, P. Foehn, and D. Scaramuzza, "Model Predictive Contouring Control for Time-Optimal Quadrotor Flight," *IEEE Transactions on Robotics*, vol. 38, no. 6, pp. 3340–3356, 12 2022.

[18] J. Ji, X. Zhou, C. Xu, and F. Gao, "CMPCC: Corridor-Based Model Predictive Contouring Control for Aggressive Drone Flight," *Springer Proceedings in Advanced Robotics*, vol. 19, pp. 37–46, 2021.

[19] A. Bertipaglia, M. Alirezaei, R. Happee, and B. Shyrokau, "Model Predictive Contouring Control for Vehicle Obstacle Avoidance at the Limit of Handling," *28th IAVSD International Symposium on Dynamics of Vehicles on Roads and Tracks*, 8 2023.

[20] N. H. Amer, H. Zamzuri, K. Hudha, and Z. A. Kadir, "Modelling and Control Strategies in Path Tracking Control for Autonomous Ground Vehicles: A Review of State of the Art and Challenges," *Journal of Intelligent and Robotic Systems: Theory and Applications*, vol. 86, no. 2, pp. 225–254, 5 2017.

[21] M. Metzler, D. Tavernini, P. Gruber, and A. Sorniotti, "On Prediction Model Fidelity in Explicit Nonlinear Model Predictive Vehicle Stability Control," *IEEE Transactions on Control Systems Technology*, vol. 29, no. 5, pp. 1964–1980, 9 2021.

[22] J. Subosits and J. C. Gerdes, "Impacts of Model Midelity on Trajectory Optimization for Autonomous Vehicles in Extreme Maneuvers," *IEEE Transactions on Intelligent Vehicles*, 2021.

[23] J. Liu, P. Jayakumar, J. L. Stein, and T. Ersal, "A Study on Model Fidelity for Model Predictive Control-based Obstacle Avoidance in High-speed Autonomous Ground Vehicles," *Vehicle System Dynamics*, vol. 54, no. 11, pp. 1629–1650, 11 2016.

[24] V. A. Laurense and J. Christian Gerdes, "Long-Horizon Vehicle Motion Planning and Control through Serially Cascaded Model Complexity," *IEEE Transactions on Control Systems Technology*, vol. 30, no. 1, pp. 166–179, 1 2022.

[25] P. Falcone, F. Borrelli, J. Asgari, H. E. Tseng, and D. Hrovat, "Predictive Active Steering Control for Autonomous Vehicle Systems," *IEEE Transactions on Control Systems Technology*, vol. 15, no. 3, pp. 566–580, 5 2007.

[26] J. Funke, M. Brown, S. M. Erlien, and J. C. Gerdes, "Collision Avoidance and Stabilization for Autonomous Vehicles in Emergency Scenarios," *IEEE Transactions on Control Systems Technology*, vol. 25, no. 4, pp. 1204–1216, 7 2017.

[27] W. Y. Choi, D. J. Kim, C. M. Kang, S. H. Lee, and C. C. Chung, "Autonomous Vehicle Lateral Maneuvering by Approximate Explicit Predictive Control," *Proceedings of the American Control Conference*, vol. 2018-June, pp. 4739–4744, 8 2018.

[28] X. Sun, Y. Cai, S. Wang, X. Xu, and L. Chen, "Optimal Control of Intelligent Vehicle Longitudinal Dynamics via Hybrid Model Predictive Control," *Robotics and Autonomous Systems*, vol. 112, pp. 190–200, 2 2019.

[29] K. Liu, J. Gong, A. Kurt, H. Chen, and U. Ozguner, "Dynamic Modeling and Control of High-speed Automated Vehicles for Lane Change Maneuver," *IEEE Transactions on Intelligent Vehicles*, vol. 3, no. 3, pp. 329–339, 9 2018.

[30] T. Novi, A. Liniger, R. Capitani, and C. Annicchiarico, "Real-time Control for At-limit Handling Driving on a Predefined Path," *International Journal of Vehicle Mechanics and Mobility*, vol. 58, no. 7, pp. 1007–1036, 7 2019.

[31] Y. Li, J. Fan, Y. Liu, and X. Wang, "Path Planning and Path Tracking for Autonomous Vehicle Based on MPC with Adaptive Dual-Horizon-Parameters," *International Journal of Automotive Technology*, vol. 23, no. 5, pp. 1239–1253, 10 2022.

[32] M. Rokonuzzaman, N. Mohajer, S. Nahavandi, and S. Mohamed, "Model Predictive Control with Learned Vehicle Dynamics for Autonomous Vehicle Path Tracking," *IEEE Access*, vol. 9, pp. 128 233–128 249, 2021.

[33] E. Asarin, T. Dang, and A. Girard, "Hybridization Methods for the Analysis of Nonlinear Systems," *Acta Informatica*, vol. 43, no. 7, pp. 451–476, 2 2007.

[34] Q. Cui, R. Ding, C. Wei, and B. Zhou, "A Hierarchical Framework of Emergency Collision Avoidance amid Surrounding Vehicles in Highway Driving," *Control Engineering Practice*, vol. 109, p. 104751, 4 2021.

[35] X. He, Y. Liu, C. Lv, X. Ji, and Y. Liu, "Emergency Steering Control of Autonomous Vehicle for Collision Avoidance and Stabilisation," *Vehicle System Dynamics*, vol. 57, no. 8, pp. 1163–1187, 8 2018.

[36] Q. Cui, R. Ding, X. Wu, and B. Zhou, "A New Strategy for Rear-end Collision Avoidance via Autonomous Steering and Differential Braking in Highway Driving," *Vehicle System Dynamics*, vol. 58, no. 6, pp. 955–986, 6 2019.

[37] K. Zhang, J. Sprinkle, and R. G. Sanfelice, "Computationally Aware Control of Autonomous Vehicles: A Hybrid Model Predictive Control Approach," *Autonomous Robots*, vol. 39, no. 4, pp. 503–517, 12 2015.

[38] F. Borrelli, P. Falcone, T. Keviczky, J. Asgari, and D. Hrovat, "MPC-based Approach to Active Steering for Autonomous Vehicle Systems," *International Journal of Vehicle Autonomous Systems*, vol. 3, no. 2-4, pp. 265–291, 2005.

[39] W. P. Heemels, B. De Schutter, and A. Bemporad, "Equivalence of Hybrid Dynamical Models," *Automatica*, vol. 37, no. 7, pp. 1085–1091, 7 2001.

[40] T. Besselmann and M. Morari, "Hybrid Parameter-varying Model Predictive Control for Autonomous Vehicle Steering," *European Journal of Control*, vol. 14, no. 5, pp. 418–431, 1 2008.

[41] D. Bernardini, S. Di Cairano, A. Bemporad, and H. E. Tseng, "Drive-by-wire Vehicle Stabilization and Yaw Regulation: A Hybrid Model Predictive Control Design," *Proceedings of the IEEE Conference on Decision and Control*, pp. 7621–7626, 2009.

[42] W. Liu, J. Zhang, D. Sun, and H. Hu, "Piecewise Affine Based Model Predictive Trajectory Tracking Control with Stability Guarantees for Autonomous Ground Vehicles," *2022 China Automation Congress (CAC)*, pp. 3664–3670, 3 2023.

[43] T. Fu, H. Jing, H. Zhou, and Z. Liu, "Mixed Logical Dynamic based Path-Tracking Model Predictive Control for Autonomous Vehicles," *IEEE Conference on Intelligent Transportation Systems, Proceedings (ITSC)*, pp. 189–196, 2022.

[44] L. Gharavi, B. De Schutter, and S. Baldi, "Efficient MPC for Emergency Evasive Maneuvers, Part I: Hybridization of the Nonlinear Problem," *IEEE Transactions on Intelligent Vehicles*, vol. 0, no. 0, 10 2023.

[45] ——, "Efficient MPC for Emergency Evasive Maneuvers, Part II: Comparative Assessment for Hybrid Control," *IEEE Transactions on Intelligent Vehicles*, vol. 00, no. 0, 2023.

[46] L. Gharavi, A. Dabiri, J. Verkuijlen, B. De Schutter, S. Baldi, and S. Member, "Proactive Emergency Collision Avoidance for Automated Driving in Highway Scenarios," *IEEE Transactions on Control Systems Technology, Special Issue*, 10 2023.

[47] A. Szucs, M. Kvasnica, and M. Fikar, "Optimal Piecewise Affine Approximations of Nonlinear Functions Obtained from Measurements," *IFAC Proceedings Volumes*, vol. 45, no. 9, pp. 160–165, 1 2012.

[48] M. Kvasnica, A. Szücs, and M. Fikar, "Automatic Derivation of Optimal Piecewise Affine Approximations of Nonlinear Systems," *IFAC Proceedings Volumes*, vol. 44, no. 1, pp. 8675–8680, 1 2011.